UNIVERSITY OF CALIFORNIA, SAN DIEGO

Two Photon Absorption and Third Harmonic Generation Micro-spectroscopy: Hemoglobin and Other Compounds

A dissertation submitted in partial satisfaction of the requirements for the degree of Doctor of Philosophy

in

Physics (Biophysics)

by

Gabriel Omar Clay

Committee in charge:

David Kleinfeld, Chair
Patrick H Diamond
Joe E Ford
Thomas Hermann
Lu J Sham

2006

The dissertation of Gabriel Omar Clay is approved,
and it is acceptable in quality and form for publication
on microfilm

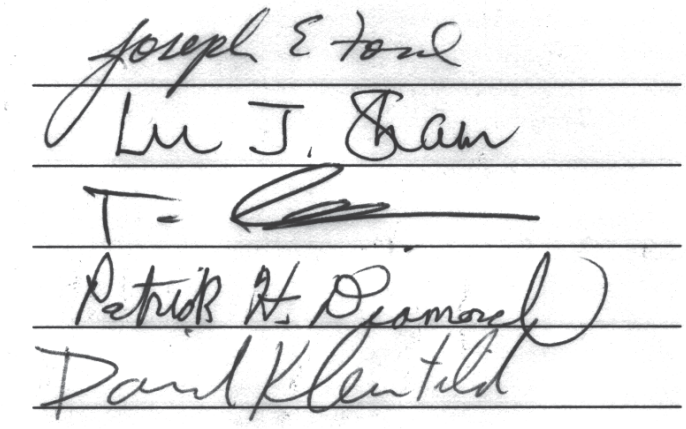

Chair

University of California, San Diego

2006

Dedication

Without a wonderful family and a group of close friends this work would not have been completed. I dedicate this dissertation to them. In acknowledgement of H.R. 3162 no specific names are mentioned.

Table of Contents

List of Figures

List of Tables

Acknowledgements

In addition to acknowledging my family, friends, and co-workers it is necessary to note the use in full or in part the following published works:

Chapter I:

Beyond observation: Microscopy with ultrashort laser pulses to probe and manipulate cortical vasculature. G. O. Clay, N. Nishimura, C. B. Schaffer, P. S. Tsai and D. Kleinfeld. SPIE International Technical Group Newsletter, Optics in Information Systems (2004)15:4-5.

Chapter II:

Spectroscopy of third harmonic generation: Evidence for resonances in model compounds and ligated hemoglobin. G. O. Clay, A. C. Millard, C. B. Schaffer, J. Aus-der-Au, P. S. Tsai, J. A. Squier and D. Kleinfeld. Journal of the Optical Society of America B (2006) 23:932-950.

Chapter III:

Large two-photon absorption cross-section of hemoglobin in the infrared range of 780 - 880 nm. G. O. Clay, C. B. Schaffer and D. Kleinfeld. submitted.

Vita

Degrees:

University California at San Diego

Ph.D.	Physics (Biophysics)		2006
M.S.	Physics		1999

University California at Santa Cruz

B.A.	Psychology	(honors)	1996
B.A.	Mathematics	(honors)	1996
B.S.	Physics	(high honors)	1996

Teaching Experience:

University California at San Diego

Teaching Assistant	Biophysics	2006
Head teaching Assistant	Introductory Quantum Physics	1999

Reuben H Fleet Center — Electromagnetism — 2001

In an outreach collaboration taught a mini-class to Fleet Center facilitators.

University San Diego — Physics and Society — 2000

Instructor Developed introductory physics concepts historically

Research Experience:

University California at San Diego

Laboratory of David Kleinfeld Research Assistant 1999-

Nonlinear optical spectrometry in biological media

University California at San Diego

Laboratory of Jackson Davis Data Analyst 1995

Human facial electromyography in response to stimuli

Related Experience:

University California Institute on Global Conflict and Cooperation

National Security Policy Making in a post 9/11 World:

Facilitator 2005

Public Policy and Biological Threats Training Program

Associate 2004-

Public Policy and Nuclear Threats Training Program

Associate 2004-

Science Policy Analysis Roundtable at University California at San Diego

Chair and founding member 2004-

Society of Photonics and Information Engineering (SPIE)

Photonics West: Biomedical Applications of Ultrafast Lasers symposium

Chair 2003

Preparing Future Physics Faculty at University California San Diego

Coordinator 2002-3

Institute for Theoretical Physics: Neuro-physics pedagogical workshop

Student Participant 2001

ABSTRACT OF THE DISSERTATION

Two Photon Absorption and
Third Harmonic Generation Micro-spectroscopy
in Hemoglobin and Other Compounds

by

Gabriel Omar Clay

Doctor of Philosophy in Physics/Biophysics

Professor David Kleinfeld, Chair

We report on third harmonic generation (THG), two photon absorption (TPA), and two-photon excited fluorescence (TPEF) micro-spectroscopy studies performed on solutions of hemoglobin, bovine serum albumin, water, benzene, and several dyes. We use focussed, ultrafast, ~2 nano-joule laser pulses at selected center wavelengths between 760- 1000 nm. We find evidence of one, two, and three photon resonances in these materials.

Previous nonlinear spectroscopy work with solution phase bio-molecules has been largely limited to fluorescent compounds. We substantially extend these studies and report on use of THG as a general means of investigating the nonlinear properties of non-fluorescent molecules.

At physiologically relevant concentrations, hemoglobin solutions are found to have large resonant TPA cross-sections, σ_{TPA} ~ 150 GM. This finding confirms theoretical predictions that the highly conjugated cyclic structure of porphryns may lead to cross-sections of such magnitudes. At some wavelengths we find a significant differences between the nonlinear properties of hemoglobin in different ligand binding states. This suggests that the nonlinear optical properties of hemoglobin may be used as a functional contrast mechanism to report blood oxygenation in nonlinear laser scanning microscopy.

Our spectral measurements on THG in water and benzene are found to be in good agreement with previous single wavelength studies. Our two-photon absorption spectra of rhodamine B and 6G are in excellent agreement with previous single wavelength TPA cross-sections studies performed on these dyes at similar concentrations. We show that large discrepancies in TPEF based cross-section studies on these dyes is largely due to concentration effects.

Introduction

Chapter Organization

The body of this work is a report on some nonlinear optical micro-spectroscopy investigations of hemoglobin and several other molecules in solution phase. Specifically we study two photon absorption and third harmonic generation induced in these samples by exposure to high intensity focused irradiation with ultrafast (~100-200 fs in duration) laser pulses at selected center wavelengths in the range of 760-1000 nm. Chapter II and III address the details of these experiments. Each chapter is free-standing and can be read independently.

Chapter II. Third harmonic generation (THG) is a coherent process in which three photons incident on a nonlinear material are transformed into a single photon at 3 times the energy. This process can be resonantly enhanced when the nonlinear material has energetic states near the first, second, or third harmonic of the incident light. In Chapter II we report on the use of THG micro-spectroscopy in a manner easily adapted to nonlinear microscopes as a means to investigate multiphoton resonances in non-fluorescent materials. We report on the THG spectra of oxy, deoxy, and carboxy- hemoglobin, bovine serum albumin, water, benzene, Fura-2, and rhodamine B [1].

Chapter III. Two-photon absorption (TPA) is the simultaneous absorption of two photons. This process allows the study of electronic states not accessible with standard one-photon absorption spectroscopy. Clearly TPA is also fundamental to the operation of two-photon excited flurorescence (TPEF) scanning microscopy. Although TPA is a likely source of photo-damage in biological samples [2], TPA studies in bio-molecules have been largely confined to fluorescent compounds [3]. This is in large part due to the difficulty in measuring TPA directly [4]. We use an extremely sensitive pump-probe technique to report on ultrafast TPA and TPEF spectroscopy measurements on oxy and carboxy- hemoglobin, rhodamine B, rhodamine 6G, and fluorescein[5].

Chapter I. However humble and meager in impact, these studies nevertheless rest in the context of, and contribute to, the tremendous ongoing historical scientific investigation into the interaction of light and matter. They also occur amid a range of exciting developments at the cross-roads of nonlinear optics, biological imaging, medicine, and chemistry. The relevance of basic science investigations, such as the nonlinear spectroscopy work presented here, may be best appreciated with a broad perspective where the incremental progress of individual studies sum to recognizable significance. In recognition of this and in acknowledgement of a significant readership pool in the non-physical science community, Section 1 of this chapter is a general and necessarily incomplete introduction to the historical development of optics, microscopy, and spectroscopy. Section 2 provides a brief, elementary introduction to the basic mathematics of nonlinear optics, and Section 3 addresses the current scientific context and specific motivations that compelled us in the research that make up

the bulk of this dissertation. The author imagines that most of Chapter 1 is accessible to college level readers, whereas the following chapters are directed towards research scientists with some familiarity with the field of nonlinear optics.

Historical Brief: through the looking glass

From the capacity of the cornea and eye-lens to form an image on the retina and the different spectral response curves of the photoreceptors lining it, to the size of the optic nerve and visual cortex, the interaction of light and matter lies at the heart of human understanding. In turn, our understanding of optical phenomenon has extended our vision (literally) and opened new windows into the material world. In this introduction we briefly consider some of the important roles that optical phenomenon and technology has played in our society and our scientific worldview and in the process introduce the historical roots of nonlinear micro-spectroscopy.

Refractive Optics. Abu Ali Hasn Ibn Al Harthan (commonly known as Al Hazain) laid out the basic principles of optical refraction in the 11th century and the use of eyeglasses for vision correction is reported to have occurred at least as early as the late 1200's in Italy. However lens-crafting technology informed by an understanding of refractive optics is not believed to have been developed until much later [6]. Galileo Galilei's innovations in these areas are reported to be in part responsible for his telescopic investigations of the moons of Jupiter (~1610) notorious for refuting the then powerful paradigm of a geocentric solar system. Skill in lens crafting was also instrumental to Anton van Leeuwenhoek and his pioneering microscopy studies from ~1660-1723 [7]. Van Leeuwenhoek was the

first to describe bacteria in saliva, the teeming life in a drop of water, and the circulation of red blood corpuscles in capillaries, which he estimated to be, "25,000 times smaller than a fine grain of sand" [8, 9]. These early microscopy studies laid the foundations of cellular biology.

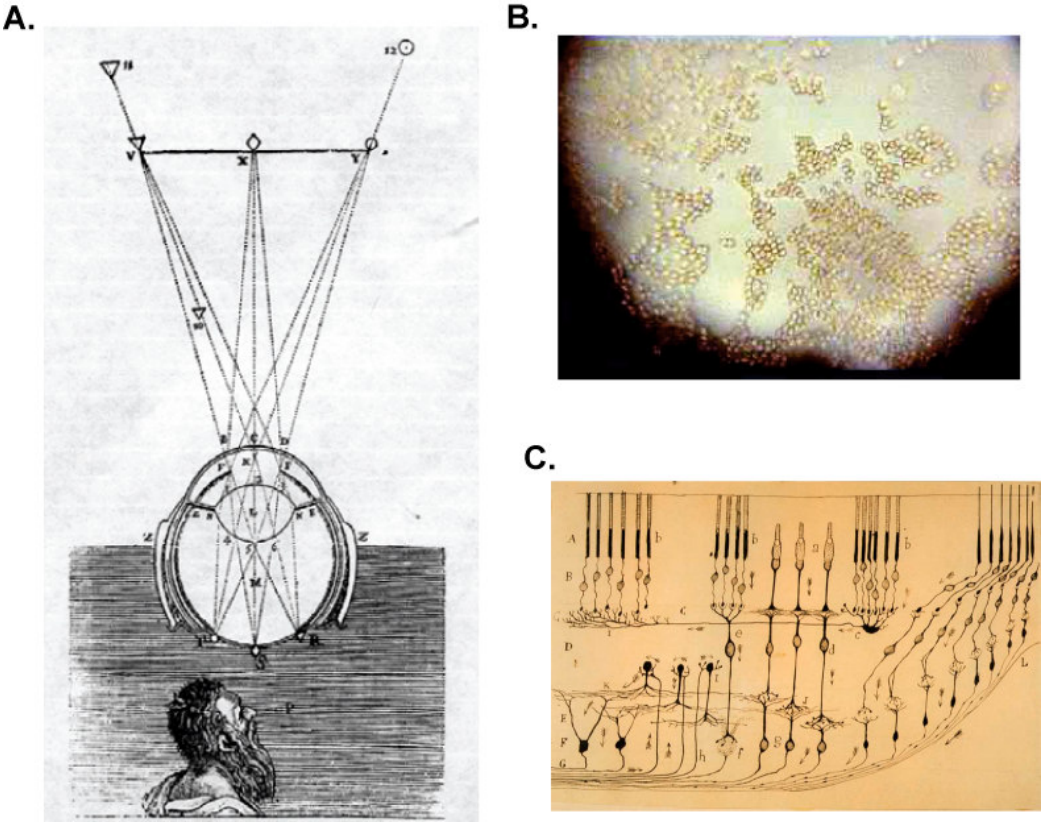

Figure 1.1. A. Woodcarving circa 1700, depicting Charles Sheiner's ray tracing technique (~1619) to illustrate focussing by the human eye [10]. **B**. Replication of Leeuwenhoek 's early microscopy studies. A single lens image of red blood cells [9, 11]. **C.** Reprint of a sketch of the photoreceptors lining the retina. Circa 1895 by S. Ramon Y Cajol [12].

Microscopy. It wasn't until many decades later that lens design and production allowed compound microscopes to out perform Leeuwenhoek's single lens systems [9]. But by the end of the 19'th century microscopes were performing at near the optical diffraction limits discovered by Ernst Abbe and the manufacture of achromatic lenses had begun [13]. By 1900 microcopists were using staining techniques to better visualize samples, had observed cellular division, and had originated the medical study of the microbial origin of disease [14]. Among the many early implications of this work was the abandonment of the previously widespread practice of letting blood to cure ailments [15] and the general acceptance of the neuron doctrine of brain architecture.

Twentieth century advancements in microscopy include the development of phase contrast by F. Zernike (~1933) and fluorescent microscopy. Fluorescent stains were used at least as early as 1911, but were not extended to live cell imaging until the 1980's [16, 17]. Recent advances in photodetectors, accessible lasers, and probe chemistry, have contributed to the rapid growth of popularity of this technique in biological and medical imaging [17-19].

Spectroscopy. Although known to the ancients, Isaac Newton apparently coined the term spectrum around 1700 to refer to the rainbow of colors that white light could be divided into using a prism. In 1801, the spectrum was shown to extend beyond the visible colors. William Herschel discovered infrared light through the use of a prism and thermometers (see Fig. 1.2A) and in the same year Johann Ritter discovered ultraviolet light through the use of a prism and a plate of silver chloride[14].

The quantitative study of spectroscopy is usually associated with Joseph von Fraunhofer who introduced a precision spectrosocope and the use of diffraction gratings in his extensive study of over 570 dark lines in solar spectrum between 1814-1823 (Fig. 1.2B.) He hypothesized that the dark lines were caused by the absence of certain wavelengths of light but died before he understood their physical origins [14]. Later these absorbtion lines would serve to identify elements present in the earths atmosphere and the outer layers of the sun. Fraunhofer's studies inspired many others. Of particular note is the work of Gustav Kirchhoff and Robert Bunsen who constructed an accurate flame spectrophotometer which they used to prove that every substance introduced into the flame emitted light that had its own unique pattern of spectral lines. In 1861, within months after publishing their results, they discovered the elements cesium and rubidium through spectroscopy, thus solidifying the spectroscopic method of chemical analysis [20]. Spectral absorption was also investigated. By 1881 W. Abney and E. R. Festing had photographed absorption spectra for 52 compounds and correlated absorption bands with the presence of certain organic groups in the molecule. This early work demonstrated that the most unique physical property of a compound may be its infrared spectra, and that certain chemical groups, even when they when incorporated into different molecules, produce absorption bands at approximately the same wavelengths.

Through the 1940's, tungsten glow lamps, prisms, gratings, filters, and light detectors largely limited spectroscopists to a narrow band from ~500-700 nm. Early commercial spectrometers were difficult to use and concentration

measurements were often made by eye through the comparison of two visual fields next to each other. Nonetheless, by 1940 there were over 800 publications on the determination of concentration of clinically relevant components in the blood and other bodily fluids [21].

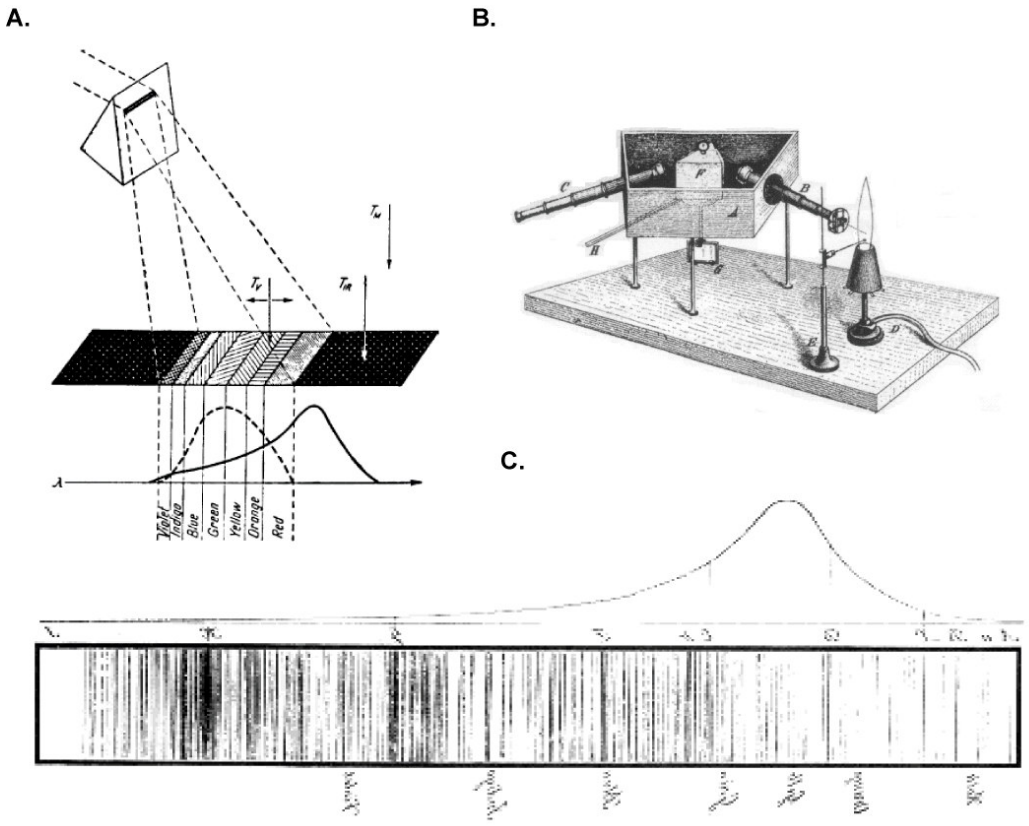

Figure 1.2. A. Diagram depicting William Herschel's (1738-1822) discovery of infrared light. Herschel placed thermometers along the spectral bands dispersed by a prism. He found greater heating in an invisible region beyond red light. The dotted curve represents the approximate spectral response of the human eye, the dark curve represents Herschel's heating results [22]. **B.** Kirchhoff and Bunsen's Flame spectrometer (circa 1860) [23]. **C.** Discrete absorption lines in the solar spectrum as recorded by Fraunhoeffer (circa 1820.) Red light is to the right and blue is to the left. The solid line shows the approximate sensitivity of the human eye (as reported by Schmidt 2005 [21].)

Quantum Spectroscopy. Beyond providing an extremely powerful tool for the discovery and identification of molecules, spectroscopy also provided the data that sparked a fundamental shift in the scientific understanding of light and matter, the quantum revolution. Spectral observations were instrumental to the development of the quantum theory, the idea that energy comes in very small discrete units called quanta, in at least two important ways. First, in 1900 Max Plank reluctantly suggested a restricted version of the quantum notion in order to account for the discrepancy between classical theoretical predictions and experimental observations of the spectral profile of light emitted from hot objects. Secondly, the discrete absorption and emission lines observed in elemental gases was interpreted by Bohr in 1913 as evidence that the electrons circulating around atoms do so in distinct well defined orbits, and that there is a discrete exchange of energy necessary for an electron to move between orbits [24]. Because light of a particular frequency is associated with a photon of a particular energy, Bohr's postulates were tantamount to a mathematical statement that atoms will only absorb light energy (i.e. photons) at certain wavelengths and that those wavelengths depend on the atoms unique electronic structure. This elementary quantum theory was enormously successful in accounting for the absorption and emission spectra of simple atoms, such as hydrogen, where it was feasible to calculate the allowed electron orbits.

Quantum Nonlinearity. In 1931, Maria Goeppert-Mayer used a much more sophisticated quantum theory to predict that an atom might simultaneously absorb two photons. She predicted that this absorption process would not require that the atom have an intermediate electronic state, such that a single photon of

the same wavelength could be absorbed. Instead she described an interaction between two photons and an atom that proceeds via a virtual electronic state that can be described as a superposition of all the electronic states intermediate to the ground and the two photon excited state. It is in honor of Maria Goppet-Mayer that the units of the two-photon cross section are now referred to as Goppert-Mayers, 1GM = 10^{-50} cm^4s /(photon molecule). She also noted that the probability that two photons would be simultaneously absorbed in a molecule would depend on the square of the excitation light intensity rather than the linear dependence on light intensity seen in the case of one photon absorption. Also, as each photon carries a unit of angular momentum, the electronic states accessible with two-photon absorption are of different parity than those accessible with one photon absorption. This implies that, in spite of the enormous amount of work in spectroscopy that had occurred by that time, there would be additional spectral absorption and emission lines in the elemental gases that had not been previously observed. However this lack of experimental verification was not considered a problem as the two-photon event would be extremely improbable and would require a very high density of photons [25]. Its observation would in fact await the development of the laser.

Nonlinear Optics. In 1960, the first flash-lamp pumped ruby laser was developed by Ted Maiman. It was capable of producing ~1 ms in duration, 3 joule laser pulses at ~694 nm [26]. In August of 1961, second harmonic generation was reported by Franken et al [27]. Several months later two-photon excited fluorescence (TPEF) was observed by Kaiser and Garret [28], who reported the TPEF efficiency to be ~$1/10^7$. In December of 1961, third harmonic generation

(THG) was detected by Terhune et al [29], who report the production of ~ 1 THG photon for every 10^6 incident on a calcite crystal. 1961 also saw the first medical application of lasers, when Koester and Campbell successfully used ruby laser pulse to photo-coagulate a retinal tumor in a human patient [30]. New nonlinear effects were being discovered at a rapid rate up through 1965 and by 1970 much of theoretical foundation for nonlinear quantum optics had been laid [31].

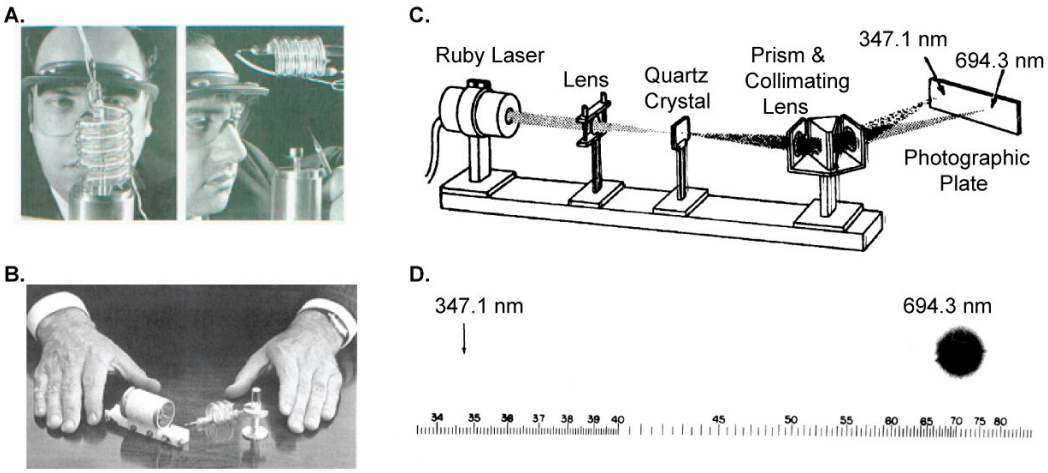

Figure 1.3. A. Howard Hughes Research Laboratories publicity photo: Ted Maiman posed with a mock up of his ruby laser, the first laser ever to be developed (1960) [32]. **B.** An actual image of Maiman's early laser- note the size difference. The publicist was not the only one less than enthusiastic about the new laser. Maiman's publication was turned down by Physical Review Letters (PRL) before its publication in Nature [32]. Some skepticism of his work also arose from those outside of the laboratory on the basis that no one reported seeing a glowing beam of light associated with the laser [33]. **C.** Schematic of the apparatus used by Franken et al to detect second harmonic light [31]. **D.** The published image of Franken et al.s photographic plate 1961 [27]. An image of the second harmonic generation should appear as indicated. The image was so faint, that the editors at PRL removed it as an undesirable smudge. No erratum ever appeared [34].

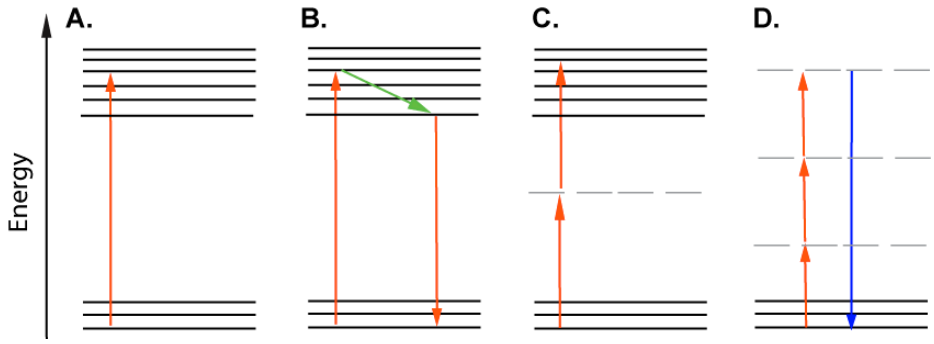

Figure 1.4. Jabolinski diagrams: Cartoon illustrating some linear and nonlinear optical transitions with respect to the energy states of a molecule. Horizontal lines represent energy levels of the molecule, with those near the top representing higher energy states. Each vertical arrow represents an energetic transition due to the absorption or emission of a photon. **A.** One photon absorption from a ground state to an excited state. **B.** One-photon absorption, followed by intermolecular relaxation and de-excitation to the ground state via fluorescence. **C.** Non-resonant two photon absorption. Two photon absorption may also be followed with fluorescent emission. The dotted energy level represents a virtual state (see text.) **D.** Non-resonant third harmonic generation. Three photons interact with a molecule and transform into a single third harmonic photon without involving any real energy states. Resonant third harmonic generation involving real states is discussed in Chapter II.

Nonlinear Spectroscopy. From 1970 onward advancements in nonlinear optics has continued to be largely tied to the development of lasers with shorter pulse durations, greater wavelength tunability, accessibility, longevity, and commercial availability. Shorter pulses allow peak powers to remain high while lowering the average power on a sample, which is an important consideration in photo-damage [35]. In addition, different physical processes can be recruited by different pulse durations. For instance electronic polarization occurs on the the femto-second time-scale, while molecular orientation is believed to take a pico-

second or longer, and thermal effects typically manifest at a time-scale closer to a millisecond [36].

The narrow tuning range and high maintenance required for many early lasers is one of the reasons that most of the early measurements of nonlinear cross-sections are at one or two wavelengths [37]. Nonetheless as early as 1972, Bradley et al [38] and Ducing et al [39] used ps in duration laser pulses to make TPEF based measurements of the two-photon cross-section in xanthene dyes at 1060 and 690 nm. The first quantitative two photon investigation of a bio-molecule may be Birge et al's 1978 report on TPEF in the visual chromophore all-trans-Retinol. In this pioneering experiment they tuned a 4mJ pulsed dye laser over the range of 620 -740nm [40]. By 1997, a relatively extensive review of quantitative nonlinear spectroscopy [3] was able to point to ~17 TPEF based studies of bio-molecules including phenylananine, tyrosine, tryptophan [41], nicotinamide adenine dinucleotide, retinal, chlorophyll, and several nucleotides.

In 1990 an transmission based 'Z-scan' technique was developed [42] that could allow absolute TPA cross-sections to be measured in non-fluorescent materials with sufficiently high cross-sections. Recent advances in this technique have allowed a direct transmission measurement of the TPA cross-section in tryptophan at 532nm and the nonlinear index of refraction to be evaluated in amino acid solutions at 775nm [43, 44]. Also in the 1990's, the introduction of a turn-key, tunable (700-1000 nm), ~100 fs pulse duration, commercial titanium sapphire laser system provided an excellent platform for multi-photon scanning microscopy and near infrared ultrafast nonlinear spectroscopy [45, 46].

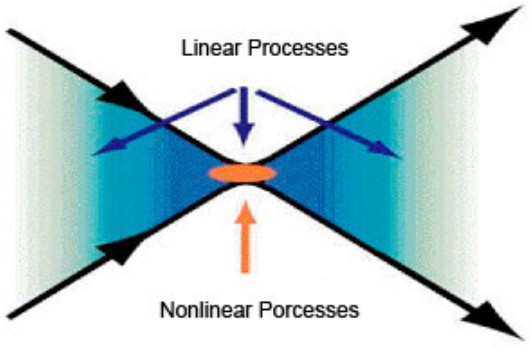

Figure 1.5. Illustration of focussed laser light. Light enters from the left and exits at the right. Linear processes can be driven throughout much of the focussing cone, however nonlinear processes are localized to a small focal volume where there exists a high intensity photon flux. This process allows nonlinear imaging to section samples in three dimensions.

Nonlinear Microscopy. With roots in fluorescent confocal microscopy and a SHG microscope built in 1974, Denk et al demonstrated a TPEF laser microsocope in 1990 [46, 47]. They used sub-picosecond, 700 nm, focused laser pulses to excite TPEF in fluorescent (or flourescently labled) samples. Scan mirrors were used to raster the laser across the sample and photo-multiplier tube detection system was used to collect the TPEF. The short pulse duration allowed higher peak to average power ratios and thus minimized photo-damage to biological specimens and photo-bleaching of fluorophores. A primary feature of this approach is intrinsic optical sectioning due to the fact that TPEF requires a large photon flux. The incident laser is only sufficiently intense to drive TPEF at the focus (see Fig.1.5.) Thus the system can resolve objects on the scale of diffraction limited focal volume. In addition because the beam can be focused

inside of samples, this technique allows for 3-dimensional imaging. The concept of using nonlinlinear contrast for 3-dimensional optical imaging has also been extended to include three-photon excited fluorescence [48], as well as second[49] and third harmonic generation microscopy [50]. An additional facet of nonlinear excitation is the possibility of using it to locally perturb the sample. For instance Denk et al's 1990 patent mentions that, "focused pulses also provide three-dimensional spatially resolved photo-chemistry which is particularly useful in photolytic release of caged effector molecules" [46]. Thus these techniques can be used to both observe and to perturb samples. Nonlinear microscopes have been used to great effect since their introduction. In Section 3. we review some of the applications of nonlinear microscopy most relevant to this dissertation.

Essential Physics

In this section we introduce the nonlinear polarizability and heuristically illustrate how harmonic generation can occur. We simplify our discussion in several ways that will be made clear as we proceed.

In conventional or linear optics, the induced macroscopic polarization field, ie. the dipole moment per unit volume, P, set up in a material in response to an applied electric field, E, is proportional to that field, in a manner that can often be described by:

(1) $$P_i(\omega) = \Sigma_j \, X^{(1)}_{ij}(\omega) \, E^j(\omega)$$

where $\mathbf{X}^{(1)}(\omega)$ is the linear susceptibility tensor of the material, the indices i and j signify the cartesian coordinates, the sum is over j =x, y, z. For simplicity, we have taken the material's response to be instantaneous and suppressed any spatial dependence. $\mathbf{X}^{(1)}(\omega)$ has 9 components. In an isotropic medium, such as the solution phase materials studied in later chapters, Eq. 1 can be written as:

(2) $$P(\omega) = X^{(1)}(\omega)\, E(\omega)$$

In general the real part of $X^{(1)}(\omega)$ is related to the index of refraction, i.e $n(\omega) = \sqrt{1 + 4\pi X_R^{(1)}(\omega)}$ and the imaginary component is proportional to the linear absorption coefficient, i.e $\alpha(\omega) = 4\pi\omega \mathrm{Im}X^{(1)}(\omega)/(n(\omega)c)$[51]. The quantum mechanical interpretation associated with the above equations is that every photon molecule interaction involves a single photon.

In most environments, this model works famously, thus for instance the phenomenal success of the superposition principle in electromagnetism. However as was first implied by Goppert-Mayer the expressions given for the polarization field above can be considered as the first term in a power series expansion. Thus a more complete accounting of the polarization field of a homogeneous medium in the presence of a monochromatic uniformly polarized electric field is given by [36]:

(3) $$P(\omega''') = X^{(1)}(\omega)\, E(\omega) + X^{(2)}(\omega)\, E(\omega')E(\omega) + X^{(3)}(\omega'')\, E(\omega)E(\omega)E(\omega) + \ldots$$
$$= P^{(1)}(\omega) + P^{(2)}(\omega') + P^{(3)}(\omega'') + \ldots$$

where in general $\chi^{(2)}(\omega)$ is a second rank tensor and $\chi^{(3)}(\omega)$ is a third rank tensor, and $P^{(1)}(\omega)$ and $P^{(1)}(\omega)$ are known as the second and third-order nonlinear polarization, respectively. The frequency arguments now carry primes to denote that they may not be equal to the fundamental.

As these nonlinearities are imagined to be electronic in origin the n'th susceptiblity tensor can be expected to be approximately the same order of magnitude as the n-1st tensor when the applied electric field is of the same order as the electronic field due to the atom. Thus the magnitude of $\chi^{(2)} \sim \chi^{(1)}/E_{atom}$. In practice, if an external field of the same magnitude as that of the atomic field was applied to a molecule not only would the perturbation expansion in Eq. 3 fail but the molecule would likely photo-ionize. Even at the peak of the pulse, the laser intensities we use here have electric fields orders of magnitude smaller than those internal to the atom.

Other than for its mention here we will not address the second-order nonlinearity for the remainder of this work. $\chi^{(2)}(\omega)$ vanishes in centro-symmetric molecules and in homogeneous media such as the solution phase samples studied here. In general $\chi^{(2)}(\omega)$ is responsible for sum and difference frequency generation and optical rectification. Second harmonic generation is the special case of sum frequency generation under monochromatic excitation.

$\chi^{(3)}(\omega)$ is associated with third harmonic generation, two photon absorption, and the nonlinear index of refraction. The experimental studies

discussed in later chapters are forms of $X^{(3)}(\omega)$ spectroscopy. If we substitute a monochromatic plane wave $E(\omega)= (Ae^{i\omega t} + A^*e^{-i\omega t})$ into the expression for the third order polarizability we get:

(4) $$P^{(3)}(\omega') = X^{(3)}(\omega') (Ae^{i\omega t} + A^*e^{-i\omega t})^3$$
$$= X^{(3)}(\omega') (A^3e^{i3\omega t} + A^{*3}e^{-i3\omega t}) + AA^*(Ae^{i\omega t} + A^*e^{-i\omega t})$$

Thus the first term of $P^{(3)}(\omega')$ in Eq. 4 has a frequency component at 3ω, thrice the incident frequency of ω. This term is third harmonic generation, the topic of chapter II. The frequency component at ω is associated with the nonlinear index of refraction, $n_2(\omega)$, where $n_2(\omega) = 3\pi \mathrm{Re}X^{(3)}(\omega)/n$ [36]. Although we do not study n_2 it arises as a possible confound in the nonlinear transmission measurements reported in Chapter III.

The imaginary component of $X^{(3)}(\omega)$ is proportional to the two-photon absorption coefficient $\beta(\omega)$ [51]:

(5) $$\beta(\omega) = 48\pi^3 \mathrm{Im}X^{(3)}(\omega')/(n^2(\omega)\lambda c).$$

This term is directly related to the two-photon absorption cross-section (Eq. 3.2) which is the primary topic of interest in chapter III.

Nonlinear Microscopy and Beyond:

Probing and Perturbing Cortical Blood Flow

A continuos noninvasive means of monitoring blood oxygenation is of fundamental interest to clinicians and research scientists. Clinically, blood oxygenation can reveal the presence of tumors and other pathologies. The near infrared region of the spectrum (700- 1000 nm) is particularly attractive to optical approaches to this problem, as in this spectral region, water demonstrates relatively low absorption, and hemoglobin remains as one of the primary tissue chromophores [52]. Many optical techniques capable of monitoring blood oxygenation have been developed, but their spatial resolution is typically low [53-58].

Understanding the microscopic details of cortical blood supply is critical both to clinical progress in the treatment of stroke and neurovascular disease, and to building a more comprehensive interpretation of blood flow based brain-imaging techniques, such as blood-oxygen-level-dependent functional magnetic resonance imaging (BOLD fMRI.) Multiphoton microscopy allows micro-vascular morphology to be mapped and blood flow dynamics visualized in live rat [59]. Furthermore micro-vascular disruption and stroke can be induced and monitored through the use of nonlinear optical excitation [60, 61]. These studies provide the immediate context of this dissertation, where we investigate the potential of nonlinear optics to query the oxygenation state of hemoglobin [1, 5].

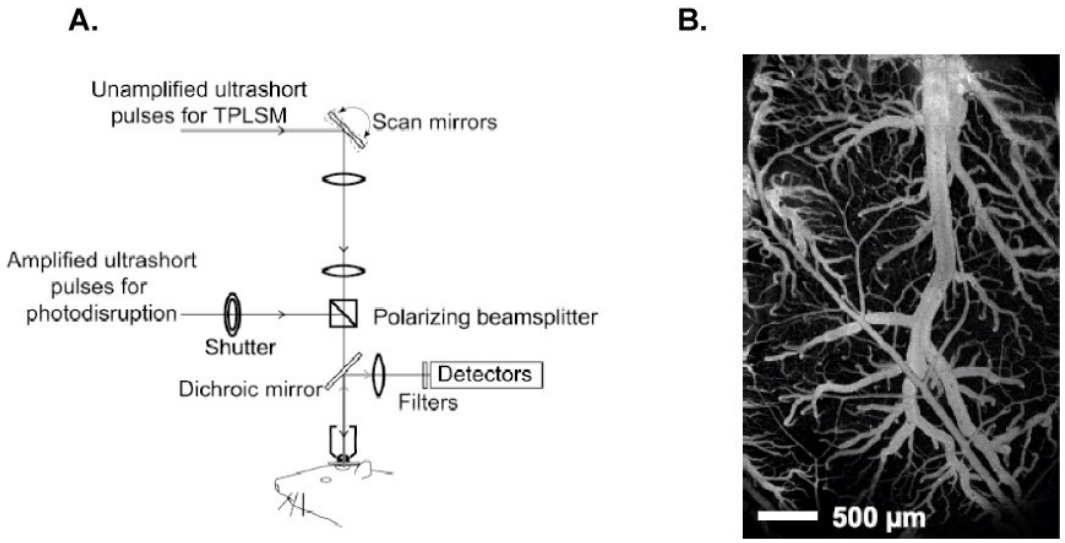

Figure 1.6. A. Schematic of the apparatus used for *in vivo* TPEF imaging and photo-disruption of rat cortical vasculature [62]. **B.** Projection of a TPLSM image stack of fluorescently labeled blood plasma in the cortical vasculature of rat [61].

Dynamic blood flow measurements in rat, *in vivo* can be accomplished by performing a craniotomy and inserting a window in the animal's skull [63] (see Fig 1.6A.) Blood flow, on the level of individual capillaries can then be imaged by labeling the plasma with a fluorescent dye [64]. As red blood cells do not take up the dye they stand out as dark spots against the labeled plasma. This allows flow velocities to be monitored in real time. This approach has been used to quantitatively compare stimulus induced changes in blood flow versus those driven by basal motion [59, 65, 66].

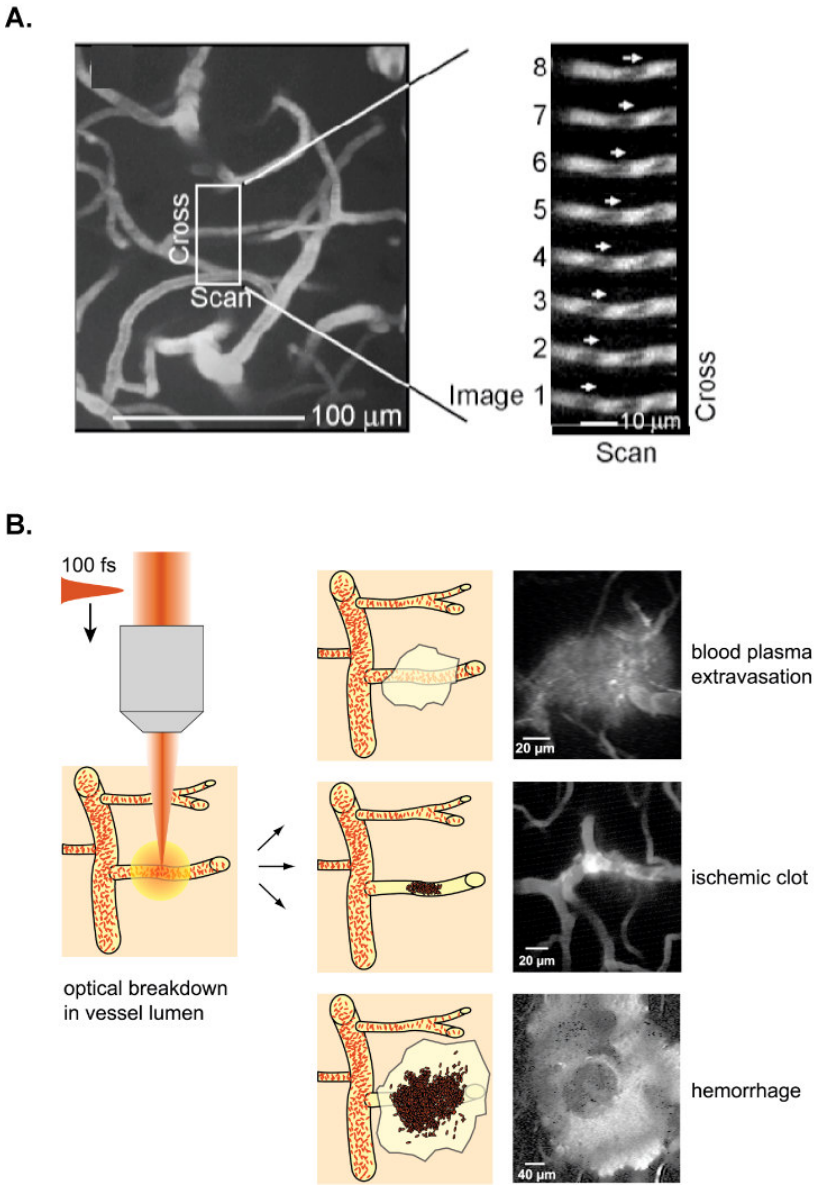

Figure 1.7. A. Dynamic blood flow imaging *in vivo* through TPEF. The blow up of a single capillary on the right hand side shows a time series of the indicated capillary [67]. The dark shadows moving through the capillary are due to red blood cells. **B.** Cartoon illustrating several levels of vascular insult initiated through photo-disruption of the vessel lumen by amplified laser light at 800 nm [60, 68].

Blood flow changes resulting from vascular insult can also be investigated using multi-photon methods [60, 61]. Blockages can be induced without the use of any exogenous agent through the use of focused amplified 800nm laser pulses [60, 68]. As the absorption of ultrafast pulses in the vessel lumen is a highly nonlinear process, localized damage can be produced up to ~500 um below the surface of the brain. Adjusting the amplified laser intensity between .1 –5 uJ allows the formation of vascular insults ranging in severity from blood plasma extravasation, i.e. small hemorrhages, and ischemic clots, to gross hemorrhages. Concurrent TPEF imaging allows the consequences of these defects to be monitored for hours afterwards. For the case of single point ischemic clots in surface vessels, related work has shown reestablishment of flow at the first downstream branch point due to flow reversal in one of the branches [67, 69] (see Fig. 1.7B.) Although reestablished flow is, on average, 50% of its initial flux, it is likely to be sufficient to maintain tissue oxygenation at physiologically viable levels. This work is ongoing but has already confirmed suggestions that a highly interconnected vascular network is robust to multiple blockages [70].

Nonlinear excitation also has the potential advantage of probing and perturbing the optical properties of endogenous molecules. The bulk of this dissertation is an investigation of the nonlinear optical properties of hemoglobin. Hemoglobin's optical properties depend on its oxygenation (ligand binding) state and thus may be a source of functional contrast. As a primary tissue chromophore it may also be a pathway to photo-damage.

Acknowledgements

This previously published material was used in part or in full for Chapter 1.

Beyond observation: Microscopy with ultrashort laser pulses to probe and manipulate cortical vasculature. G. O. Clay, N. Nishimura, C. B. Schaffer, P. S. Tsai and D. Kleinfeld. SPIE International Technical Group Newsletter, Optics in Information Systems (2004)15:4-5.

References

1. Clay, G., et al., *Spectroscopy of third-harmonic generation: evidence for resonances in model compounds and ligated hemoglobin.* Journal of the Optical Society of America B, 2006. **23**(5): p. 932-950.

2. Konig, K., et al., *Cellular response to near-infrared femtosecond laser pulses in two-photon microscopes.* Optics Letters, 1997. **22**: p. 135-138.

3. Callis, P.R., *Two-Photon Induced Fluorescence.* Annual Reviews Physical Chemistry, 1997. **48**: p. 271-297.

4. Tian, P. and W. Warren, *Ultrafast measurement of two-photon absorption by loss modulation.* Optics Letters, 2002. **27**: p. 1634-1636.

5. Clay, G., C.B. Schaffer, and D. Kleinfeld, *Large two-photon absorption cross-section of hemoglobin in the infrared range of 780 - 880 nm.* Optics Letters, 2006: p. (in submissions).

6. Hecht, E., *Optics*. 2002, San Francisco: Addison Wesley.

7. Suplee, C., *Milestones of Science*. 2000, Washington DC: National Geographic Society.

8. Segaller, S., *Red Gold: An Epic History of Medicine and Commerce*. 2002, The Educational Broadcasting Corporation.

9. Ford, B.J., *First Steps in Experimental Microscopy.* The Microscope, 1995. **43**: p. 47-57.

10. Tassignon, M.-J.B. and F. Van de Velde. *New Optics of the Human Eye*. in *New Optics of the Human Eye*. 2004. Brussels, Belgium: European Science Foundation.

11. Ford, B.J., *Brian J Ford Science Website*. 2006. p. http://www.brianjford.com/wavrbcs.htm.

12. Cajal, S.R., *Histology of the Nervous System*, ed. L. Azoulay. Vol. 1. 1995, New York: Oxford University Press.

13. Sterrenburg, F.A.S., *Microscopy Primer*, in *Micscape Magazine*. 2002.

14. Taton, R., *Science in the Nineteenth Century*. 1965, New York: Basic Books Inc.

15. Seigworth, G.R., *Bloodletting Over the Centuries.* New York State Journal of Medicine, 1980: p. 2022-2028.

16. Taton, R., *Science in the Twentieth Century*. 1966, New York: Basic Books Inc.

17. Michalet, X., et al., *The Power and Prospects of Fluorescence Microscopies and Spectroscopies.* Annual Review Biophysical and Biomolecular Structures, 2003. **32**: p. 161-182.

18. Gillenwater, A., R. Jacob, and R. KRichards-Kortum, *Fluorescence Spectroscopy: A technique with potential to improve the early detection of aerodigestive tract neoplasia.* Head and Neck, 1998: p. 556-561.

19. Lackowitz, J.R., *Principles of Fluorescence Spectroscopy*. 1983, Plenum: New York.

20. Schrenk, W.G., *Historical Development of Flame Excitation Sources for Analytical Spectroscopy.* Applied Spectroscopy, 1986. **40**: p. 14-27.

21. Schmidt, W., *Optical Spectroscopy in Chemistry and Life Sciences*. 2005, Weinheim: Wiley-VCH Verlag.

22. Davies, T., *The history of near infrared spectroscopic analysis: Past, present, and future.* Analusis Magazine, 1998. **26**: p. 17-20.

23. Kirchhoff, G. and R. Bunsen, *Chemical Analysis by Observation of Spectra.* Annalen der Physik und der Chemie, 1860. **110**: p. 161-189.

24. Bohr, N., *On the Constitution of Atoms and Molecules.* Philosophical Magazine, 1913. **26**: p. 1-25.

25. Masters, B.R. and P.T.C. So, *Antecedents of Tso-Photon Excitation Laser Scanning Microscopy.* Microscopy Research and Technique, 2003(63): p. 3-11.

26. Maiman, T.H., *Stimulated Optical Emission in Ruby.* Nature, 1960(187): p. 493.

27. Franken, P.A., et al., *Generation of Optical Harmonics.* Physical Review Letters, 1961. **17**: p. 118-121.

28. Kaiser, W. and C.G.B. Barrett, *Two-Photon Excitation in CaF2:Eu2+.* Physical Review Letters, 1961. **7**: p. 229-233.

29. Terhune, R.W., P.D. Maker, and C.M. Savage, *Observation of Saturation Effects in Optical Harmonic Generation.* Applied Physics Letters, 1963. **2**: p. 54-55.

30. Rosenberg, N., A.C. Celijns, and H. Dawkins, *Sources of Medical Technology: Universities and Industry*. 1995, Washington DC: National Academy Press.

31. Shen, Y.R., *Laser Science: Past, Present, and Future.* AAPPS Bulletin, 2005. **15**(2): p. 22-31.

32. Hecht, J., *Laser Pioneers*. 1991: Academic Press. 298.

33. Garwin, L. and T. Lincoln, *A Century of Nature: Twenty-One Discoveries that Changed Science and the World*. 2003, Chicago: University of Chicago Press.

34. Bloembergen, N., *Nonlinear Optics: Past, Present, and Future.* IEEE Journal on selected topics in quantum electronics, 2000. **6**: p. 876-880.

35. Konig, K., et al., *Pulse-length dependence of cellular response to intense near-infrared laser pulses in multiphoton microscopes.* Optics Letters, 1999. **24**: p. 113-115.

36. Boyd, R.B., *Nonlinear Optics, Second Edition*. 2003: Academic Press.

37. Swofford, R.L. and A.C. Albrecth, *Nonlinear Spectroscopy.* Annual Reviews Physical Chemistry, 1978. **29**: p. 421-440.

38. Bradley, D.J., M.H.R. Hutchinson, and H. Koetser, *Interactions of Picosecond Laser Pulses with Organic Molecules. II. Two-Photon Absorption Cross-Sections.* Proceedings of the Royal Society of London. Series A, Mathematical and Physical Sciences, 1972. **329**: p. 105-119.

39. Hermann, J.P. and J. Ducuing, *Dispersion of the Two-Photon Cross Section in Rhodamine Dyes.* Optics Communications, 1972. **6**: p. 101-105.

40. Birge, R.R., et al., *Two-Photon Spectroscopy of the Visual Chromophores: Evidence for a Lowest Excited State Ag- Like pi pi* State in all-trans-Retinol (Vitamine A).* Journal of the American Chemical Society, 1978. **100**: p. 1533-1539.

41. Jiang, S.-P., et al., *Two Photon Excitation of Proteins.* Chemical Physics Letters, 1984. **104**: p. 109-111.

42. Sheik-Bahae, M., A. Said, and E. Van Stryland, *High-sensitivity, single-beam n2 measurements.* Optics Letters, 1989. **14**: p. 955.

43. Sengupta, P., et al., *Determination of the absolute two-photon absorption cross secton of tryptophan.* Multiphoton Microscopy in the Biomedical Sciences: Proceedings of SPIE, 2001.

44. Rodrigues, J.J., et al., *Femtosecond Z-scan measurements of nonlinear refraction in amino acid solutions.* Optics Materials, 2002: p. 153-157.

45. Spence, D.E., P.N. Kean, and W. Sibbett, *60-fsec pulse generation from a self-mode-locked Ti:sapphire laser.* Optics Letters, 1991. **16**: p. 42-45.

46. Masters, B.R. and P.T.C. So, *Antecedents of Two-Photon Excitation Laser Scanning Microscopy.* Microscopy Research and Technique, 2003(63): p. 3-11.

47. Denk, W., J.H. Strickler, and W.W. Webb, *Two-photon laser scanning fluorescence microscopy.* Science, 1990. **248**: p. 73-76.

48. Hell, S.W., et al., *Three-photon excitation in fluorescence microscopy.* Journal of Biomedical Optics, 1996. **1**: p. 71-74.

49. Campanola, P.J., et al., *Applications in nonlinear optical microscopy.* Cell Vision, 1997. **4**: p. 191-192.

50. Squier, J., et al., *Third harmonic generation microscopy.* Optics Express, 1998. **3**: p. 315-321.

51. Sutherland, R., *The Handbook of Nonlinear Optics*. 2003, New York: Marcel Dekker, Inc.

52. Cheng, X., et al., *Breast cancer detection by mapping hemoglobin concentration and oxygen saturation.* Applied Optics, 2003. **42**: p. 6412-6421.

53. Duduran, T., et al., *Diffuse optical measurement of blood flow, blood oxygenation, and metabolism in a human brain during sensorimotor cortex activation.* Optics Letters, 2004. **29**: p. 1766-1768.

54. Faber, D.J., et al., *Toward assessment of blood oxygen saturation by spectroscopic optical coherence tomography.* Optics Letters, 2005. **30**(1015-1017).

55. Liu, H., et al., *Noninvasive Investigation of Blood Oxygenation Dynamics of Tumors by Near-Infrared Spectroscopy.* Applied Optics, 2000. **39**.

56. Esenaliev, R.O., et al., *Optoacoustic Technique for Noninvasive Monitoring of Blood Oxygenation: A Feasibility Study.* Applied Optics, 2002. **41**: p. 4722-4731.

57. Iftimia, N.V., et al., *Toward noninvasive measurement of blood hematocrit using spectral domain low coherence interferometry and retinal tracking.* Optics Express, 2006. **14**: p. 3377.

58. Beard, P., et al., *Shedding Light on the Human Body*, in *The Royal Society's Science Exhibition 2006*. 2006, The Royal Society.

59. Kleinfeld, D., et al., *Fluctuations and stimulus-induced changes in blood flow observed in individual capillaries in layers 2 through 4 of rat neocortex.* Proceedings of the National Academy of Sciences USA, 1998. **95**: p. 15741-15746.

60. Nishimura, N., et al. *Targeted disruption of deep-lying neocortical microvessels in rat using ultrashort laser pulses*. in *Proceedings of SPIE, Commercial and Biomedical Applications of Ultrafast Lasers IV*. 2004. San Jose: SPIE.

61. Schaffer, C.B., et al., *Two-Photon Imaging of Cortical Surface Microvessels Reveals a Robust Redistrubition in Blood Flow after Vascular Occlusion.* PLOS Biology, 2006(4): p. 1-13.

62. Clay, G., et al., *Beyond observation: Microscopy with ultrashort laser pulses to probe and manipulate cortical vasculature.* SPIE International Technical Group Newsletter: Optics in Information Systems, 2004. **15**: p. 4-5.

63. Villringer, A., et al., *Confocal laser microscopy to study microcirculation on the rat brain surface in vivo.* Brain Research, 1989. **504**: p. 159-160.

64. Kleinfeld, D. and W. Denk, *Two-photon imaging of neocortical microcirculation*, in *Imaging Neurons: A Laboratory Manual*, R. Yuste, F. Lanni, and A. Konnerth, Editors. 2000, Cold Spring Harbor Laboratory Press: Cold Spring Harbor. p. 23.1-23.15.

65. Kleinfeld, D., ed. *Cortical blood flow through individual capillaries in rat vibrissa S1 cortex: Stimulus induced changes are comparable to underlying fluctuations in flow*. Brain Activation and Cerebral Blood Flow Control, ed. M. Tomita. Vol. 892. 2002, Elsevier International Congress Series: Tokyo.

66. Chaigneau, E., et al., *Two-photon imaging of capillary blood flow in olfactory bulb glomeruli.* Proceedings of the National Academy of Sciences USA, 2003. **100**: p. 13081-13086.

67. Schaffer, C.B., et al. *Arteriole blood flow reverses direction at the first branch that lies downstream from a localized photothrombotic clot*. in *Society of Neuroscience*. 2003. New Orleans, LA.

68. Nishimura, N., et al. *Photodisruption with amplified femtosecond laser pulses induces three-dimensionally localized clots in neocortical vasculature in rat*. in *Society for Neuroscience*. 2003. New Orleans, LA.

69. Friedman, B., et al., *Heterogeneous changes in blood flow in response to single vessel blockages and MCA occlusions in rat parietal cortex as revealed by in vivo two-photon laser imaging.* Stroke, 2004. **35**: p. 81.

70. Hudetz, G.A., *Percolation phenomenon: The effect of capillary network rarefaction.* Microvascular Research, 1993. **45**: p. 1-10.

Third Harmonic Spectroscopy:
Multi-photon resonances in model compounds
and ligated hemoglobin

Abstract

We use third harmonic generation light generated from the interface of biomolecular solutions and a glass substrate as a means to probe resonant contributions to their nonlinear absorption spectra that could serve as contrast mechanisms for functional imaging. Our source was near-infrared, 100-fs laser pulses whose center wavelength was varied from 760 to 1000 nm. These infrared pulses undergo coherent conversion to pulses of ultraviolet light, parameterized by the third-order susceptibility $\chi^{(3)} \equiv \chi^{(3)}(3\omega, \omega, \omega, \omega)$, in a manner that depends on the electronic structure of the fluid. Our measurements yield the ratio of the third-order susceptibility of a sample relative to that of glass, *i.e.*, $\chi^{(3)}_{\text{sample}}(3\omega) \big/ \chi^{(3)}_{\text{glass}}(3\omega)$, where past results claim that $\chi^{(3)}_{\text{glass}}(3\omega)$ is approximately constant over our range of frequencies. A comparison of $\chi^{(3)}_{\text{sample}}(3\omega) \big/ \chi^{(3)}_{\text{glass}}$ with linear absorption spectra and two-photon action spectra reveals both even and odd parity absorption features that resonantly enhance third harmonic generation (THG). We find evidence of a two-photon resonance in the $\chi^{(3)}_{\text{sample}}(3\omega) \big/ \chi^{(3)}_{\text{glass}}$ spectrum for aqueous solutions of rhodamine B, Fura-2, and hemoglobin, and a three-photon resonance in the $\chi^{(3)}_{\text{sample}}(3\omega) \big/ \chi^{(3)}_{\text{glass}}$ spectrum for solutions of bovine serum albumin (BSA). Consistent

with past work, we find evidence of a one-photon resonance for the $\chi^{(3)}_{\text{sample}}(3\omega)\,/\,\chi^{(3)}_{\text{glass}}$ spectrum for water, while confirming a lack of resonant enhancement for the $\chi^{(3)}_{\text{sample}}(3\omega)\,/\,\chi^{(3)}_{\text{glass}}$ spectrum for benzene. At physiological concentrations, hemoglobin in different in ligand binding states could be distinguished based on features of their THG spectrum.

Introduction

The nonlinear spectroscopy of fluids has assumed new relevance with the advent and proliferation of nonlinear microscopies[1]. In these techniques, an ultrashort pulse of laser light is tightly focused into a material so that optical excitation is confined to a focus where the photon flux is highest. This provides intrinsic three-dimensional optical sectioning for two-photon laser scanning microscopy[2-4], second harmonic generation[5], three-photon laser scanning microscopy[6-9], and third harmonic generation[10-14] (THG). While contrast in two-photon and three-photon scanning microscopy is typically achieved through the use of fluorescent indicators, contrast in harmonic generation relies on optical interfaces and intrinsic chromophores. *A priori*, THG will depend directly on one-, two-, and three-photon absorption resonances[15] and thus may be expected to report changes in the function properties of biologically active molecules. An understanding of the nonlinear resonant properties of endogenous molecules is of further importance as a means to indicate pathways for phototoxicity and shadowing by multiphoton absorption.

Under tight focusing conditions, the extent of THG increases dramatically when the focus spans an interface between two optically different materials[10, 16]. This allows imaging based on THG to resolve otherwise transparent interfaces and inhomogeneities within the resolution of the confocal parameter and without the use of dyes[11, 13, 17-19]. Mitochondria[20], red blood cells[21, 22], embryonic development[18, 23], neurons[13], plasma flows[24, 25], muscle fibers[26], and skin biopsy samples[27] have been visualized in this manner. Third harmonic imaging contrast has also been linked to the density of optical solids[24], the aggregation state of polymers[28-30], and the concentration of intracellular [Ca^{2+}] in cultured human glial cells[31]. Finally, a near-field THG scanning imaging study of a dried red blood cell by Schaller *et al* [22] qualitatively showed that their image contrast was best when their excitation beam was spectrally tuned near an anticipated three-photon resonance in hemoglobin. This past work motivates the need for a systematic study of possible functional THG signals.

Beyond issues of imaging, nonlinear optical spectroscopy *per se* provides insight into the structure and electronic properties of materials that is complimentary to that provided by linear spectroscopy[32-38]. Over the last two decades, third harmonic generation has emerged as a useful nonlinear spectroscopy tool[39-43] that has been widely used to identify two and three-photon resonances in solids and thin films[29, 35, 37, 38, 44-48] and indicate a sensitive THG dependence on the molecular structures and interactions of solutes and solvents[49-51].

Here we report on THG at the solution/glass interface as a means to explore the contribution of electronic resonances to THG spectra of solution phase bio-

compounds. We first consider several model solutions with known one- and two-photon absorption spectra as a means to calibrate our methodology[52-55]. We then focus on physiological solutions of bovine serum albumin (BSA) as well as different ligation states of hemoglobin, *i.e.*, oxyhemoglobin, carboxyhemoglobin, and deoxyhemoglobin. Serum albumin and hemoglobin are the primary constituents of blood plasma and red blood cells, respectively and have been the subjects of extensive study. Hemoglobin also has distinct changes in its linear spectrum between ligated and nonligated states[56] that are expected to be reflected in THG.

Theory

Third harmonic generation is the coherent conversion of light with frequency ω to light with frequency 3ω, *i.e.*, wavelength $\lambda/3$, in a material that undergoes intense irradiation. It involves the absorption of three identical photons of energy $\hbar\omega$ and the emission a single photon of energy $3\hbar\omega$ within the temporal uncertainty interval of $\omega^{-1} \sim 10^{-16}$ s. The resultant light propagates in the forward dimension. A material's susceptibility to a given nonlinear conversion process is described by the susceptibility tensors, $\chi^{(n)}$, that relate the polarization field, denoted *P*, induced in the material to the electric field, denoted *E*, of the incident photon. Of the eighty-one independent elements included in the third-order nonlinear susceptibility tensor $\chi^{(3)}_{ijkl}(\omega_i, \omega_j, \omega_k, \omega_l)$, we are only interested in the terms associated with a uniformly polarized, single frequency excitation field, *i.e.*, $\omega_j = \omega_k = \omega_l$. This allows the fourth-rank tensor status of the susceptibility tensor to be suppressed and the THG polarization field $P^{(3)}(3\omega)$ to be expressed as

$$P^{(3)}(3\omega) = \chi^{(3)}(3\omega)\, E^3(\omega)\ . \qquad (1)$$

In a solution or other isotropic media, the measured value for $\chi^{(3)}(3\omega)$ is averaged over orientation and equal to $\frac{1}{3}\left[\chi^{(3)}_{xxxx}(3\omega)+\chi^{(3)}_{yyyy}(3\omega)+\chi^{(3)}_{zzzz}(3\omega)\right]$. The susceptibility $\chi^{(3)}(3\omega)$ is the term we seek to measure.

Resonant Enhancement

The underlying molecules that facilitate THG need not have real states available whose excitation energy corresponds at the incident photon energy or any multiple thereof. However, the THG process is resonantly enhanced if real energy levels are present at the fundamental (ω), second harmonic (2ω), or third harmonic (3ω) frequency. Thus the third-order susceptibility tensor may be dominated by either resonant or non-resonant mechanisms, which makes it convenient to write

(2) $$\chi^{(3)}_{\text{Total}}(3\omega) \equiv \chi^{(3)}_{\text{non-resonant}}(3\omega) + \chi^{(3)}_{\text{resonant}}(3\omega).$$

Under the assumption that all molecules are in the electronic ground state prior to excitation, the resonance term generated in a perturbation expansion is[57]

(3) $$\chi^{(3)}_{\text{resonant}}(3\omega) = \sum_{lkj} \frac{N\mu_{0l}\mu_{lk}\mu_{kj}\mu_{j0}}{\hbar^3\left(\omega_{l0}-3\omega-i\gamma_{l0}\right)\left(\omega_{k0}-2\omega-i\gamma_{k0}\right)\left(\omega_{j0}-\omega-i\gamma_{j0}\right)}$$

where *N* is the number of molecules and the indices refer to different electronic states. Thus μ_{j0} is the electric dipole transition moment between the j-th state and the ground state, γ_{j0}, is the phenomenological damping coefficient that is inversely proportional to the decay rate from the j-th state to the ground state, and $\hbar\omega_{j0}$ is the energy difference between the j-th state and the ground state. The intermediate states are those closest to multiples of the incident photon energy, $\hbar\omega$, and the energies of the various states satisfy the relation $\hbar\omega_{l0} \geq \hbar\omega_{k0} \geq \hbar\omega_{j0}$.

Resonance occurs as $\omega_{l0} \rightarrow \omega$, $\omega_{k0} \rightarrow 2\omega$, or $\omega_{j0} \rightarrow 3\omega$ (Eq. 2), corresponding to one-, two-, and three-photon resonance, respectively, and can significantly increase the magnitude of the susceptibility[17, 57]. Implicit in this formalism is the notion that all photons in the excitation field have the same polarization, or parity, as well as energy.

One- and three-photon resonance. The selection rules, based on conservation of parity, for enhancement by a single photon resonance also apply to enhancement by a three-photon resonance. Thus the presence of peaks in the linear absorption spectrum of the solution, at frequencies ω and 3ω, is a good indication of whether such resonances are likely to be involved in THG (Eq. 3). It is important to note that such resonant enhancement may be self-limiting in thick samples. When one- and three-photon resonances are strong, one- and three-photon absorption by the material will deplete the incoming fundamental and outgoing third harmonic wave, respectively.

Two-photon resonance. Two-photon absorption is an even-parity process while, as above, linear absorption is as odd-parity process. Thus, although, parity selection rules relax in non-centrosymmetric molecules[58] two-photon resonant absorption does not always correspond with peaks in the linear absorption spectra at frequency 2ω. As two-photon absorption does not involve energy levels that have allowed single photon transitions with the ground state, two-photon resonance can lead to enhancements of the susceptibility without a significant loss of optical power.

Further, two-photon resonance is not likely to affect the index of refraction and thus the phase-matching of a given nonlinear process[17].

Non-resonant contributions. In the case that the non-resonant component of $X^{(3)}(3\omega)$ is dominant, several semi-empirical scaling laws have been proposed to account for the spectral dependence of $\chi^{(3)}(3\omega)$[57, 59-61]. Miller's rule has been found to account for much of the spectral dependence of ionic crystals, for which

$$\chi^{(3)}_{\text{non-resonant}}(3\omega) \propto \chi^{(1)}(3\omega)\left[\chi^{(1)}(\omega)\right]^3 \propto \left[n^2(3\omega)-1\right]\left[n^2(\omega)-1\right]^3 . \quad (4)$$

Wang's rule[60] has been found to account for much of the spectral dependence of gasses, for which

$$\chi^{(3)}_{\text{non-resonant}}(3\omega) \propto \left[\chi^{(1)}(\omega)\right]^2 \propto \left[n^2(\omega)-1\right]^2 . \quad (5)$$

Lastly, Boling's rule[62] includes local field effects and should be more generally valid in the fluid phase, *i.e.*,

$$\chi^{(3)}_{\text{non-resonant}}(3\omega) \propto \left[n^2(\omega)+2\right]^2\left[n^2(\omega)-2\right]^2 . \quad (6)$$

Microspectroscopy

The third harmonic intensity that is generated from an axially symmetric material with susceptibility $\chi^{(3)}(3\omega)$ when irradiated by a tightly focused Gaussian beam, denoted $P(3\omega)$, is[10]

$$P(3\omega) = C(\omega)\left| b(\omega)\int_{-\infty}^{\infty} d\phi e^{ib\Delta\kappa\phi}\frac{\chi^{(3)}(3\omega,\phi)}{(1+i2\phi)^2}\right|^2 P^3(\omega) \quad (7)$$

where C(ω) is a formulation of pre-factors that depends on the geometry and efficiency of the collection system but are independent of the sample, P(ω) is the incident power, b(ω) is the confocal parameter, and the integration is over the normalized distance $\phi = z/b$ with the focus at $\phi = 0$. In diffraction-limited geometries the confocal parameter is given by

(8) $$b(\omega) = 2\pi n(\omega)\frac{w_o^2}{\lambda} = \frac{2n(\omega)\lambda}{\pi}\frac{\left[n^2(\omega)\text{-}NA^2\right]}{NA^2}$$

where n(ω) is the index of refraction and w_o is the radius of the beam waist at the focal plane, expressed in terms of the numerical aperture (NA) of the objective. Lastly, the wave-vector mismatch between the excitation and emitted third harmonic field, denoted, $\Delta\kappa$, is[57]

(9) $$\Delta\kappa = 6\pi\frac{n(\omega) - n(3\omega)}{\lambda}.$$

Significant generation of THG in the far field occurs when the fundamental field can constructively drive the third harmonic field. Under tight focussing conditions this corresponds to the case where values of the product $b\Delta\kappa$ are close to unity.

Since the elements of the nonlinear susceptibility are generally small in magnitude, *e.g.*, $\chi^{(3)}(3\omega) \sim 10^{-14}$ esu for many solutions and $\chi^{(3)}(3\omega) \sim 10^{-17}$ esu for gases, THG signals from bulk samples tend to be small[15, 57], *i.e.*, $P(3\omega)/P(\omega) \sim 10^{-8}$ for incident irradiance of $\sim 10^{10}$ W/cm^2. More significantly, in an isotropic medium, the Gouy phase-shift encountered as a light wave traverses the focus causes the THG produced on one side of a focus to destructively interfere with THG produced on the other side and thus cancel the third harmonic wave in the far field[63]. However the

cancellation will be imperfect if the optical properties of the sample, *i.e.*, the index of refraction and the nonlinear susceptibility, differ across the focal volume[10, 15]. Tsang[16] and Barad[10] have shown that the far field third harmonic intensity can be increased by many orders of magnitude when the focus spans an interface between two optically different materials. This renders THG microscopy particularly sensitive to optical interfaces and inhomogeneities on the spatial scale of the focal volume[11, 13, 17-19].

It follows from equation 7 that the THG intensity from a Gaussian beam focused on a flat interface between two infinite homogeneous slabs of material is

$$P(3\omega)_{Slab_1/Slab_2} = C(\omega)\left|\chi^{(3)}_{Slab_1}\, b_{Slab_1} J(b_{Slab_1}\Delta\kappa_{Slab_1}) - \chi^{(3)}_{Slab_2}\, b_{Slab_2} J(b_{Slab_2}\Delta\kappa_{Slab_2})\right|^2 P^3(\omega) \quad (10)$$

where we have neglected reflection and absorption and make use of the dimensionless phase matching integral, J(bΔκ), defined as

$$J(b\Delta\kappa) \equiv \int_0^\infty d\phi\ \frac{e^{ib\Delta\kappa\phi}}{\left(1+i2\phi\right)^2}. \quad (11)$$

An absolute measurement of $\chi^{(3)}(3\omega)$ is complicated by the need to determine the factors in $C(\omega)$[64, 65]. Yet a relative value of $\chi^{(3)}(3\omega)$ is often of sufficient utility. In particular, the value of $\chi^{(3)}(3\omega)$ for a solution is measured relative to the glass substrate, typically fused silica, that forms the sample container[15, 52, 54, 66]. This paradigm is implemented by collecting third harmonic light from both the interface between the sample solution and the glass, with intensity $P(3\omega)_{solution/glass}$, and from the interface between the glass and air, with intensity $P(3\omega)_{glass/air}$. It follows from equation 10 that the ratio of these measurements is

(12)

$$\frac{P(3\omega)_{solution/glass}}{P(3\omega)_{glass/air}} = \left[\frac{\chi^{(3)}_{glass}(3\omega) b_{glass}(\omega)\, J(b_{glass}\Delta\kappa_{glass}) - \chi^{(3)}_{solution}(3\omega) b_{solution}(\omega)\, J(b_{solution}\Delta\kappa_{solution})}{\chi^{(3)}_{glass}(3\omega) b_{glass}(\omega)\, J(b_{glass}\Delta\kappa_{glass}) - \chi^{(3)}_{air}(3\omega) b_{air}(\omega)\, J(b_{air}\Delta\kappa_{air})} \right]^2 .$$

Noting that $\chi^{(3)}_{air}(3\omega)$ ~ 0, this becomes

(13) $$\frac{P(3\omega)_{solution/glass}}{P(3\omega)_{glass/air}} \cong \left[1 - \frac{\chi^{(3)}_{solution}(3\omega)\, b_{solution}(\omega)\, J(b_{solution}\Delta\kappa_{solution})}{\chi^{(3)}_{glass}(3\omega)\, b_{glass}(\omega)\, J(b_{glass}\Delta\kappa_{glass})} \right]^2 .$$

Solving for the susceptibilities leads to

(14) $$\frac{\chi^{(3)}_{solution}(3\omega)}{\chi^{(3)}_{glass}(3\omega)} = \frac{J(b_{glass}\Delta\kappa_{glass}) b_{glass}(\omega)}{J(b_{solution}\Delta\kappa_{solution}) b_{solution}(\omega)} \left(1 \pm \sqrt{\frac{P(3\omega)_{solution/glass}}{P(3\omega)_{glass/air}}} \right) .$$

The resolution of the sign ambiguity requires additional information that is gathered through consideration of resonances or, as will be discussed in the Results section, are obtained by comparative measurements. The general validity of this approach was examined by Barille *et al.*[52], who demonstrated remarkable consistency between their femtosecond measurements at an excitation wavelength of 1.5 μm and previous picosecond measurements[52, 53, 67] at an excitation wavelength of 1.9 μm.

In the case of a solution composed of a solute and a solvent, the different components may contribute to equation 14 with opposite signs. The correct value of the susceptibility ratio of the hydrated solute, defined as $\chi^{(3)}_{solute}(3\omega)/\chi^{(3)}_{glass}(3\omega)$, may be determined from the measured power ratio of the solution, denoted $P(3\omega)_{solution/glass}/P(3\omega)_{glass/air}$, given knowledge of both the power ratio and the susceptibility

ratio of the solvent, *i.e.*, $P(3\omega)_{solvent/glass}/P(3\omega)_{glass/air}$ and $\chi^{(3)}_{solvent}(3\omega)/\chi^{(3)}_{glass}(3\omega)$ respectively. In the case where the solute and solvent occur with solvated volume fractions of υ and 1 - υ, respectively, the measured power ratio of the dissolved solute is

$$\frac{\chi^{(3)}_{solute}(3\omega)}{\chi^{(3)}_{glass}(3\omega)} = \frac{J(b_{glass}\Delta\kappa_{glass})\, b_{glass}(\omega)}{J(b_{solution}\Delta\kappa_{solution})\, b_{solution}(\omega)} \times \left(1+\frac{1}{\upsilon}\left[\pm\sqrt{\frac{P(3\omega)_{solution/glass}}{P(3\omega)_{glass/air}}} - (1-\upsilon)\sqrt{\frac{P(3\omega)_{solvent/glass}}{P(3\omega)_{glass/air}}}\right]\right). \quad (15)$$

Note that the sign of the solvent term has been taken to be negative (Results) and the index and dispersion of the dissolved solute is correctly taken to be the same as the solution, as these are properties of the bulk. The remaining sign ambiguity must be resolved independently.

Methods

Imaging

Our imaging apparatus consists of a laser scanning microscope[68] with the collection of transmitted light for THG imaging and epi-emitted light for simultaneous two-photon excited fluorescence laser scanning microscopy (Fig. 2.1). The excitation source for imaging was a locally constructed 1.054 µm Nd:glass oscillator with an 80-MHz repetition rate and ~100-fs duration pulses. We used a 40x 0.65-NA Zeiss excitation objective (f = 4 mm) and a fused-silica collection lens (f = 6 mm). The detectors were Hamamatsu R6357 photomultipliers (PMTs) with quartz windows that were connected to a resistive load and amplified. Colored glass filters (Corning UG-11) were used to block all but the third harmonic light from reaching the photomultiplier tube. For two-photon excited fluorescence, bandpass (550 ± 25-nm) and colored glass filters (Corning BG-39) were used to block extraneous light.

Microspectroscopy

Apparatus and materials. Spectroscopic measurements were performed without the use of the x-y scan mirrors (Fig. 2.1). The excitation source was a Ti:Sapphire oscillator (Mira 900-F with 10-W Verdi pump, Coherent Inc., Santa Clara, CA) with a 76 MHz repetition rate and ~ 100-fs duration; this source was tuned over a wavelength range of 760 to 1000 nm. We used 40x 0.65 and 0.75 NA Zeiss excitation objectives. The detector was a Hamamatsu R6353 PMT with quartz windows that was connected to a resistive load and amplified. As with imaging, colored glass filters (Corning UG-11) were used to block all but the third harmonic light from reaching the photomultiplier tube. For fundamental wavelengths below 810 nm, the colored glass filters were supplemented with a 265-nm bandpass filter.

Our sample containers were micro-cuvettes (3520; Vitrocom, Mountain Lakes, NJ) with flat 200-µm thick glass walls (Duran 8340) and a 500-µm wide chamber to hold the solution. The Duran 8340 glass has optical properties similar to those of fused silica (Appendix B).

Our samples consisted of deionized water, neat benzene (BX0212-6; Omni Solv, Charlotte, NC), and aqueous solutions of 1 mM rhodamine B chloride (R-6626; Sigma-Aldrich, St. Louis, MO), 0.5 mM solution of Fura-2 pentasodium salt (F-6799; Molecular Probes, Eugene, OR) with 3.3 mM EGTA (E-478; Fisher Scientific, Pittsburgh, PA), 0.5 mM Cascade-Blue trisodium salt (C-687; Molecular Probes), 0.75mM BSA (81-066-1; Miles Scientific, Naperville, IL), and hemoglobin. The

hemoglobin solutions are at physiological concentrations 2 mM (~ 17 g/dL) and represent three different ligand binding states. These include a 98 % (v/v) oxy-hemoglobin (HbO_2) solution (300881R0; Instrumentation Laboratories, Lexington, MA), a mixed 60 % (v/v) carboxylated and 40 % (v/v) oxygenated, carboxyhemoglobin (HbCO) solution (300879R0; Instrumentation Laboratories), and a deoxygenated (Hb) solution (> 80 % based on spectroscopic measurements) that was formed by bubbling N_2 through the oxyhemoglobin solution.

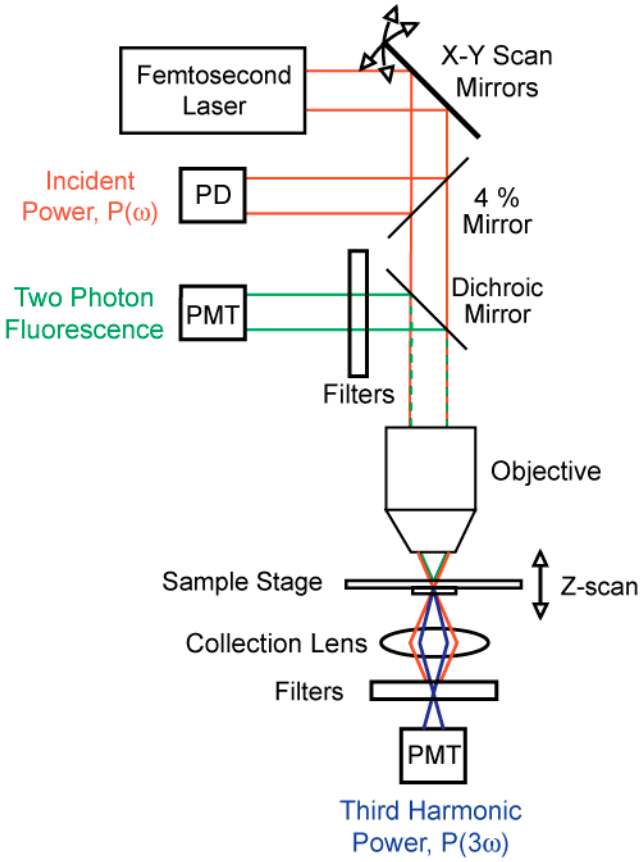

Figure 2.1 Multi-photon imaging and THG spectroscopy apparatus. Images were collected using a 1.054-µm, 100-fs Nd:Glass pulsed laser. Spectroscopic measurements were made using a Ti:Sapphire laser with 100 fs pulses and wavelengths between 760 and 1000 nm.

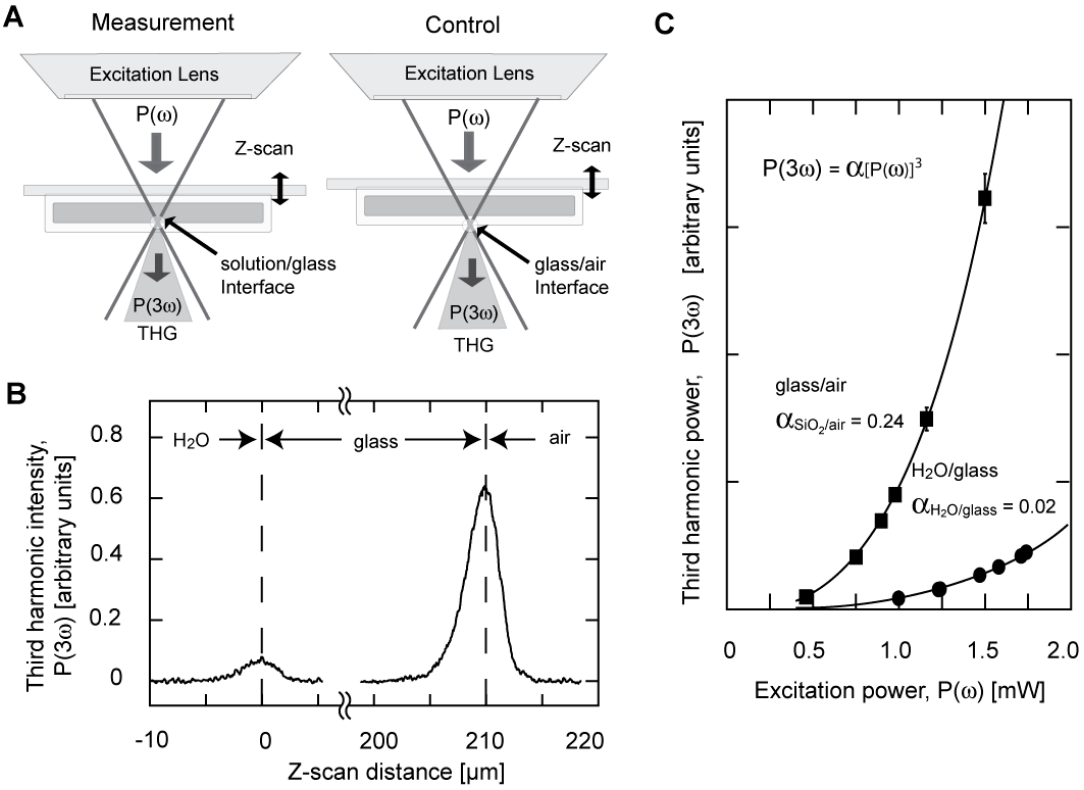

Figure 2.2 The third harmonic spectroscopic measurement procedure applied to de-ionized water. **(A)** Close up of the sample and apparatus. Third harmonic generated light is collected from both the sample/vessel interface and the vessel/air interface and their ratio is used to infer sample properties. **(B)** A THG signal is generated as an interface is scanned through the focus of the beam. The peak of the THG intensity profile is measured for different incident laser powers. The half-width at half-maximum is proportional to the confocal parameter b. **(C)** The THG intensity from both the sample/vessel interface and the vessel/air interface demonstrate the anticipated cubic dependence on laser power.

THG measurement. We seek to derive the third-order susceptibility ratio of our solution relative to glass, $\chi^{(3)}_{\text{solution}}(3\omega)/\chi^{(3)}_{\text{glass}}(3\omega)$, by measuring the ratio of THG power from the solution/glass and glass/air interfaces, *i.e.*, $\mathrm{P}(3\omega)_{\text{solution}}/\mathrm{P}(3\omega)_{\text{glass/air}}$. Measurements were made in a manner similar to the method employed by Barille *et al.*[52]. We scanned through the solution-filled micro-cuvette along the propagation

axis of the incident beam and collected third harmonic light from both the solution/glass and glass/air interface (Fig. 2.2A). The third harmonic power, $P(3\omega)$, traces out two bell shaped profiles as the focus is swept across the two interfaces (Fig. 2.2B). The peak of the profile centered on the lower solution/glass interface corresponds to $P(3\omega)_{solution/glass}$ and the peak of the profile centered on the bottom of the glass side corresponds to $P(3\omega)_{glass/air}$ (Fig. 2.2B). The half-widths at half-maximum of each profile indicates the extent of the confocal parameter (Eq. 8)[10]. The THG signal was averaged over ~ 20 such sweeps. The maximum incident irradiance at the sample was ~ 10^{10} W/cm^2 and the maximum THG efficiency was $P(3\omega)/P(\omega) \sim 5 \times 10^{-7}$.

The measurement of peak third harmonic power was repeated at different incident powers to form graphs of $P_{solution/glass}(3\omega)$ and $P_{glass/air}(3\omega)$ versus the incident power $P(\omega)$ (Fig. 2.2C). The relation between the two measured third harmonic powers was fit as a cubic function of incident power, *i.e.*, $P_{solution/glass}(3\omega) = \alpha_{solution/glass}P(\omega)^3 + P_{dark}$ and $P_{glass/air}(3\omega) = \alpha_{glass/air}P(\omega)^3 + P_{dark}$, where $\alpha_{solution/glass}$, $\alpha_{glass/air}$, and P_{dark} are the fit coefficients. The parameter P_{dark} was fit to the two interfaces simultaneously and corrected for dark noise in the PMT. This procedure, as opposed to a measurement of THG at a single incident power, increases the signal-to-noise of our measurement. It further minimizes potentially confounding effects that have non-cubic scaling with the incident power, such as excited state absorption and the nonlinear refraction[59].

Data Reduction

Prior to additional corrections, the ratio of third harmonic powers is given by $R_{THG}(\omega) = \alpha_{solution/glass}(\omega) / \alpha_{glass/air}(\omega)$. This ratio must be corrected for reflection at interfaces and linear absorption by the glass cuvette.

Linear absorption. Linear absorption and transmission spectra, between 250 and 1000 nm of all model solutions were obtained with a Cary 50 (Varian, Palo Alto, CA) spectrophotometer. Those for the different ligation states of hemoglobin are taken from published measurements[56] (Fig. 2.7A). The near-infrared absorption spectra of water was further culled from the literature[69]. Duran glass measurements are from manufactures literature (Vitrocom) and corrected to account for reflection at normal incidence using the Fresnel equation for the reflectivity, $r(\omega)$, *i.e.*,

(16) $$r(\omega)_{SiO2/solution} = \frac{n_{glass}(\omega) - n_{solution}(\omega)}{n_{solution}(\omega) + n_{glass}(\omega)},$$

and measurements for benzene (Fig. 2.10B) are a composite of data taken over wavelengths that ranged from 0.78 to 1.25 μm[70] and 1.33 to 1.8 μm[71].

Reflection coefficients. To account for the different third harmonic and fundamental powers transmitted through each interface, the reflection coefficients $r(\omega)$ and $r(3\omega)$ were calculated using the Fresnel equation (Eq. 16). The absorptivity $a(\omega)$ of the glass substrate was extracted from linear transmission measurements, $t(\omega)$, with use of the calculated reflection coefficients, $r(\omega)$, and the formula $a(\omega) = \{[1 - r(\omega)]^2 - t(\omega)\}/[1 - r(\omega)]^2$.

Linear dispersion. Calculation of the reflection coefficients, $r(\omega)$, the diffraction limited confocal parameter, b(ω) (Eq. 8), and the wave-vector mismatch, $\Delta\kappa(\omega)$ (Eq. 9), depends on prior knowledge of the dispersion of the linear refractive index, n(ω). Unfortunately, precise refractive index measurements and models do not exist for many materials. This is especially notable at wavelengths shorter than 400 nm, which are important in estimations of $\Delta\kappa(\omega)$ and $r(3\omega)$. The uncertainty in $\Delta\kappa(\omega)$ is graphically illustrated in the case of benzene (Fig. 2.3A), where we plot the results from two dispersion models for benzene (Appendix A), each of which fit all available dispersion data equally well at visible wavelengths, but which significantly diverge for ultraviolet wavelengths.

Confocal parameter. The confocal parameter, b(ω), can be measured directly from the axial extent of the THG profile (Fig. 2.2B)[10] as noted above. In diffraction limited geometries, where the linear dispersion of the sample is known, the confocal parameter can be calculated with equation 8. We use both approaches and note that diffraction limited THG measurements can simultaneously be used as a means to independently measure the linear index through this correspondence. Typical confocal parameters for this experiment were between 5 and 7 μm.

Volume fractions. Calculation of the susceptibility ratio (Eq. 15) for the case of solutions requires an estimate of the hydrated volume fraction of the solute under study. The volume of the hydrated complex is relevant because the electronic interaction between solute and solvent is integral to the solution's nonlinear optical

properties[49, 50, 72-74]. Thus we are essentially interested in measuring the susceptibility of the solvated complex.

As a means to estimate the hydrodynamic volume of rhodamine B in water, and thus the volume fraction of solvated rhodamine B chloride in a 1 mM aqueous solution, we make use of the rotational relaxation time of rhodamine B in solution[73] and approaches based on functional groups[75, 76]. We note that close to 50 % (w/v) of the rhodamine B may be dimerized at a concentration of 1 mM[77, 78]. We use this estimate for rhodamine B and the ratios of volume estimates from functional group based approaches[75, 76] to calculate the hydrated volume fraction of Fura-2 dye in a 0.5 mM aqueous solution. Literature measurements also contribute to our volume fraction estimates of BSA and hemoglobin solutions[79, 80].

Corrected ratio of THG power

The corrected, fitted ratio of THG power is

$$R_{THG}(\omega) \equiv \frac{\alpha_{solution/glass}(\omega)}{\alpha_{glass/air}(\omega)} \frac{\left[1-r^2(\omega)_{glass/solution}\right]^3 \left[1-a(\omega)_{glass}\right]^3}{\left[1-r^2(3\omega)_{glass/solution}\right]\left[1-a(3\omega)_{glass}\right]}. \quad (17)$$

This measure controls for linear absorption, reflections, some of the inter-capillary and inter-sample variation, and mitigates drift in laser parameters and sample orientation. The susceptibility ratio for solvents (Eq. 14) is re-expressed as

$$\frac{\chi^{(3)}_{solution}(\omega)}{\chi^{(3)}_{glass}(\omega)} = \frac{J(b_{glass}\Delta\kappa_{glass})\, b_{glass}(\omega)}{J(b_{solution}\Delta\kappa_{solution})\, b_{solution}(\omega)} \left\{\beta(\omega)\rho(\omega) \pm \sqrt{R_{THG}(\omega)}\right\} \quad (18)$$

where the coefficient

$$\beta(\omega) \equiv \frac{J(b_{glass\text{-}solution}\Delta\kappa_{glass})\, b_{glass\text{-}solution}(\omega)}{J(b_{glass\text{-}air}\Delta\kappa_{glass})\, b_{glass\text{-}air}(\omega)} \quad (19)$$

accounts for the possibility of changes in the confocal parameter of the glass at the two interfaces due to aberrations and the coefficient

(20) $$\rho(\omega) = \sqrt{\frac{\left[1 - r^2(\omega)_{\text{glass/solution}}\right]^3}{\left[1 - r^2(3\omega)_{\text{glass/solution}}\right]}}$$

accounts for reflections at the interfaces of the cuvette. The former term is typically unity but in some experiments was found to be close to 0.8 while the latter term is greater than 0.9. The phase integral J(bΔκ) (Eq. 11) can be numerically evaluated[25, 52] as a function of the product bΔκ (Fig. 2.3B). Lastly, for the case of a solution, the corrected susceptibility expression (Eq. 15) is

(21)

$$\frac{\chi^{(3)}_{\text{solute}}(\omega)}{\chi^{(3)}_{\text{glass}}(\omega)} = \frac{J(b_{\text{glass}}\Delta\kappa_{\text{glass}})b_{\text{glass}}(\omega)}{J(b_{\text{solution}}\Delta\kappa_{\text{solution}})b_{\text{solution}}(\omega)}\left\{\beta(\omega)\rho(\omega) + \frac{1}{v}\left[\pm\sqrt{R_{\text{THG}}_{\text{solution}}(\omega)} - (1-v)\sqrt{R_{\text{THG}}_{\text{solvent}}(\omega)}\right]\right\}$$

with β(ω) and ρ(ω) given above (Eqs. 19 and 20).

Experimental Results

We consider first the image formation characteristics of THG solely as motivation for our spectroscopic studies. We then consider a systematic study of model solutions, *i.e.*, water, benzene, rhodamine B, Fura-2, and bovine serum albumin solutions, followed by different functions states of hemoglobin in solution, *i.e.*, oxy-, carboxy-, and deoxy-hemoglobin solutions. In all cases, the above theoretical framework is used to interpret our measurements of THG intensity, P(3ω), in terms of the third-order nonlinear susceptibility $\chi^{(3)}(3\omega)$.

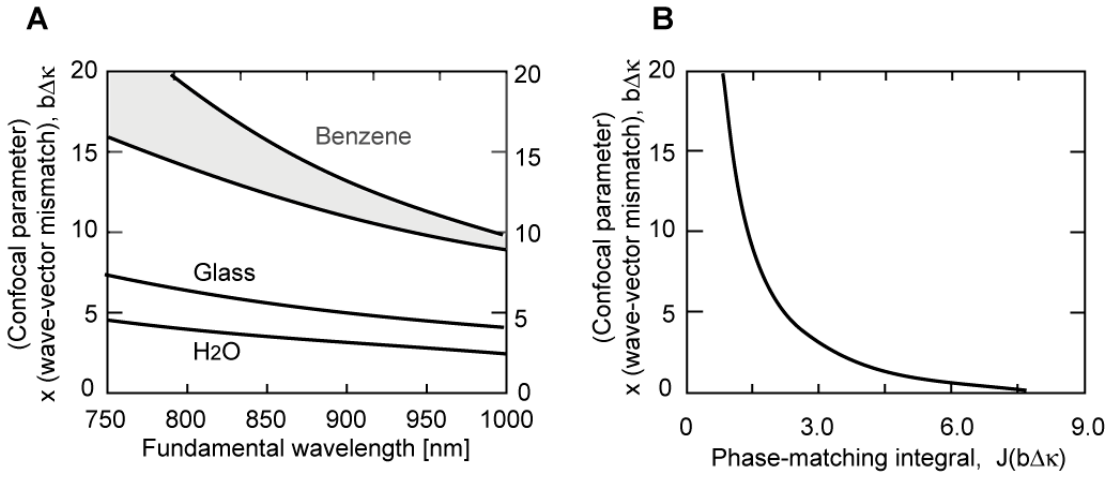

Figure 2.3 (A) Theoretical curves of the confocal parameter times the wave vector mismatch, bΔκ. Curves are calculated from linear dispersion models for water, benzene, and Duran glass in the case of diffraction limited geometry. The band representing benzene is bounded by the curves predicted by two different models of dispersion[32, 87]. **(B)** The phase-matching integral[25], J(bΔκ).

THG Imaging

The enhancement of THG at an interface is illustrated through a comparison two-photon excited fluorescence and THG imaging of 10-µm diameter fluorescein-labeled microspheres versus equally sized unlabeled glass beads that sit in a drop of water on a glass coverslip (Fig. 2.4A). The microspheres are readily resolved in entirety with two-photon fluorescence, while only the interfaces normal to the incident beam, either at the microsphere/water or water/glass interface, yield third harmonic light (Fig. 2.4A). The elongation of images for either modality is a consequence of the difference in axial resolution (z_o = 5.0 µm) compared to lateral resolution (r_o = 1.0 µm). The top surfaces of the beads appear dark as a result of the absorption of the third harmonic light by the fluorescent beads. The shadowing on the glass surface results from distortion of the excitation beam as it passes through

the bead. Critically, there is no fluorescent signal for the case of imaging glass beads, yet THG at the water/glass interface leads to an image of the top and bottom surfaces of the beads (Fig. 2.4A).

As motivation for our studies on the THG by hemoglobin, we applied THG imaging to human red blood cells in solution without the use of dyes. A maximal projection through a 5 μm stack of unprocessed images leads to the well known view of red blood cells as concave disks (Fig. 2.4B).

Microspectroscopy

We now turn to quantitative spectroscopy of model compounds and hemoglobin in solution. We report our measurements in terms of the corrected and fitted ratio of third harmonic power at the solution/glass interface relative to that at the glass/air interface (Eq. 17). These are used, when appropriate, to derive the corresponding ratio of susceptibilities (Eqs. 18 and 19). A discussion of the uncertainty in all terms is presented toward the end of this section.

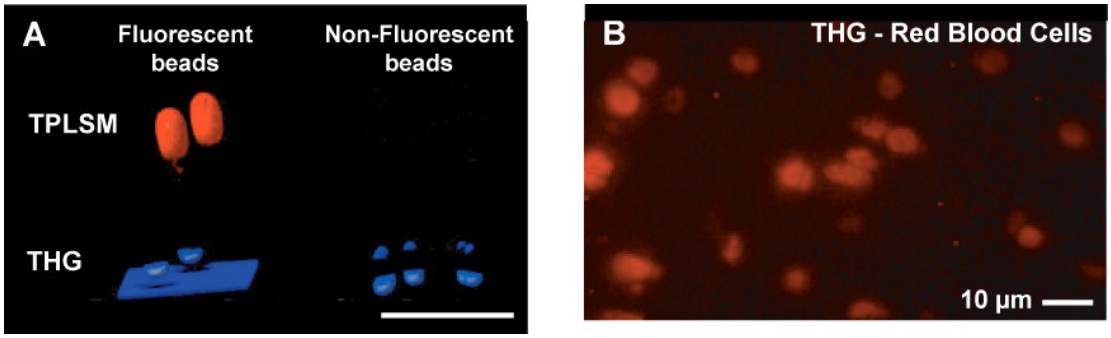

Figure 2.4. Two-photon excited fluorescence and THG imaging. **(A)** A comparison of two-photon excited fluorescence and THG images. Unlike two-photon excited fluorescence, THG can be collected from both fluorescent and non-fluorescent beads. Third harmonic generation can be seen to be primarily produced at interfaces perpendicular to the excitation beam including the coverslip beneath the fluorescent samples. In this case a shadow of the beads is cast on the coverslip due to the distortion of the excitation beam. **(B)** Third harmonic image showing the high contrast of red blood cells in solution without the use of dyes.

Model solvents. Measurements of THG at the water/glass interface relative to the glass/air interface show that $R_{THG}(\omega)$, the ratio of third harmonic powers (Eq. 17), decreased as a monotonic function of wavelength (Fig. 2.5A). The sign ambiguity in the susceptibility ratio $\chi^{(3)}_{H_2O}(3\omega) \big/ \chi^{(3)}_{glass}$ (Eqs. 18 to 20) is resolved by considering the spectral trend in $R_{THG}(\omega)$ to be related to a one-photon resonance near a wavelength of 970 nm (Fig. 2.5A'). The errors bars in figures 2.5A and 2.5A' capture an ~ 11 % uncertainty in the measurement of $R_{THG}(\omega)$, while the additional systematic uncertainty in $\chi^{(3)}_{H_2O}(3\omega) \big/ \chi^{(3)}_{glass}$ is expected to be less than 4 %.

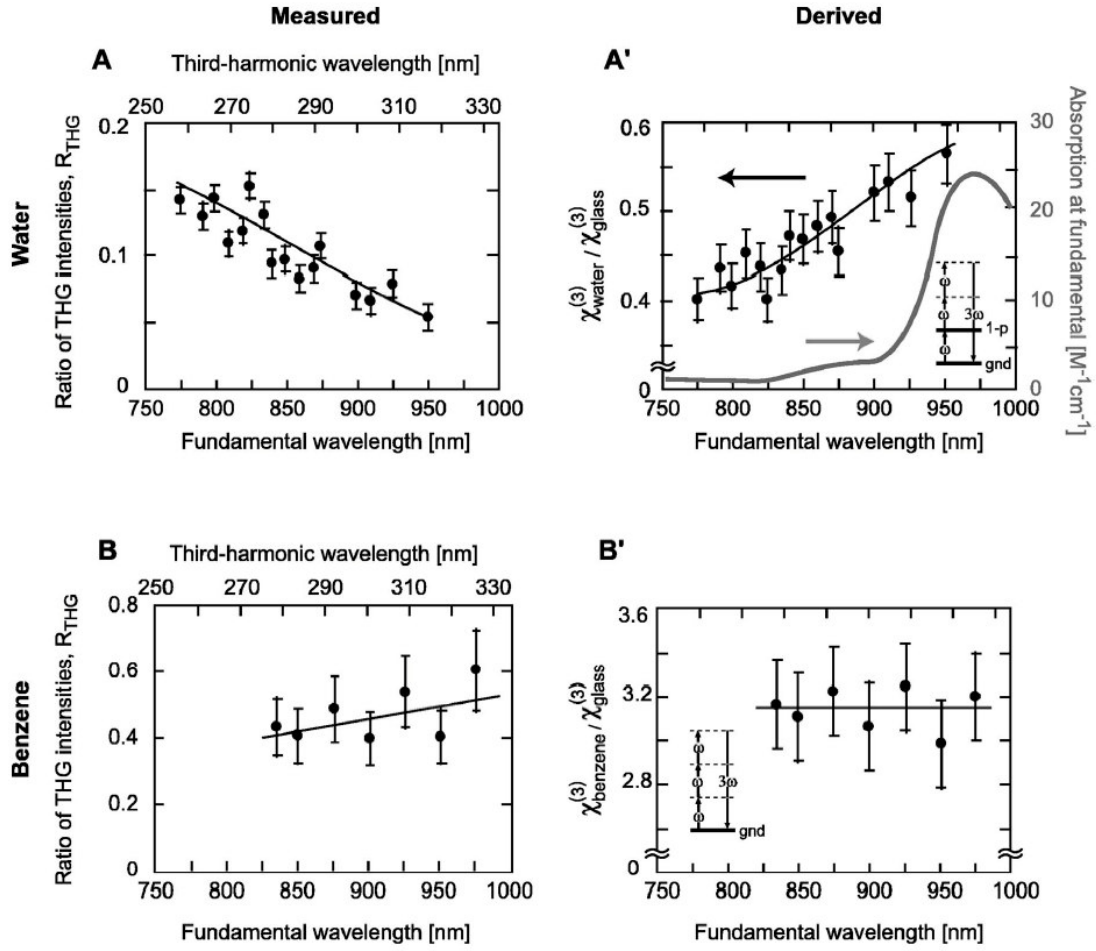

Figure 2.5. Third harmonic spectra of water and benzene; each datum is the mean ± SE. Linear absorption spectra between 250 to 1000 nm were obtained with a Cary 50 spectrophotometer. **(A)** The third harmonic intensity ratio, $R_{THG}(\omega)$, of deionized water. The term $R_{THG}(\omega)$ is the ratio of the cubic fit coefficients of the sample/vessel interface to that of the vessel/air interface and is related to the ratio of the third-order susceptibility ratio by equation 18. **(A')** We show the derived third-order susceptibility ratio of water and glass, $\chi^{(3)}_{H_2O}(3\omega) \Big/ \chi^{(3)}_{glass}$, and the linear absorption of water at the fundamental wavelength. The correspondence between the THG and linear absorption spectrum indicates a one-photon resonant enhancement. The energy diagram in the inset illustrates a one photon resonance. Arrows direct the reader to the appropriate vertical scale for the two graphs. **(B)** The third harmonic intensity ratio, $R_{THG}(\omega)$, of neat benzene. **(B')** The calculated third-order susceptibility ratio of benzene and glass is relatively constant suggesting that the dominant contribution to $\chi^{(3)}(3\omega)$ of benzene is non-resonant. The energy diagram in the inset illustrates a lack of resonant enchancement.

The third harmonic spectrum of benzene is essentially constant over the range of measured wavelengths (Figs. 2.5B and 2.5B'), consistent with an absence of one- and two-photon resonances over the range of our measurements. The third harmonic spectrum does not reflect the long wavelength tail of the ultraviolet absorption band in benzene that, in principle, could contribute to a three-photon resonance; this suggests that the dominant contribution to $\chi^{(3)}(3\omega)$ of benzene is non-resonant. The sign ambiguity in the estimate of $\chi^{(3)}_{\text{benzine}}(3\omega)\big/\chi^{(3)}_{\text{glass}}$ (Eqs. 18 and 19) is resolved to be positive based on two considerations. First, the hyperpolarizabilities associated with double bonds between carbon atoms in benzene are anticipated to lead to a much larger $\chi^{(3)}(3\omega)$ values for this molecule than for distilled water[51, 81, 82]. Second, a choice of the negative root in equation 14 leads to comparable values for $\chi^{(3)}(3\omega)$ in water and benzene over the range of 875 to 950 nm. The systematic uncertainty in the susceptibility ratio of benzene is ~ 17 %.

Aqueous solutions. The third harmonic spectrum of a 1 mM solution of rhodamine B chloride shows a sharp decrease with increasing wavelength, with a break in the slope near 850 nm (Figs. 2.6A and 2.6A'). The sign ambiguity in the estimate of $\chi^{(3)}_{\text{rhodamine}}(3\omega)\big/\chi^{(3)}_{\text{glass}}$ (Eqs. 19 to 21) is easily resolved if we assume that the susceptibility of the rhodamine B solution is greater than that of pure water. We use equation 21 through 18 to find $\chi^{(3)}_{\text{rhodamine}}(3\omega)\big/\chi^{(3)}_{\text{glass}}$ and note that it mirrors the

two-photon excited fluorescent cross-section measurements[83] in rhodamine B; this suggests the presence of a strong two-photon resonance (Fig. 2.6A'). The systematic error introduced into $\chi^{(3)}_{\text{rhodamine}}(3\omega)\big/\chi^{(3)}_{\text{glass}}$ by our estimate of the volume fraction, υ = 0.0004, is ~ 50 % (Eq. 15).

The third harmonic spectrum of a solution of 0.5 mM Fura-2 pentasodium salt and 3.3 mM EGTA shows a sharp decrease with increasing wavelength with a break in the slope at a wavelength of 800 nm (Fig. 2.5C). Unlike the case of rhodamine B, the $R_{THG}(\omega)$ solvent background is a 3.3 mM EGTA solution (data not shown). The sign ambiguity in the estimate of $\chi^{(3)}_{\text{Fura-2}}(3\omega)\big/\chi^{(3)}_{\text{glass}}$ (Eq. 21) is resolved by assuming that the susceptibility of the dye solution is greater than that of water alone. Our estimate of the volume fraction of the hydrated Fura-2 complex at ~ 0.07 % introduces an ~ 70 % systematic error in our derived value of $\chi^{(3)}_{\text{Fura-2}}(3\omega)\big/\chi^{(3)}_{\text{glass}}$. The susceptibility ratio, $\chi^{(3)}_{\text{Fura-2}}(3\omega)\big/\chi^{(3)}_{\text{glass}}$ shows a spectral profile very similar to the measured[84-86] two-photon excited fluorescent cross-section of Fura-2 (Fig. 2.6B'). This suggests a strong two-photon resonance.

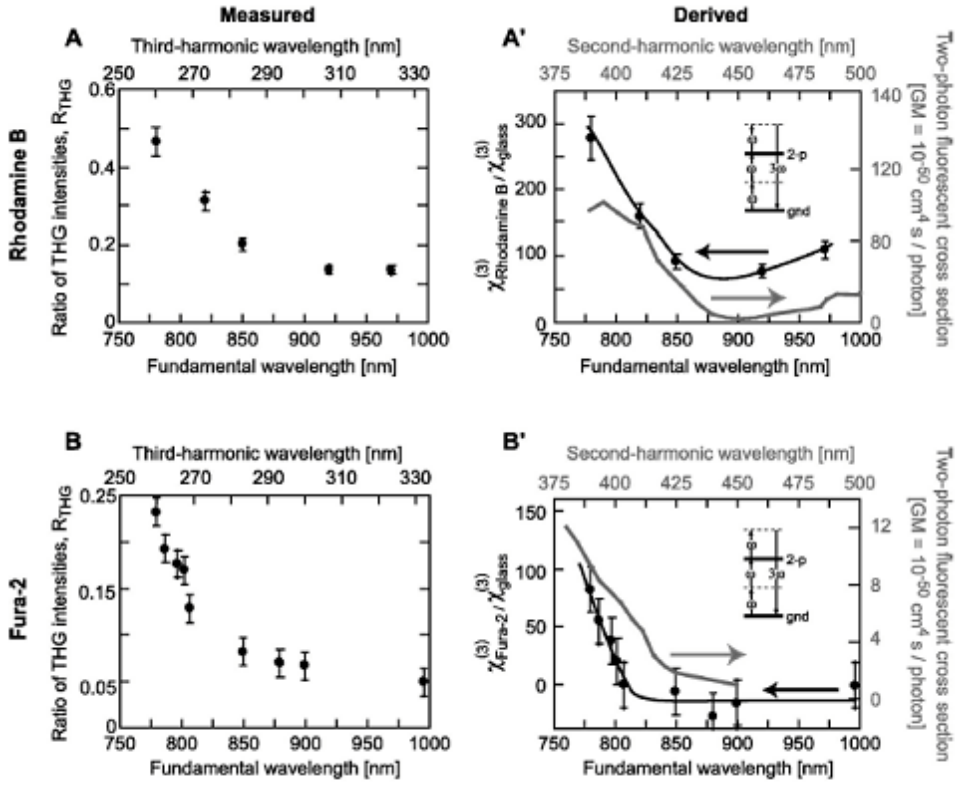

Figure 2.6. Third harmonic spectrum of rhodamine B, Fura-2, and BSA; each datum is the mean ± SE. The primed figures include an energy diagram in the inset illustrating the resonant enhancement mode and arrows direct the reader to the appropriate vertical scale for the two graphs.**(A)** We show the third harmonic intensity ratio, $R_{THG}(\omega)$, of an aqueous solution of 1 mM rhodamine B. **(A')** We show the derived third-order susceptibility ratio of rhodamine B, $\chi^{(3)}_{\text{rhodamine}}(3\omega) \big/ \chi^{(3)}_{\text{glass}}$, and the two-photon action cross-section[83]. The correspondence between the THG and two-photon action indicates a strong two-photon resonant enhancement in rhodamine B below 850 nm. **(B)** The third harmonic intensity ratio, $R_{THG}(\omega)$, of an aqueous solution of 0.5 mM Fura-2. **(B')** The third-order susceptibility ratio of Fura-2, $\chi^{(3)}_{\text{Fura-2}}(3\omega) \big/ \chi^{(3)}_{\text{glass}}$, and the two-photon action cross-section[84-86] track each other indicating a two-photon resonant enhancement.

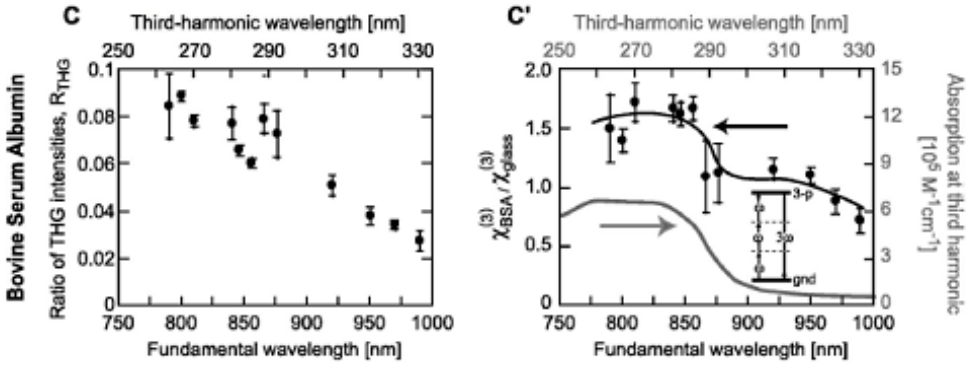

Figure 2.6 (continued). (C) The third harmonic intensity ratio, $R_{THG}(\omega)$, of a 0.75 mM solution of BSA. **(C')** The calculated third-order susceptibility ratio of BSA and glass, $\chi^{(3)}_{\mathrm{BSA}}(3\omega)\big/\chi^{(3)}_{\mathrm{glass}}$ suggests that $\chi^{(3)}(3\omega)$ for BSA has a three-photon resonant enhancement from 750 to 850 nm. We display the linear absorption of BSA over the region relevant to three-photon resonance.

The THG spectrum of a 0.75 mM solution of BSA also shows a decrease with increasing wavelength (Fig. 2.6C). The sign ambiguity in the estimate of $\chi^{(3)}_{\mathrm{BSA}}(3\omega)\big/\chi^{(3)}_{\mathrm{glass}}$ (Eq. 21) is resolved if we assume that the susceptibility of the albumin is enhanced by a three-photon resonance in the linear absorption spectrum of albumin (Fig. 2.6C'). Dispersion and volume fraction uncertainties result in a less than 12 % systematic uncertainty in our value for $\mathrm{X}^{(3)}_{\mathrm{BSA}}(3\omega)\big/\mathrm{X}^{(3)}_{\mathrm{glass}}$.

Hemoglobin solutions. The linear absorption spectrum of hemoglobin shows a prominent Soret absorption band that peaks near a wavelength of 420 nm (Fig. 2.7A; central gray). The corresponding dip in the measured value of $R_{THG}(\omega)$ of these solutions (Fig. 2.8) is highly suggestive of a two-photon resonance. We use this correspondence to resolve the sign ambiguity in equation 21. We use the

refractive index estimate of oxyhemoglobin (Fig. 2.7B; see Appendix A for derivation) to estimate the wave-vector mismatch (Eq. 9). We estimate that the volume fraction of hemoglobin in a 2 mM solution to be ~ 12 % for the various hemoglobin solutions[79, 80] and estimate that this introduces a systematic error of ~ 6.5 % in our susceptibility ratios $\chi^{(3)}_{\mathrm{O_2\text{-}Hb}}(3\omega) \big/ \chi^{(3)}_{\mathrm{glass}}$. An unaccounted for feature at long wavelengths may reflect the additional involvement of a three-photon resonance (left-hand gray band in figure 2.7A) or the solvent.

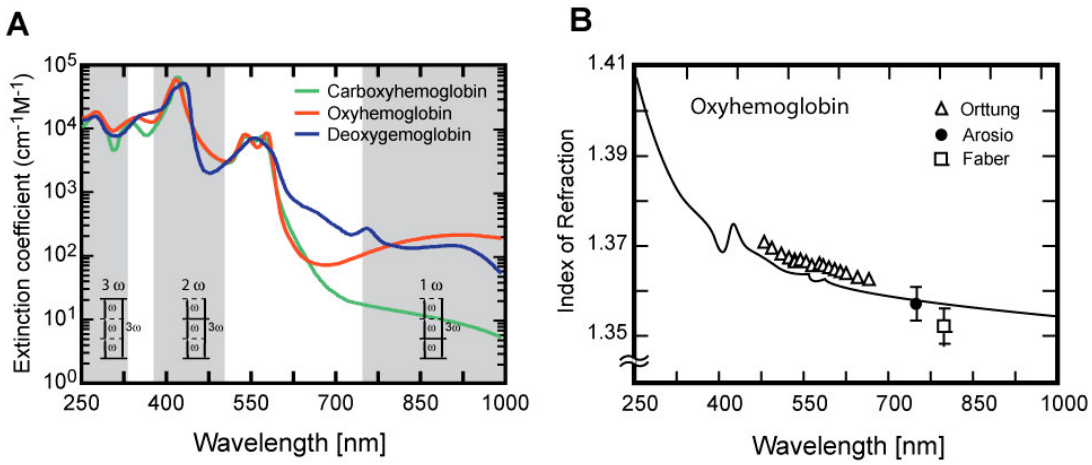

Figure 2.7. (A) The linear absorption spectrum of oxy-, deoxy-, and carboxyhemoglobin[56]. The wavelength bands corresponding to potential one-photon, two-photon, and three-photon resonances are highlighted and labeled. **(B)** The estimated refractive index of oxyhemoglobin (Appendix A) and point index measurements taken by Orttung *et al.*[118] (500 to 650 nm), Arosio *et al.*[80] (750 nm) and Faber *et al.*[80] (800 nm).

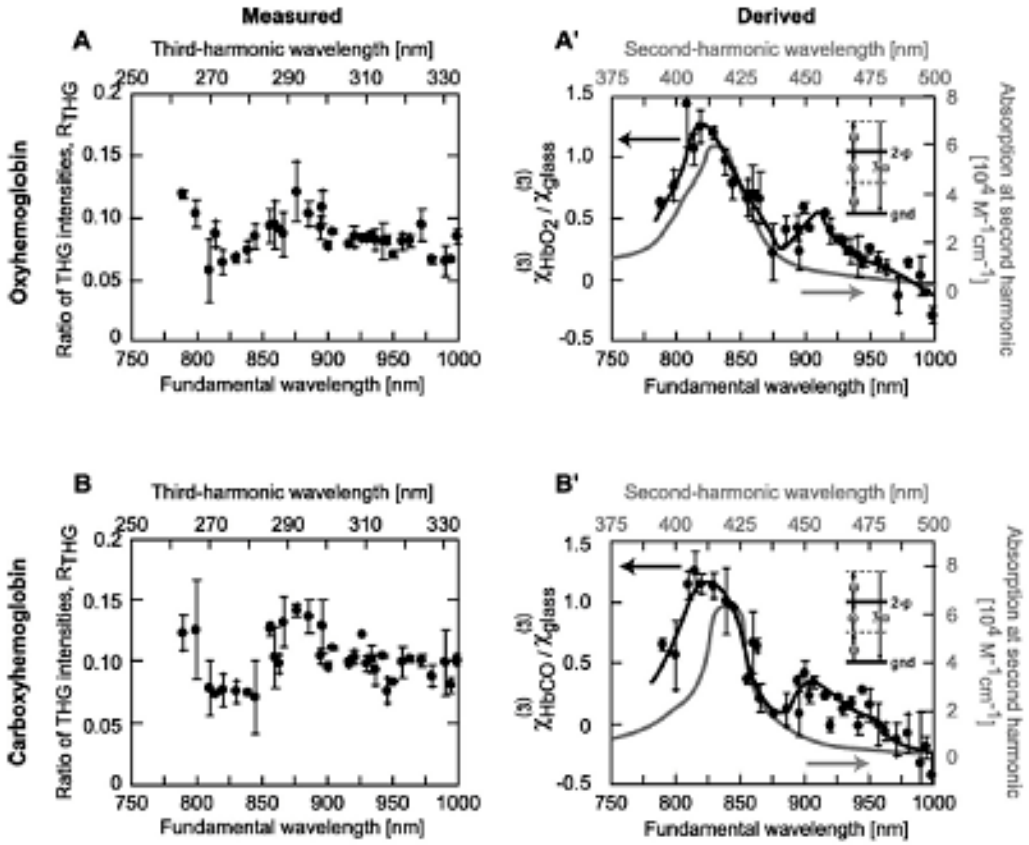

Figure 2.8. Third harmonic spectrum of oxy-, carboxy-, and deoxyhemoglobin solutions (this work) together with linear absorption measurements[56]; each datum is the mean ± SE. The primed figures include an energy diagram in the inset illustrating two-photon resonant enhancement and arrows direct the reader to the appropriate vertical scale for the two graphs. **(A)** The third harmonic intensity ratio, $R_{THG}(\omega)$, of a 2 mM oxyhemoglobin solution. **(A')** The correspondence between the derived third-order susceptibility ratio of oxyhemoglobin, $\chi^{(3)}_{\mathrm{HbO_2}}(3\omega)\big/\chi^{(3)}_{\mathrm{glass}}$, and the linear absorption from 375 to 500 nm indicates a two-photon resonant enhancement. **(B)** We show the third harmonic intensity ratio, $R_{THG}(\omega)$, of a 2 mM, 60 % (v/v) carboxylated hemoglobin solution. **(B')** The derived third-order susceptibility ratio of 60 % (v/v) carboxyhemoglobin, $\chi^{(3)}_{\mathrm{HbCO}}(3\omega)\big/\chi^{(3)}_{\mathrm{glass}}$, and the linear absorption in the two-photon resonance range suggests a two-photon resonant enhancement.

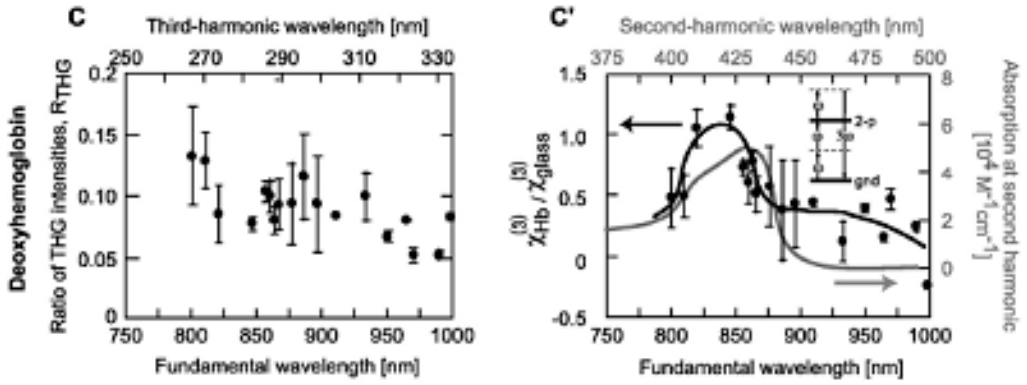

Figure 2.8. (Continued.) (C) The third harmonic intensity ratio, $R_{THG}(\omega)$, of a 2 mM, ~ 95 % (v/v) deoxygenated hemoglobin solution. **(C')** The calculated third-order susceptibility ratio of deoxyhemoglobin and glass, $\chi^{(3)}_{\mathrm{Hb}}(3\omega)\big/\chi^{(3)}_{\mathrm{glass}}$ and the linear absorption of deoxyhemoglobin in the two-photon absorption regime.

Uncertainty. The standard deviation of the measured peak THG power was between 1.5 and 5.5 % of the peak value across the wavelength range of 760 to 1000 nm, with the exact percentage dependent upon the incident power, the interface, and the sample. The uncertainties in the cubic fits of the peak THG power led to uncertainties as high as 6 % in the value of $R_{THG}(\omega)$ (Eq. 17) within the same session. Measurements of the same substance on different days could lead to variations as large as 13 % in the values of $R_{THG}(\omega)$. The experimental errors are represented as standard errors of the mean (SE) in the graphs of $R_{THG}(\omega)$ and $\chi^{(3)}_{\mathrm{solution}}(3\omega)\big/\chi^{(3)}_{\mathrm{glass}}$ (Figs. 2.5, 2.6 and 2.8). They result from an average over two to five estimates of $R_{THG}(\omega)$, where we recall that each estimate involves the ratio of cubic equations fit through 6 to 10 data points for both solution/glass and glass/air interfaces (Fig. 2.2C). The standard errors are on the same order as uncertainties in absolute measurements of the susceptibility in glass[65].

Additional, systematic uncertainties in the susceptibility ratios (Tables 2.1 and 2.2) result from the propagation of uncertainty in the dispersion of relevant materials. The dipersion of Duran 8340 glass (Eq. A1), benzene[87] (Eqs. A2 and A3), water[88] (Eq. A4), BSA (Eq. A5), rhodamine B, Fura-2, and hemoglobin (Fig. 2.7B) are approximated by numerical formulas (Appendix A). The uncertainty in the values of the susceptibility ratio introduced by these approximations are maximal at the blue side of the spectrum, where there are few published measurements of the refractive index to constrain models (Appendix A). At an excitation wavelength of 750 nm, we estimate that the uncertainty in $\chi^{(3)}_{\text{solution}}(3\omega) \big/ \chi^{(3)}_{\text{glass}}(3\omega)$ that results from uncertainty in the linear dispersion is < 3 %, ~ 17 %, < 1 %, < 5 %, and < 5 % for Duran 8340, benzene, water, BSA, and hemoglobin respectively (Table 2.1).

A second source of uncertainty in the susceptibility ratios concerns the volume of solution (Eqs. 15 and 21) occupied by the solvated form of rhodamine B, Fura-2, BSA, and hemoglobin in 1 mM, 0.5 mM, 0.75 mM, and 2 mM solutions is estimated to be 0.04 %, 0.07 %, 7 %, and 12 % respectively. Uncertainties in the volume fraction estimates dominate the systematic uncertainty in the derived susceptibility ratios for these solutions (Table 2). This large uncertainty in values gleaned from the literature is due in part to the presence of a substrate where adsorption may play a role[72, 90-94].

Table 2.1: Dispersion Estimates and Uncertainties at λ = 250 and 750 nm

	n(3ω)	$\frac{\delta n(3\omega)}{n(3\omega)}$	n(ω)	$\frac{\delta n(\omega)}{n(\omega)}$	Uncertainty in $\frac{X^{(3)}_{solute}(3\omega)}{X^{(3)}_{glass}(3\omega)}$
Duran glass*	1.530	< 0.2 %	1.469	< 0.1 %	< 3 %
Benzene[87]	1.610	1.7 %	1.480	0.4 %	17 %
Water[89]	1.379	< 0.01 %	1.329	< 0.001%	< 1 %
Dyes[89]	1.384	2 %	1.332	1 %	~ 30 %
BSA*	1.390	< 1 %	1.337	< 0.5 %	< 5 %
Hemoglobin*	1.410	< 1 %	1.360	< 0.05 %	< 5 %
	λ= 250 nm		λ = 750 nm		λ = 750 nm

✶: Appendix

Table 2.2: Volume Fraction Estimates and Uncertainties of Solutes in Solution

	Hydro-Dynamic radius	Conc-entration	Volume Fraction, υ	Uncertainty in υ	Uncertainty in $\frac{X^{(3)}_{solute}(3\omega)}{X^{(3)}_{glass}(3\omega)}$
Rhod. B[73, 76]	0.5 nm	1.0 M	0.04 %	45 %	50 %
Fura2[73, 76]	0.7 nm	0.5 mM	0.07 %	50 %	70 %
BSA[79, 80]	3.14 nm	0.75 mM	7 %	20 %	7.5 %
Hemoglobin[79, 80]	2.96 nm	2.0 mM	12 %	11 %	6.5 %

Spectral discrimination of hemoglobin ligand states. The final issue concerns the ability to discriminate among the three ligation states of hemoglobin based on their relative THG spectra, $R_{THG}(\omega)$. In principle, this can be accomplished wherever the spectra do not intercept. However, for the signal-to-noise ratios achieved in our measurements, we could distinguish among all three states (95 % confidence level) in a 20-nm wide band only near a center wavelength of 960 nm (Fig. 2.9). At other center wavelengths two of the three possible states could be distinguished (Fig. 2.9).

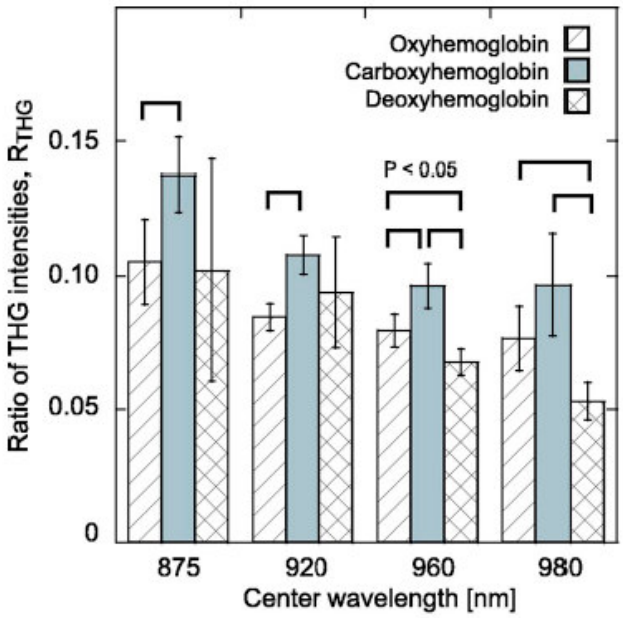

Figure 2.9. The third harmonic intensity ratio of hemoglobin in different oxidation states averaged over 20-nm bands. Error bars represent two standard errors; significance at the 95 % confidence level is indicated by a bar.

Discussion

We confirm that far field THG is significantly enhanced when the focal volume is bisected by an optical interface[11, 13, 17-19] (Fig. 2.4). We use this phenomenon to investigate the nonlinear spectra of solutions over the wavelength range of 750 to 1000 nm by collecting THG from the interface of sample solutions and their glass containers[52, 54] (Fig. 2.2). The susceptibility ratio of pure solutions, $\chi^{(3)}_{\text{solution}}(3\omega)\big/\chi^{(3)}_{\text{glass}}$ (Eq. 16) is inferred from power dependent measurements of the THG from the solution/glass and glass/air interfaces[11, 52, 54]. This calculation requires sample specific models of linear dispersion (Fig. 2.7B), which we generate and collate in Appendix A. We further derive the susceptibility ratios of hydrated solutes $\chi^{(3)}_{\text{solute}}(3\omega)\big/\chi^{(3)}_{\text{glass}}$ from THG measurements on solutions, by 'subtracting' the THG due to the solvent from the total THG from the solution (Eqs. 15 and 21). Miller's rule (Eq. 4) indicates that the nonlinear susceptibility, $\chi^{(3)}_{\text{glass}}$ of the glass substrate is approximately constant over the 750 to 1000 nm range of wavelengths, which implies that spectral features in the susceptibility ratio $\chi^{(3)}_{\text{sample}}(3\omega)\big/\chi^{(3)}_{\text{glass}}$ reflects features in the susceptibility, $\chi^{(3)}_{\text{sample}}(3\omega)$, of the sample (Appendix B).

To evaluate the accuracy of our spectroscopic approach in pure solutions, we compare our measured values of the nonlinear susceptibility ratio of de-ionized water and benzene to measurements in the literature[52, 54, 55, 66, 67] (Fig. 2.10). Most literature measurements are made relative to fused silica (SiO_2), so an accurate comparison with our results requires that we first scale our results by the ratio of the susceptibility of our Duran glass to that of SiO_2. This scaling factor is achieved by

applying Miller's rule (Eq. 4) and indicates that the glass/SiO_2 susceptibility ratio is ~ 1.17 (Appendix B).

The scaled values of $\chi^{(3)}_{\text{sample}}(3\omega) \Big/ \chi^{(3)}_{\text{SiO}_2}$ for benzene and water found here (Fig. 2.10) are in good correspondence with those measured at different wavelengths and with different approaches. Literature values are plotted with the measurements made here and error bars are included whenever they are available. Systematic errors in our values are not accounted for in the figure (Tables 1 and 2). The close agreement among measurements made with pulse-widths ranging from 30 ns to 40 fs supports the understanding of THG as a purely electronic effect, not unduly modulated by the nonlinear index of refraction or short time scale solvation processes[95-98].

The microspectroscopy approach[52, 54, 99] adopted here relies on tightly focused ~ 100 fs pulse-width, ~ 1 nJ laser pulses to sample ~ 50 μm^3 volumes of solution. It can be performed with exactly the same pulse shape[100-102], energy, and duration used in laser scanning nonlinear imaging. Previous spectroscopic studies based on the Maker fringe technique relied on softly focused 10 ns or longer, ~ 1 mJ laser pulses to sample much larger volumes[39, 53, 66, 103]. While the Maker fringe technique yields third harmonic phase information, which is discarded in the present technique, both approaches appear to have similar experimental errors.

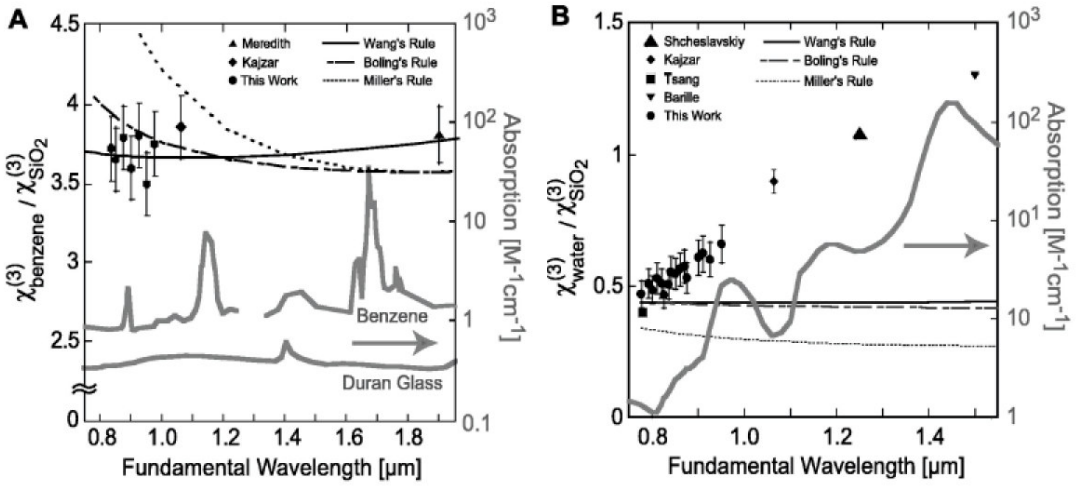

Figure 2.10. Comparison of THG and linear absorption spectra with semi-empirical rules, and linear absorption spectra. The data from THG measurements made here have been shifted by the ratio of Miller's rules for Duran glass and SiO_2 in order to compare with values reported in the literature (this factor is ~ 1.17, Appendix B). An arrow directs the reader to the right hand side vertical scale for linear absorption measurements. **(A)** Benzene: The THG measurement at 1.06 μm used 13 ns pulses and a maker-fringes technique[66] while the 1.9 μm measurement used ~ 30 ns pulses and a triple wedge technique[53, 67]. Linear absorption measurements in benzene are piecewise composed from measurements over wavelengths of 0.78 to 1.25 μm[70] and 1.33 and 1.8 μm[71]. Linear absorption values for the Duran glass are based on transmission measurements and are corrected to account for reflection using the Fresnel equations (Eq. 15). **(B)** Water: the THG measurement at 780 nm used 100 fs pulses and a variant of the Maker-fringes approach[16], those at 1.25 and 1.5 μm used 40 to 130 fs pulses and an experimental protocol similar to that used here[52, 54], while the measurement at 1.06 μm used 13 ns pulses and a Maker-fringes technique[66]. Linear absorption measurements are due to Segelstein[69].

We also compare the various semi-empirical rules for calculating $\chi^{(3)}(3\omega)$ values (Eqs. 4 to 6) with those found here and in the literature for the cases of benzene and water (Fig. 2.10). These formulations are not expected to perform well in solutions or near resonance. However Wang's rule[60] (Eq. 5) and to a lesser extent Boling's rule[59, 62] (Eq. 6) predict the relatively flat spectrum of benzene (Fig. 2.10A), which may indicate a broader utility for use with non-resonant solutions.

Nonlinear Spectra

Comparisons between linear and nonlinear spectra show common features and demonstrate one-, two-, and three-photon resonances in THG spectra that correspond with linear absorption features at the fundamental, second, and third harmonic of the excitation beam as well as two-photon absorption resonances. We find evidence of a one-photon resonance in the $\chi^{(3)}(3\omega)$ spectra of water (Figs. 2.5A' and 2.10B); a two-photon resonance in the $\chi^{(3)}(3\omega)$ of rhodamine B, Fura-2, and hemoglobin (Figs. 2.6A', 2.6B' and 2.7'), a three-photon resonance in the $\chi^{(3)}(3\omega)$ of BSA (Fig. 2.6C'), and no resonance in benzene (Fig. 2.5B). The two-photon resonances in the rhodamine B and Fura-2 spectra are identified by comparison with two-photon excited fluorescence cross-sections spectra (Figs. 2.6A' and 2.6B') and confirm that THG may be used as a probe of two-photon excited states that are not accessible with linear absorption measurements[86].

The degree of modulation in $\chi^{(3)}(3\omega)$ associated with a resonant enhancement varies dramatically between compounds. For example, Fura-2 shows a greater than 20-fold increase in $\chi^{(3)}(3\omega)$ associated with 10- to 10^2-times increase in its two-photon action $\sigma(\omega)$, while rhodamine B shows an ~ 3-fold increase in $\chi^{(3)}(3\omega)$ associated with an ~10^2-fold increase in the $\sigma(\omega)$ (Fig. 2.6'). In part, these differences follow from the variable contribution of non-resonant terms to the susceptibility (Eq. 2) as the resonant modulation $\chi^{(3)}_{\text{resonant}} / \chi^{(3)}_{\text{non-resonant}}(3\omega)$ is most appreciable for compounds such as oxy-hemoglobin and Fura-2, where the non-resonant value is relatively low.

Potential application to Imaging

The ratio of THG powers, $R_{THG}(\omega)$, represents image luminosity as collected in a THG microscope. $R_{THG}(\omega)$ is not directly proportional to the nonlinear susceptibility (Eq. 18), as a result resonance enhancements may appear as an increase or a decrease in THG luminosity (Figs. 2.5A, 2.5A' and 2.6). Nonetheless $R_{THG}(\omega)$ spectra can be used to distinguish different solutions. We also find that at physiological concentrations (~ 2 mM), hemoglobin solutions consisting of 98 % (v/v) oxy-hemoglobin, 60 % (v/v) carboxy- and 40 % (v/v) oxy-hemoglobin (corresponding with heavy smoke inhalation), or 90 % (v/v) deoxyhemoglobin show significant differences in their $R_{THG}(\omega)$ spectra when averaged over 20-nm spectral bands (Fig. 2.9).

Additional factors are needed to enhance the signal-to-noise ratio before THG can be used to determine the oxidation state of hemoglobin in flowing red blood cells. This appears to be the case, even though distinguishing oxiation states would only require that differences in THG contrast be imaged and no corrections for index, absorption, or reflections would be necessary. It is possibe that THG from red blood cells may provide a higher contrast then the hemoglobin solution/glass interface[92, 104], though such measurements would require a tight focus so as to minimize the orientation effects of the cell. It is also possible that successive single-power measurements might be more useful for discriminating between oxidation states. Acquisition of repeated measurements at the same power has the advantage allowing rapid comparisons across cells while surrendering the potential to extract

accurate absolute values for the third-order susceptibility. Finally, simultaneous laser trapping and THG spectroscopy may provide the acquisition time necessary to distinguish between oxidation states *in vivo*.

The two-photon absorption resonance in the THG spectrum of hemoglobin (Figs. 2.8A', B' and C') does not lead to a significantly larger value for the nonlinear susceptibility than the value found for BSA (Fig. 2.6C'). This suggests that damage induced under nonlinear excitation will not be preferentially driven in either compound. In capillaries with diameters on the order of a few confocal parameters, hemoglobins two-photon resonace implies, that provided the fluorescent dye used to label the plasma does not also have strong local spectral features, 820 nm is an optimal wavelength for visualizing red blood cell shadows[105, 106]. . Conversely irradiating at 880 nm would be best the best way to minimize photodamage to hemoglobin.

The large two-photon resonance in the rhodamine B and Fura-2 indicates that common fluorescent dyes used for two-photon microscopy may have a latent information channel available in THG. In all cases the THG channel will preferentially probe dyes in the vicinity of interfaces effectively creating a complimentary contrast mechanism.

Appendix A

Dispersion. We discuss the derivation and application of the phenomenological formulae used to calculate the refractive indices of silicone dioxide, Duran 8340 glass, benzene, water, and solutions of Rhodamine B, Fura-2, BSA, and Hemoglobin.

SiO_2 and Duran Glass. The dispersion of SiO_2 is fit by a well known formula[107], while that for Duran 8340 glass is approximated by this dispersion equation to fit reported index values in the visible range[108]. We have:

(A1)
$$n_{SiO2\ or\ Duran}(\lambda) = \sqrt{1 + \frac{n_1}{1-\left(\frac{\lambda_1}{\lambda}\right)^2} + \frac{n_2}{1-\left(\frac{\lambda_2}{\lambda}\right)^2} + \frac{n_3}{1-\left(\frac{\lambda_3}{\lambda}\right)^2}}$$

where the common parameters are $n_1 = 0.897479$, $\lambda_1 = 3145.816$ nm, $n_2 = 0.4079426$, and $\lambda_2 = 340.9419$ nm. For SiO_2, $n_3 = 0.6961663$ and $\lambda_3 = 261.5422$ nm, while for Duran glass, $n_4 = 0.7376285665$ and $\lambda_4 = 279.6276303$ nm.

Benzene. Significant differences in the value of $\Delta\kappa$ arise when comparing refractive index models for benzene constructed in the visible wavelength[32, 87] (Fig. 2.2A). Comparison of the model calculation with existing refractive index measurements does not allow for a clear choice between models[109]. We use the average index of the two models. The first is[87]

(A2) $$n_{benzene}(\lambda) = n_0\left[1 + \left(\frac{\lambda_0}{\lambda}\right)^2\right]$$

with $n_0 = 1.21501$ and $\lambda_0 = 76.56803$ nm, and the second is[32]

(A3) $$n_{benzene}(\lambda) = n_0\sqrt{1 + \frac{n_1}{1-\left(\frac{\lambda_1}{\lambda}\right)^2}}$$

with $n_0 = 1.205$, $n_1 = 0.501$, and $\lambda_1 = 170$ nm.

Water. Models of the refractive index, n(ω) of water as in the case of benzene, exhibit significant divergence at wavelengths in the ultraviolet part of the spectrum[32, 110]. Our choice of models[89] is dictated by favorable comparison with reported measurements across the full 250 to 750 nm range of wavelengths. We use[110]

(A4)

$$n_{water}(\lambda,S,T) = n_0 + \left(n_1 + n_2T + n_3T^2\right)S - n_4T^2 + \frac{n_5 + n_6S + n_7T}{\lambda} - \left(\frac{n_8}{\lambda}\right)^2 + \left(\frac{n_9}{\lambda}\right)^3$$

where S is salinity in parts per thousand, T is temperature in Celsius, λ is in nanometers, and the parameter values are $n_0 = 1.31405$, $n_1 = 1.779\times10^{-4}$, $n_2 = -1.05\times10^{-6}$, $n_3 = 1.60\times10^{-6}$, $n_4 = 2.02\times10^{-6}$, $n_5 = 15.868$, $n_6 = 1.155\times10^{-2}$, $n_7 = -4.23\times10^{-2}$, $n_8 = 66.20$, and $n_9 = 103.681$.

Dye solutions. The wavelength dependence of the index of the dye solutions is approximated by scaling the dispersion curve of salt-water[89] (Eq. A4) to match an existing measurement[111] of the concentration dependent index increment, dn(ω)/dc

of rhodamine B solutions at a wavelength of 780 nm. This gives an effective salinity of 2 % (v/v) (S = 20) for 1 mM solutions of rhodamine B; the same index increment was used for a 0.5 mM solution of Fura2.

BSA. We use existing measurements of dn(ω)/dc at various wavelengths[112-114] (see Table 3) to construct a concentration dependent dispersion increment model for BSA

(A5) $$\frac{\mathrm{dn}_{\mathrm{BSA}}(\lambda)}{\mathrm{dc}} = -\frac{\lambda}{118} + 162 + \frac{15000}{\lambda} + \left(\frac{0.056}{\lambda}\right)^2$$

where λ is in nanometers.

Table 2.3: Linear Dispersion Increment of Bovine Serum Albumin

Wavelength	436 nm	488 nm	546 nm	578 nm	1060 nm
dn(ω)/dc [ml/g]	0.1924	0.12	0.1854	0.1901	0.181
Reference	114	113	114	112	113

Hemoglobin. We estimate the dispersion of oxy-hemoglobin solutions with a Taylor expansion of the Kramers-Kronig integral that relates the real and imaginary components of the complex refractive index[115] $n_c(\omega) = n(\omega) + i\, n'(\omega)$. The imaginary component of the refractive index is related to the molar absorption coefficient $\varepsilon(\omega)$ by[116]

(A6) $$n'(\omega) = c\ln(10)\frac{\varepsilon(\omega)}{2\omega}$$

where c is the speed of light and $\omega = 2\pi c/\lambda$. We approximate the local dispersion features of oxy-hemoglobin by fitting the $n'(\omega)$ absorption spectra in the 250 to 1000 nm wavelength range, with *r* Gaussians representing *r* absorption bands, such that $n'(\omega)$ can be expressed as the sum

(A7) $$n'(\omega) = \sum_r A_r e^{-\frac{(\Omega_r - \omega)^2}{2\sigma_r^2}}$$

where $\sigma_r(\omega) \equiv (\Omega_r - \omega_{1/2}) \Big/ \sqrt{2ln(2)}$, Ω_r is the resonance angular frequency, $\omega_{1/2}$ is the frequency at half of the peak height, and A_r is the maximum value of $n'(\omega)$ for the r'-th absorption band. Variations in the index due to local absorption bands can then be expressed as[117]

(A8) $$\Delta n(\omega) = \sqrt{2}\sum_r \frac{A_r}{\sigma_r}(\Omega_r - \omega) e^{-\frac{(\Omega_r - \omega)^2}{2\sigma_r^2}}$$

The results of this approach are then scaled and provided with a linear offset to fit existing measurements of dn(ω)/dc in oxy-hemoglobin over the 450 to 800 nm wavelength range[80, 115, 118] (Table 4; Fig. 2.7B).

Table 2.4: Linear Dispersion Increment of Oxyhemoglobin

Wavelength	500 nm	650 nm	750 nm	800 nm
dn(ω)/dc [ml/g]	0.198	0.1900	0.170±0.01	0.143±0.02
Reference	118	118	80	115

Appendix B

Schott's Duran 8340 glass, also designated as Corning 7740 Pyrex, is a borosilicate glass (81 % SiO_2, 13 % B_2O_3, and 4 % AlO_3) with very similar optical properties ($n\nu$ = 1.474 and Abbe number of 65.7) to pure fused SiO_2 ($n\nu$ = 1.458 and Abbe number of 67.8)[108]. Boron is added primarily to reduce the melting temperature and is not thought to change the nonlinear properties of the glass[119]. Nonetheless, according to Miller's rule (Eq. 4) the third-order susceptibility of the Duran glass is 17.9 to 17.2 % larger than the value of $\chi^{(3)}(3\omega)$ for fused SiO_2 over the 750 to 1000 nm wavelength range. Measurements of $\chi^{(3)}(3\omega)$ in glasses of different indices support the magnitude of this estimate[119-121], although the difference in $\chi^{(3)}(3\omega)$ values[59, 61] may be as large as 100 %. Miller's rule also indicates that the value of $\chi^{(3)}(3\omega)$ for either glass will smoothly decrease by about 10 % over the same range of wavelengths. This has been generally supported by measurements in fused SiO_2 and borosilicate glass at wavelengths ranging from 1.064 to 2.1 μm, which show a less than 20 % change (with 7 to 15 % variation) in the value $\chi^{(3)}(3\omega)$ for a given glass[59, 65].

Acknowledgements

We thank Zvi Kam for the gift of a quartz lens and Earl Dolnick for assistance with the electronics. Financial support was provided by the NSF IGERT program (GOC), the Burroughs Welcome funded La Jolla Interfaces in Science (ACM and CSB), the David and Lucille Packard Foundation (DK), the NIH/NCRR (DK and JAS), and the NIH/NIBIB (DK and JAS).

This previously published material was used in part or in full for Chapter II.

Spectroscopy of third harmonic generation: Evidence for resonances in model compounds and ligated hemoglobin. G. O. Clay, A. C. Millard, C. B. Schaffer, J. Aus-der-Au, P. S. Tsai, J. A. Squier and D. Kleinfeld. Journal of the Optical Society of America B (2006) 23:932-950.

References

1. W. R. Zipfel, R. M. Williams, and W. W. Webb, "Nonlinear magic: Multiphoton microscopy in the biosciences," Nature Biotechnology **21**, 1369-1377 (2003).

2. W. Denk, "Two-photon scanning photochemical microscopy: Mapping ligand-gated ion channel distributions," Proceedings of the National Academy of Sciences USA **91**, 6629-6633 (1994).

3. W. Denk and K. Svoboda, "Photon upmanship: Why multiphoton imaging is more than a gimmick," Neuron **18**, 351-357 (1997).

4. W. Denk, J. H. Strickler, and W. W. Webb, "Two-photon laser scanning fluorescence microscopy," Science **248**, 73-76 (1990).

5. P. J. Campanola, D. W. Young, A. E. Cowan, C. Roychoudhuri, and L. M. Loew, "Applications in nonlinear optical microscopy," Cell Vision **4**, 191-192 (1997).

6. D. L. Wokosin, V. E. Centonze, S. Crittenden, and J. White, "Three-photon excitation fluorescence imaging of biological specimens using an all-solid-state laser," Bioimaging **4**, 1-7 (1996).

7. I. Graczynski, H. Malak, and J. R. Lakowicz, "Multi-photon excitation of DNA stains DAPI and Hoechst," Bioimaging **4**, 138-148 (1996).

8. S. W. Hell, K. Bahlmann, M. Schrader, A. Soini, H. Malak, I. Grycznyski, and J. R. Lakowicz, "Three-photon excitation in fluorescence microscopy," Journal of Biomedical Optics **1**, 71-74 (1996).

9. S. Maiti, J. B. Shear, R. M. Williams, W. R. Zipfel, and W. W. Webb, "Measuring serotonin distribution in live cells with three-photon excitation," Science **275**, 530-532 (1997).

10. Y. Barad, H. Eisenberg, M. Horowitz, and Y. Silberberg, "Nonlinear scanning laser microscopy by third harmonic generation," Applied Physics Letters **70**, 922-924 (1997).

11. J. Squier, M. Muller, G. J. Brakenhoff, and K. Wilson, "Third harmonic generation microscopy," Optics Express **3**, 315-321 (1998).

12. D. Oron, D. Yelin, E. Tal, S. Raz, R. Fachima, and Y. Silberberg, "Depth-resolved structural imaging by third-harmonic generation microscopy," Journal of Structural biology (147), 3-11 (2004).

13. D. Yelin and Y. Silberberg, "Laser scanning third-harmonic microscopy in biology," Optics Express **5**(8), 169 (1999).

14. D. Yelin, D. Oron, E. Korkotian, M. Segal, and Y. Silberberg, "Third-harmonic microscopy with a titanium-sapphire laser," Applied Physics B **74**, 97-101 (2002).

15. J. M. Schins, T. Schrama, J. Squier, G. J. Brakenhoff, and M. Müller, "Determination of material properties by use of third-harmonic generation microscopy," Journal of the Optical Society of America B **19**(7), 1627-1634 (2002).

16. T. Y. F. Tsang, "Optical third harmonic generation at interfaces," Physical Review A **52**, 4116 (1995).

17. J. Reintjes, *Nonlinear Optical Parametric Processes in Liquids and Gases* (Academic Press, INC, Washington, DC, 1984).

18. S.-W. Chu, S.-Y. Chen, T.-H. Tsai, T.-M. Liu, C.-Y. Lin, H.-J. Tsai, and C.-K. Sun, "In vivo developmental biology study using noninvasive multi-harmonic generation microscopy," Optics Express **11**(23), 3093-3099 (2003).

19. M. Muller, J. Squier, K. R. Wilson, and G. J. Brakenhoff, "3D-microscopy of transparent objects using third harmonic generation," Journal of Microscopy **191**, 266-274 (1998).

20. V. Barzda, C. Greenhalgh, J. Aus der Au, J. Squier, S. Elmore, and J. H. G. M. van Beek, "Second- and third-harmonic generation and multiphoton excitation fluorescence microscopy from simultaneous imaging of cardiomyocytes," presented at the Commercial and Biomedical Applicatrions of Ultrafast Lasers IV, 2004.

21. A. C. Millard, P. W. Wiseman, D. N. Fittinghoff, K. Wilson, J. Squier, and M. Muller, "Third-harmonic generation microscopy by use of a compact, femtosecond fiber laser source," Applied Optics **38**, 7393-7397 (1999).

22. R. D. Schaller, J. C. Johnson, and R. J. Saykally, "Nonlinear chemical imaging microscopy: Near-field third harmonic generation imaging of human blood cells," Analytical Chemistry **72**, 5361-5364 (2000).

23. D. Debarre, W. Supatto, E. Farge, B. Moulia, M. C. Schanne-Klein, and E. Beaurepaire, "Velocimetric third-harmonic generation microscopy: Micrometer-scale quantification of morphogenetic movements in unstained embryos," Optics Letters **29**, 2881-2883 (2004).

24. S. Y. Chen, A. Maksimichuk, E. Esarey, and D. Umstadter, "Observation of phase-matched relativistic harmonic generation," Physical Review Letters **84**, 5528-5531 (2000).

25. A. N. Naumov, D. A. Sidorov-Biryukov, A. B. Fedotov, and A. M. Zheltikov, "Third-harmonic generation in focused beams as a method of 3D microscopy of a laser-produced plasma," Optics Spectroscopy **90**, 778 (2001).

26. S.-W. Chu, S.-Y. Chen, G.-W. Chern, T.-H. Tsai, Y.-C. Chen, B.-L. Lin, and C.-K. Sun, "Studies of $\chi(2)/\chi(3)$ tensors in submicron-scaled bio-tissues by polarization harmonics optical microscopy," Biophysical Journal **86**, 3914-3922 (2004).

27. C.-K. Sun, C.-C. Chen, S.-W. Chu, T.-H. Tsai, Y.-C. Chen, and B.-L. Lin, "Multiharmonic-generation biopsy of skin," Optics Letters **28**(24), 2488-2490 (2003).

28. D. A. Akimov, A. A. Ivanov, M. V. Alfimov, E. P. Grabchak, A. A. Shtykova, A. N. Petrov, A. A. Podshivalov, and A. M. Zheltikov, "J-aggregation visualized with two-photon resonant third-harmonic generation," Journal of Raman Spectroscopy **34**, 1007-1012 (2003).

29. T. Hasegawa, K. Ishikawa, T. Kanetake, T. Koda, K. Takeda, H. Kobayashi, and K. Kubodera, "Excitonic resonant effect in the third-order nonlinear optical properties of blue- and red form polydiacetylene films," Chemical Physics Letters **171**, 239-244 (1990).

30. R. D. Schaller, J. C. Johnson, K. R. Wilson, L. F. Lee, L. H. Haber, and R. J. Saykally, "Nonlinear chemical imaging nanomicroscopy: From second and third harmonic generation to multiplex (broad-bandwidth) sum frequency generation near-field scanning optical microscopy," Journal of Physical Chemistry B **106**, 5143-5154 (2002).

31. L. Canioni, S. Rivet, L. Sarger, R. Barille, P. Vacher, and P. Voisin, "Imaging of Ca2+ intracellular dynamics with a third-harmonic generation microscope," Optics Letters **26**, 515 (2001).

32. R. H. Hellwarth, "Third-order optical susceptiblilities of liquids and solids," Progress in Quantum Electronics **5**, 1 (1977).

33. R. L. Swofford and A. C. Albrecht, "Nonlinear spectroscopy," Annual Review of Physical Chemistry **29**, 421-440 (1978).

34. T. Hasegawa, Y. Iwasa, H. Kishida, T. Koda, Y. Tokura, H. Tachibana, and Y. Kawabata, "Two-photon resonant third-harmonic generation in polysilanes," Physical Review B **45**, 6317-6320 (1992).

35. M. A. Diaz-Garcia, F. Agullo-Lopez, W. E. Torruellas, and G. I. Stegeman, "Identification of two-photon states in phthalocyanines by third harmonic generation spectroscopy," Chemical Physics Letters **235**, 535-540 (1995).

36. P. R. Callis, "Two-photon induced fluorescence," Annual Review of Physical Chemistry **48**, 271-297 (1997).

37. A. Schulzgen, Y. Kawabe, E. Hanamura, A. Yamanaka, P. A. Blanche, J. Lee, H. Sato, M. Naito, N. T. Dan, S. Uchida, Y. Tanabe, and N. Peyghambarian, "Two-photon resonant third-harmonic generation in La2CuO4," Physical Review Letters **86**, 3164-3167 (2001).

38. A. B. Schumacher, J. S. Dodge, M. A. Carnahan, R. A. Kaindl, D. S. Chemla, and L. L. Miller, "Parity-Forbidden Excitation of Sr2CuO2Cl2 Revealed by Optical Third-Harmonic Spectroscopy," Physical Review Letters **87**, 1-4 (2001).

39. P. D. Maker and R. W. Terhune, "Study of optical effects due to an induced polarization third order in the electric field strength," Physical Review **137**, A801-A818 (1965).

40. J. Jerphagnon and S. K. Kurtz, "Maker fringes: A detailed cmparison of theory and experiment for isotropic and uniaxial crystals," Journal of Applied Physics **41**, 1667-1681 (1970).

41. H. Tajalli, J. P. Jiang, J. T. Murray, N. R. Armstrong, A. Schmidt, M. Chandross, S. Maxumdar, and N. Peyghambarian, "Spectra of third-order optical nonlinear susceptibilities of epitaxial chloro-indium-phthalocyanines," Applied Physics Letters **67**, 1639-1641 (1995).

42. R. R. Tykwinski, U. Gubler, R. E. Martin, F. Diederich, C. Bosshard, and P. Gunter, "Structure-Property Relationships in Third-Order Nonlinear Optical Chromophores," Journal of Physical Chemistry B **102**, 4451-4465 (1998).

43. S. O. Konorov, D. A. Akimov, A. A. Ivanov, M. V. Alfimov, S. Botti, R. Ciardi, L. D. Deominicis, L. S. Asilyan, A. A. Podshivalov, D. A. Sidorov-Biryukov, R. Fantoni, and A. M. Zheltikov, "Femtosecond optical harmonic generation as a non-linear spectroscopic probe for carbon nanotubes," Journal of Raman Spectroscopy **34**, 1018-1024 (2003).

44. W. E. Torruellas, D. Neher, R. Zanoni, G. I. Stegeman, F. Kajzar, and M. Leclerc, "Dispersion measurements of the third-order nonlinear susceptiblity of polythiophene thin films," Chemical Physics Letters **175**, 11-16 (1990).

45. J. C. Baumert, G. C. Bjorklund, D. H. Jundt, M. C. Jurich, H. Looser, R. D. Miller, J. Rabolt, R. Sooriyakumaran, J. D. Swalen, and R. J. Twieg, "Temperature dependence of the third-order nonlinear optical susceptiblities in polysilanes and polygermanes," Applied Physics Letters **53**, 1147-1149 (1988).

46. C. Halvorson, R. Wu, D. Moses, F. Wudl, and A. J. Heeger, "Third harmonic generation spectra of degenerate ground state derivatives of poly(1,6-heptadiyene)," Chemical Physics Letters **212**, 85-89 (1993).

47. J. McElvain, M. Cha, H. Yu, N. Zhang, F. Wudl, and A. J. Heeger, "Third harmonic generation spectrum of a degenerate ground state conjugated polymer. Direct evidence of simultaneous two- and three-photon resonance," Chemical Physics Letters **247**, 221-226 (1995).

48. H. S. Nalwa, M. Hanack, G. Pawlowski, and M. K. Engel, "Third-order nonlinear optical properties of porphyrazinne, phtalocyanine and napthalocyanine germanium derivities: Demonstrating the effect of pi-

conjugation length on third-order optical nonlinearity of two-dimensional molecules," Chemical Physics **245**, 17-26 (1999).

49. S. R. Marder, J. W. Perry, G. Bourhill, C. B. Gorman, B. G. Tiemann, and K. Mansour, "Relation between bond-length alternation and second electronic hyperpolarizability of conjugated molecules," Science **261**, 186-189 (1993).

50. J. Y. Huang and M. H. Wu, "Nonlinear optical studies of binary mixtures of hydrogen bonded liquids," Physical Review E **50**(5), 3737-3746 (1994).

51. I. Ledoux, I. D. W. Samuel, J. Zyss, S. N. Yaliraki, F. J. Schattenmann, R. R. Schrock, and R. J. Silbey, "Third-order microscopic noninearities of very long chain polyenes: Saturation phenomena and conformational effects," Chemical Physics **245**, 1-16 (1999).

52. R. Barille, L. Canioni, S. Rivet, L. Sarger, and G. Rivoire, "Nonlinearity measurements of thin films by third-harmonic-generation microscopy," Physical Review E **66**, 67602 (2002).

53. G. R. Meredith, B. Buchalter, and C. Hanzlik, "Third-order optical susceptibility determination by third harmonic generation. 2," Journal of Chemical Physics **78**(3), 1533-1542 (1983).

54. V. Shcheslavskiy, G. Petrov, and V. V. Yakovlev, "Nonlinear optical susceptibility measurements of solutions using third-harmonic generation on the interface," Applied Physics Letters **82**(22), 3982-3984 (2003).

55. T. Tsang, "Third- and fifth-harmonic generation at the interfaces of glass and liquids," Physical Review A **54**, 5454 (1996).

56. P. Lemberg and J. W. Legge, *Hematin Compounds and Bile Pigments* (Interscience Publishers, Inc., New York, 1949).

57. R. B. Boyd, *Nonlinear Optics, Second Edition* (Academic Press, 2003).

58. E. J. Sanchez, L. Novotny, G. R. Holtom, and X. S. Xie, "Room-temperature fluorescence imaging and spectroscopy of single molecules by two-photon excitation," The Journal of Physical Chemistry A **101**, 7019-7023 (1997).

59. C. Bosshard, U. Gubler, P. Kaatz, W. Mazerant, and U. Meier, "Non-phase-matched optical third-harmonic generation in noncentrosymmetric media: Cascaded second-order contributions for the calibration of third-order nonlinearities," Physical Review B **61**, 10688-10701 (2000).

60. C. Wang, "Empirical relation between the linear and the third-order nonlinear optical susceptibilities," Physical Review B **2**, 2045-2048 (1970).

61. N. Sugimoto, H. Kanbara, S. Fujiwara, K. Tanaka, and Y. Shimizugawa, "Third-order optical nonlinearities and their ultrafast response in Bi2-O3-B2O3-SiO2 glasses," Journal of the Optical Society of America B **16**(11), 1904-1908 (1999).

62. N. L. Boling, A. J. Glass, and A. Owyoung, "Empirical relationships for predicting nonlinear refractive index changes in optical solids," IEEE Journal of Quantum Electronics **QE-14**, 601-608 (1978).

63. R. W. Boyd, *Nonlinear Optics* (Academic Press, New York, 1992).

64. J. R. Heflin, Y. M. Cai, and A. F. Garito, "Dispersion measurements of electric-field-induced second-harmonic generation and third-harmonic generation in conjugated linear chains," Journal of the Optical Society of America B **8**, 2132-2147 (1991).

65. U. Gubler and C. Bosshard, "Optical third-harmonic generation of fused silica in gas atmosphere: Absolute value of the third-order nonlinear susceptibility $\chi^{(3)}$," Physical Review B **61**, 10702-10710 (2000).

66. F. Kajzar and J. Messier, "Third-harmonic generation in liquids," Physics Review. A **32**(4), 2352 (1985).

67. G. R. Meredith, B. Buchalter, and C. Hanzlik, "Third-order optical susceptibility determination by third harmonic generation. 1," Journal of Chemical Physics **78**(3), 1533-1542 (1983).

68. P. S. Tsai, N. Nishimura, E. J. Yoder, E. M. Dolnick, G. A. White, and D. Kleinfeld, "Principles, design, and construction of a two photon laser scanning microscope for in vitro and in vivo brain imaging," in *In Vivo Optical Imaging of Brain Function*, R. D. Frostig, ed. (CRC Press, Broca Raton, 2002), pp. 113-171.

69. D. J. Segelstein, "The complex refractive index of water," Masters (University of Missouri, Kansas City, 1981).

70. K. I. Hildrum, T. Isaksson, T. Naes, and A. Tandberg, *Near Infra-red Spectroscopy: Bridging the gap between data analysis and NIR applications*, Ellis Horwood Series in Analytical Chemistry (Ellis Horwood, New York, 1992), p. 473.

71. K. Murayama, B. Yuan, Y. Ozaki, M. Tomida, and S. Era, "Near-infrared spectroscopy for liquids of microliter volume using capillaries with wall transmission," Analyst **128**, 957-959 (2003).

72. B. Halle and M. Davidovic, "Biomolecular hydration: From water dynamics to hydrodynamics," Prooceedings of the National Academy of Sciences **100**, 12135-12140 (2003).

73. J. L. Dela Cruz and G. J. Blanchard, "The influence of chromophore structure on intermolecular interactions. A study of selected rhodamines in polar protic and aprotic solvents," Journal of Physical Chemistry A **106**, 10718-10724 (2002).

74. G. R. Fleming and M. Cho, "Chromophore-solvent dynamics," Annual Review of Physical Chemistry **47**, 109-134 (1996).

75. A. Bondi, "van der Waals volumes and radii," The Journal of Physical Chemistry **68**, 441-451 (1964).

76. H. T. Edward, "Molecular volumes and the Stokes-Einstein equation," Journal of Chemical Education **47**, 261-270 (1970).

77. J. E. Selwyn and J. I. Steinfeld, "Aggregation equilibria of xanthene dyes," The Journal of Physical Chemistry **76**, 762-774 (1971).

78. F. L. Arbelo, P. R. Ojeda, and I. L. Arbeloa, "On the aggregation of rhodamine B in ethanol," Chemical Physics Letters **148**, 253-258 (1988).

79. H. G. Elias, *Makromolekule* (Wiley-VCH Verlag GmbH, 1990).

80. D. Arosio, H. E. Kwansa, H. Gering, G. Piszczek, and E. Bucci, "Static and dynamic light scattering approach to the hydration of hemoglobin and its supertetramers in the presence of osmolites," Biopolymers **63**, 1-11 (2002).

81. B. F. Levine and C. G. Bethea, "Molecular hyperpolarizabilities determined from conjugated and nonconjugated organic liquids," Appied Physics Letters **24**, 445-447 (1973).

82. H. Reis, M. G. Papadopoulos, and D. N. Theodorou, "Calculation of refractive indices and third-harmonic generation susceptibilities of liquid benzene and water: Comparison of continuum and discrete local-field theories," Journal of Chemical Physics **114**, 876881 (2000).

83. C. Xu and W. W. Webb, "Measurement of two-photon excitation cross sections of molecular fluorophores with data from 690 to 1050 nm," Journal Optical Society of America **13**, 481-491 (1996).

84. D. L. Wokosin, C. M. Loughrey, and G. L. Smith, "Characterization of a range of Fura dyes with two-photon excitation," Biophysical Journal **86**, 1726-1738 (2004).

85. C. Xu, R. M. Williams, W. Zipfel, and W. W. Webb, "Multiphoton excitations cross-sections of molecular fluorophores," Bioimaging **4**, 198-207 (1996).

86. C. Xu, W. Zipfel, J. B. Shear, R. M. Williams, and W. W. Webb, "Multiphoton fluorescence excitation: New spectral windows for biological nonlinear microscopy," Proceedings of the National Academy of Sciences USA **93**, 10763-10768 (1996).

87. H. El-Kashef, "Study of the refractive properties of laser dye solvents: Toluene, carbon disulphide, chloroform, and benzene," Optical Materials **20**, 81-86 (2002).

88. L. V. Butov, A. Zrenner, G. Abstreiter, A. V. Petinova, and K. Eberl, "Direct and indirect magnetoexcitons in symmetrical $In_xAg_{1-X}As/GaAs$ coupled quantum-wells," Physical Review B **52**, 12153-12157 (1995).

89. X. Quan and E. Fry, "Empirical equation for the index of refraction of seawater," Applied Optics **34**, 3477-3480 (1995).

90. M. L. Ferrer, R. Duchowicz, B. Carrasco, J. G. de la Torre, and A. U. Acuñ, "The conformation of serum albumin in solution: A combined phosphorescence depolarization-hydrodymic modeling study," Biophysical Journal **80**, 2422-2430 (2001).

91. T. Lazaridis, "Solvent reorganization energy and entropy in hydrophobic hydration," Journal of Physical Chemistry B **104**, 4964-4979 (2000).

92. K. E. S. Tang and V. A. Bloomfield, "Excluded volume in solvation: Sensitivity of scaled-particle theory to solvent size and density," Biophysical Journal **79**, 2222-2234 (2000).

93. C. E. Giacomelli, M. J. Esplandiu, P. I. Ortiz, M. J. Avena, and C. P. De Pauli, "Ellipsometric study of bovine serum albumin adsorped onto Ti/TiO_2 electrodes," Journal of Colloid and Interface Science **218**, 404-411 (1999).

94. A. Samokhvalov and R. Naaman, "Wavelength- and time-dependent two-photon photoemission spectroscopy of dye-coated silicon surface," Journal of Physical Chemistry B **104**, 11248 (2000).

95. W. P. de Boeij, M. S. Pshenichnikov, and D. A. Wiersma, "Ultrafast solvation dynamics explored by femtosecond photon echo spectroscopies," Annual Review of Physical Chemistry **49**, 99-123 (1998).

96. A. B. Myers, "Molecular electronic spectral broadening in liquids and glasses," Annual Review of Physical Chemistry **49**, 267-295 (1998).

97. P. Vohringer, D. C. Arnett, R. A. Westervelt, M. J. Feldstein, and N. F. Scherer, "Optical dephasing on femtosecond time scales: Direct measurement and calculation from solvent spectral densities," Journal of Chemical Physics **102**, 4027-4036 (1994).

98. M. Sinclair, D. Moses, K. Akagi, and A. J. Heeger, "Anisotropy of the third-order nonlinear-optical susceptibility in a degenerate ground state conjugated polymer: trans-(CH)x," Physical Review B **38**, 724-733 (1988).

99. V. Shcheslavskiy, G. I. Petrov, S. Saltiel, and V. V. Yakovlev, "Quantitative characterization of acqueous solutions probed by the third-harmonic generation microscopy," Journal of Structural Biology **147**, 42-49 (2004).

100. A. H. Buist, M. Muller, R. I. Ghauharali, G. J. Brakenhoff, J. A. Squier, C. J. Bardeen, V. V. Yakeovlev, and K. R. Wilson, "Probing microscopic chemical environments with high-intensity chirped pulses," Optics Letters **24**, 244-246 (1999).

101. J. A. Squier, K. R. Wilson, V. V. Yakovlev, C. Bardeen, A. Buist, M. Muller, and G. J. Brakenhoff, "Effect of pulse phase and shape on the efficiency of multiphoton processes: Implications for fluorescence microscopy," presented at the Conference on Lasers and Electro-Optics, Baltimore, 1999.

102. H. Kawano, Y. Nabekawa, A. Suda, Y. Oishi, H. Mizuno, A. Miyawaki, and K. Midorikawa, "Attenuation of photobleaching in two-photon excitation fluorescence from green fluorescent protein with shaped excitation pulses," Biochemical and Biophysical Research Communications **11**, 592-596 (2003).

103. F. Kajzar and J. Messier, "Original technique for third-harmonic-generation measurements in liquids," Reviews of Scientific Instruments **58**(11), 2081-2085 (1987).

104. I. E. Borissevitch, N. Rakov, G. S. Maciel, and C. B. de Araujo, "Changes in porphyrin nonlinear absorption owing to interaction with bovine serum albumin," Applied Optics **39**, 4431-4435 (2000).

105. D. Kleinfeld, P. P. Mitra, F. Helmchen, and W. Denk, "Fluctuations and stimulus-induced changes in blood flow observed in individual capillaries in layers 2 through 4 of rat neocortex," Proceedings of the National Academy of Sciences USA **95**, 15741-15746 (1998).

106. E. Chaigneau, M. Oheim, E. Audinat, and S. Charpak, "Two-photon imaging of capillary blood flow in olfactory bulb glomeruli," Proceedings of the National Academy of Sciences USA **100**, 13081-13086 (2003).

107. I. H. Malitson, "Interspecimen comparison of refractive index of fused silica," Journal of the Optical Society of America **55**, 1205-1209 (1965).

108. E. I. Optics, "Glass Materials Table," www.edmundoptics.com, ed. (2001).

109. J. M. Resa, C. Gonzalez, S. O. de Landaluce, and J. Lanz, "Densities, excess molar volumes, and refractive indices of ethyl acetate and aromatic hydrocarbon binary mixtures," Journal of Chemical Thermodynamics **34**, 995-1004 (2002).

110. P. D. T. Huibers, "Models for the wavelength dependence of the index of refraction of water," Applied Optics **36**, 3785-3787 (1997).

111. S. Yaltkaya and R. Aydin, "Experimental investigation of temperature effect on the refractive index of dye laser solutions," Turkish Journal of Physics **26**, 41-47 (2002).

112. G. E. Perlmann and L. G. Longsworth, "The specific refractive increment of some purified proteins," Journal of the American Chemical Society **70**, 2719-2724 (1948).

113. H. J. Coles, B. R. Jennings, and V. J. Morris, "Refractive Index Increment Measurement for Bacterial Suspensions," Physics in Medicine and Biology **20**, 310-313 (1975).

114. M. Halwer, G. C. Nutting, and B. A. Brice, "Molecular weight of lactoglobulin, ovalbumin, lysozyme and serum albumin by light scattering," Journal of the American Chemical Society **73**, 2786-2790 (1951).

115. D. Faber, E. G. Mik, Aalders, and T. G. van Leeuwen, "Oxygen saturation dependent index of refraction of hemoglobin solutions assessed by OCT," presented at the Proceedings of the SPIE, 2003.

116. J. Noack, D. X. Hammer, G. D. Noojin, B. A. Rockwell, and A. Vogel, "Influence of pulse duration on mechanical effects after laser-induced breakdown in water," Journal of Applied Physics **83**(12), 7488-7495 (1998).

117. P. Latimer, "Anomalous Dispersion of CS2 and ChCl3: Theoretical predictions," Journal of the Optical Society of America **51**, 116-118 (1961).

118. W. Orttung and J. Warner, "Refractive index dispersion in equine hemoglobin solutions," The Journal of Physical Chemistry **69**, 3188-3190 (1965).

119. E. M. Vogel, S. G. Kosinski, D. M. Krol, J. L. Jackel, S. R. Friberg, M. K. Oliver, and J. D. Powers, "Structural and optical study of silicate glasses for nonlinear optical devices," Journal of Non-Crystalline Solids **107**, 244-250 (1989).

120. H. Nasu, J. Matsuoka, and K. Kanichi, "Second- and third-order optical non-linearity of homogeneous glasses," Journal of Non-Crystalline Solids **178**, 23-30 (1994).

121. D. W. Hall, M. A. Newhouse, B. N. F., W. H. Dumbaugh, and D. L. Weidman, "Nonlinear optical susceptibilities of high-index glasses," Applied Physics Letters **54**(14), 1293-1295 (1989).

Ultrafast Two Photon Absorption Spectroscopy: Hemoglobin and Xanthene dyes

Abstract

Two-photon absorption (TPA) spectroscopy was performed on solutions of hemoglobin and xanthene dyes. We used a variant of the pump-probe technique capable of reaching a fractional sensitivity of 3×10^{-6} to directly detect the change in transmission induced by TPA, at selected wavelengths between 780 and 880 nm. Hemoglobin was found to have a TPA cross-section with a peak value of $\sigma_{TPA} \sim 150$ GM at 825 nm, near a Soret band related resonance. This confirms theoretical claims that the highly conjugated cyclic structure of porphryns leads to unusually large cross-sections. We also found a significant difference in the cross-section of carboxy- versus oxy-hemoglobin; *e.g.*, $\sigma_{TPA} = 61$ GM versus $\sigma_{TPA} = 18$ GM, respectively, at 850 nm. Our measurements of the TPA cross-sections for the dyes rhodamine 6G and B, *i.e.*, $\sigma_{TPA} = 13.5$ GM and $\sigma_{TPA} = 21$ GM respectively at 800 nm, are consistent with previously reported values. We also report on TPA and fluorescence measurements on these dyes and fluorescein at other wavelengths. We use a concentration scaling argument to compare these values with previous fluorescence based TPA derivations.

Introduction

Two-photon absorption (TPA) provides both a means to measure even parity electronic transitions that cannot be studied with one-photon processes[1] and, with advent of nonlinear laser scanning microscopy, a basis for contrast in biological imaging[2]. Interest in TPA is also motivated by applications in optical power limiters[3], photolithography[4], photodynamic therapy[5], and three-dimensional optical data storage[6]. Two-photon excited fluorescence (TPEF) is the primary means of investigating solution-phase TPA that is driven by ultrafast, *i.e.,* ~ 100 fs, duration laser pulses. These approaches require assumptions about the TPEF fluorescent yield and are clearly limited to use with fluorescent materials. TPA in non-fluorescent biomolecules is of interest theoretically and of importance to the understanding of cellular photo-damage[7, 8], targeted photo-disruption[9], photodynamic therapy[10, 11], and contrast in quantitative nonlinear imaging of biological samples[12, 13]. However TPEF studies make use of the spectral separation between the excitation beam and fluorescence emission rendering them far more accessible than direct measurements of TPA[14].

In vivo TPEF laser scanning microscopy studies have imaged cortical blood flow with fluorescently labeled blood plasma[15, 16]. Two-photon absorption by hemoglobin is considered both a possible route for photo-damage and a potential contrast mechanism to report blood oxygenation. Two-photon absorption in hemoglobin is also of theoretical relevance as calculations on porphyrins predict that a number of the Soret band states have two-photon cross-sections that exceed 100 GM[17].

Here, we performed nonlinear transmission measurements on hemoglobin in solution at the physiologically relevant concentration of 2-mM, *i.e.*, ~ 17-g/dL, which corresponds to the *average* concentration in blood; the concentration in red blood cells is about two-times higher. We measured TPA in a 98 % (v/v) oxy-hemoglobin (HbO_2) solution and a mixed 60 % (v/v) carboxy- / oxy-hemoglobin (HbCO) solution (nos. 300881R0 and 300879R0 respectively; Instrumentation Laboratories).

We also investigated TPA and TPEF in solutions of rhodamine 6G (no. R4127-100G; Sigma-Aldrich) and rhodamine B chloride (no. R-6626; Sigma-Aldrich) in methanol and solutions of fluorescein () in ethanol. These xanthene dyes have been well studied and their TPEF spectra have been published over the wavelength range of interest (see Appendix III.A & B.) There are also several previously published nonlinear transmission measurements on rhodamine B and 6G which measure TPA directly and can serve as a basis of comparison for the measurements made here.

Experimental

Pump-Probe Spectroscopy: The nonlinear optical properties of a sample allow optical mixing to occur between two beams (the pump and the probe) that are co-focussed on the sample. If the beams are frequency tagged (f1 and f2) and overlapped in space and time, optical mixing at the sample will result in sum and difference frequency modulations in the transmitted beams.

We used a "double modulation" variant of pump probe spectroscopy similar to that described by Frolov and Vardeny[18] as a means to directly detect TPA in solution phase material. This approach, which actually involves three modulation frequencies in its implementation here, enhances the signal-to-noise ratio of traditional pump-probe techniques by upconverting the optical signal to radio frequencies (~0.62 MHz) where ~1/f laser noise is minimal. After the probe light is collected with a photodiode, the signal is electronically downconverted to audio frequencies (7.6 kHz) in order to enable the use of an audio frequency (AF) lock-in amplifier which has a superior signal to noise than those operating at radio frequencies.

Apparatus: Our laser source was a variable wavelength Ti:Sapphire oscillator (Mira 900-F with 10-W Verdi pump; Coherent Inc.) with a 76-MHz repetition rate. The laser beam was divided into a pump and a probe beam. An acoustic optical modulator (AOM) (no. 1205C-2; Isomet) was used to impose a 0.62-MHz modulation to the pump beam, a dual beam mechanical chopper (no. 3501; New Focus) imparted an additional 3.2-kHz modulation to the pump and a 4.5-kHz modulation to the probe beam (Fig 3.1.) Auto-correlation of both beams revealed a temporally Gaussian pulse profile. The duration of the probe pulse was ~ 100 fs while that of the pump was stretched by dispersion in the AOM to ~ 200 fs. The beams were co-focused (0.3 NA 10-X Neofluar; Zeiss) in the sample and collected independently with a pair of reverse biased photodiodes (Det210; Thorlabs). After collection, the probe signal is down-converted electronically (no. ZP3 Mixer; MiniCircuits) at 0.62 MHz and phase-sensitive detection (no. SR530; Stanford Research Systems) is used to phase-lock to the (AF) sum-

frequency signal at 7.6 kHz. This process sensitively detected modulations in the probe beam that were caused by optical mixing with the pump beam.

Samples were mounted on a stage and could be translated along the optical axis of the objective (Z-scanned). In all cases, our sample containers were micro-cuvettes (no. 3520; Vitrocom) with flat, 200-µm thick glass (Duran type 8340) walls and a 200-µm wide internal chamber. Room temperature was maintained at 21C.

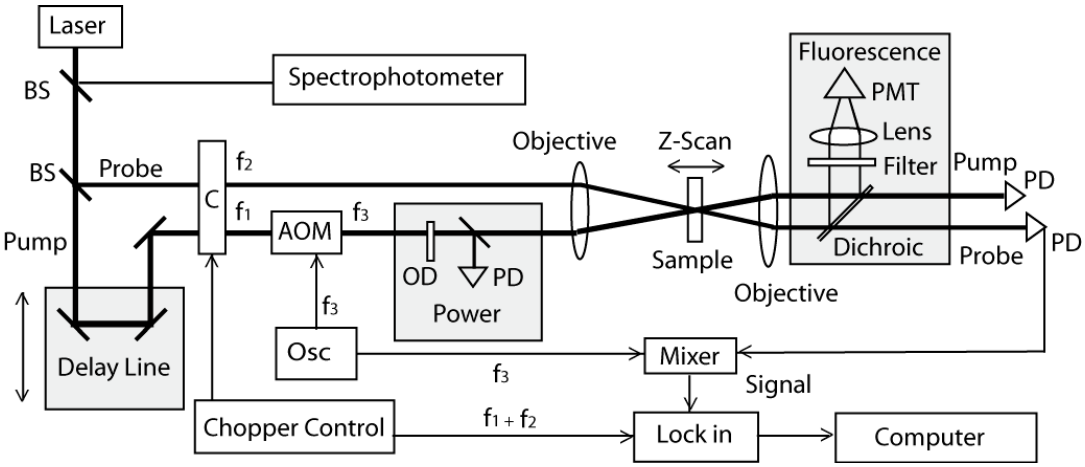

Figure 3.1. Double Modulation TPA and TPEF Spectroscope. BS = Beam Splitter; C = dual channel Chopper; AOM= Acoustic Optical Modulator; Osc = Oscillator; OD = neutral optical density filter wheel; PD = Photodiode; PMT = Photomultiplier tube. The pump and probe beam lines are depicted in thick black. The delay line (shown in grey) is used to adjust pump beam pulses to be coincident or lagging in time relative to the probe beam pulses at the focus. The chopper and AOM are used to frequency tag the probe and pump beams at f_2, and both f_1 and f_3, respectively. The pump power can be adjusted by a optical density filter wheel (OD) and is monitored by a photodiode (PD) (see power section in grey). The sample is mounted on a stage that can be Z-scanned through the focus. TPEF can be collected via a long pass dichroic, an infrared blocking filter, and a PMT (see fluorescence section in grey). Photodiodes collect both beams. Electronic lines are depicted in thin grey with arrows indicating the direction of signal and frequency markers where appropriate. The mixer downconverts the detected signal at the AOM modulation frequency f_3. The signal is then detected at the chopper sum frequency $f_1 + f_2$. The linear spectrophotometer is a Carey 50. Unterminated photodioces and PMT can also be routed through the mixer and the lock-in.

Measurement of TPA: Typical TPA measurements were performed by positioning the sample at the center of the focus and recording the difference in the sum-frequency signal when the beams were temporally overlapped and when the pump pulse lagged the probe in time by about ~10 ps, to generate a background signal. Differencing in this way controlled for background offset in the detection scheme. The measurement was performed at various pump powers and the resulting differential sum-frequency signal verses pump power data were fit with a line. In our hands, this approach provided better sensitivity than using a dual channel differential lock-in to continually difference the sum frequency signal between two co-focused probe beams (collected independently with matched photodiodes) where one beam was coincident in time with the pump and the other temporally offset.

The sum-frequency signal represents multi-photon absorption events in which at least one photon is absorbed from each of the pump and the probe pulses. The sum-frequency signal is proportional to TPA events provided that, first, all of the transmitted probe light is collected to avoid systematic complications that stem from the nonlinear index and, second, that the excitation power is limited such that excited state absorption and higher-order nonlinearities are not significantly recruited. Under these conditions, the sum-frequency signal increases linearly with the optical power in the pump beam (Fig. 3.2).

Calibration: A thin plate of gallium phosphide (GaP) was used for absolute calibration of the transmission change measured with the pump-probe technique. The fractional intensity loss of the transmitted probe beam induced by mixing with the pump beam, denoted $\Delta T/T$, can be directly measured in GaP. Measurements of $\Delta T/T$ in GaP were typically in the range of 1.5×10^{-3} to 8×10^{-3} for a for focal pump power, denoted Pref, in the range of 20 to 50 mW. This allowed us to equate the power dependent slope of the differenced sum-frequency signal from GaP, denoted V_{GaP}, to the absolute change in transmission of the probe beam, $\Delta T/T_{GaP}$, thereby providing absolute calibration. The fractional intensity loss of each sample at pump power Pref, denoted $\Delta T/T_{sample}$, was then be determined by taking the ratio of the measured power dependent slope of the sum-frequency signal from the sample, denoted V_{sample}, to that of GaP, denoted V_{GaP}, and then multiplying by $\Delta T/T_{GaP}$, *i.e.*, $\Delta T/T_{sample} = (V_{sample}/V_{GaP}) \times \Delta T/T_{GaP}$. In this manner we routinely measured fractional sensitivities of $\Delta T/T \sim 5 \times 10^{-6}$.

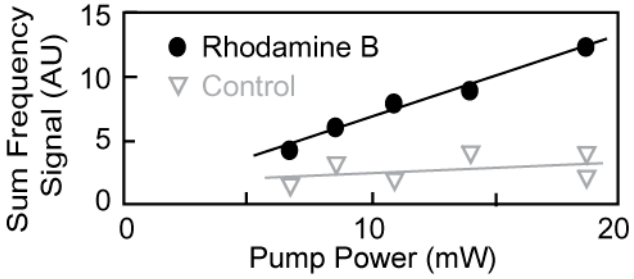

Figure 3.2. A single-trial TPA measurement on rhodamine B (8.3-mM in methanol) at 880 nm shows the linearity of the sum-frequency signal with the pump beam power. Control data was collected with the rhodamine sample placed in the beam path but outside of the focal region. All experiments were performed at 21C.

Analysis

Optical absorption proceeds according the relation

$$\frac{dI}{dz} = \alpha I + \beta I^2 , \quad (1)$$

where I is the incident intensity, z is the optical path length, α is the one photon absorption coefficient and β is the two-photon absorption coefficient. The two–photon cross-section, denoted σ_{TPA}, is proportional to the two-photon absorption coefficient, *i.e.*,

$$\sigma_{TPA} = \frac{h\omega}{N} \beta , \quad (2)$$

where $\hbar\omega$ is the energy of the excitation photon and N is the number density of scatterers.

The two-photon cross-section is further related to the fractional change in transmission $\Delta T/T$ of the probe induced by the pump, under the conditions of our apparatus, by[19]

$$\sigma_{TPA} = \frac{h\omega}{N} \frac{1+\eta}{\sqrt{2}\,\eta} \frac{A}{L} \frac{1}{P_{ref}} \frac{\Delta T}{T} , \quad (3)$$

where $\eta \approx 0.69$ is the ratio of the cross-sectional areas of the pump to the probe beams, L is the axial length of the overlap of the co-focused beams, and A is an effective cross-sectional area of the overlap volume of the beams at the focus. L was estimated by collecting the TPEF profile of a fluorescent sample while Z-scanning, thus at full width half maximum L ~ 94 μm (Appendix III.A.) The area A is estimated in two ways. First, through the relation $A = \lambda_o b/(2n)$, where λ_o is the center wavelength of the pulse and b is the confocal parameter of a single beam; the parameter b is also measured through TPEF Z-scanning while electronically phase locking onto the beam of interest. Second, the parameter A is estimated through the relation $A = (\lambda_o^2 / \pi)(1 - NA^2_{eff})/NA^2_{eff}$, where NA_{eff} = NA x (beam size) / (back aperture size) and NA is the stated numerical aperture of the air objective. The relations for A were evaluated by measuring the ratio of the beam areas at the back aperture of the excitation objective with the area of the back aperture. We use the average of the two methods to find A/L ~ 5 ± 1 μm.

Theoretical Limit: It is of interest to compare the ratio of the experimental σ_{TPA} value with theoretical predictions. There is a particular interest in understanding what molecular structures lead to large cross-sections[20]. For this reason it has been suggested that the measured values σ_{TPA} be compared with the maximum off-resonance TPA cross-section theoretically possible for the measured molecule[21, 22]. This maximum value of σ_{TPA} is given by[22]:

(4) $$\sigma_{TPA\_MAX} = 64.1E^2\left[\frac{1}{n^2}\left(\frac{n^2+2}{3}\right)^4\right]\left[\frac{\Gamma_{20}}{E_{20}}+2\frac{\Gamma_{10}}{E_{10}}\right]\left(\frac{N_{ef}^2}{E_{10}^5}\right)$$

where n is the index of refraction of the solution, E is the incident photon energy in eV, E_{10} and E_{20} are the energies (in eV) between the ground state and the first and second excited states respectively, Γ_{10} and Γ_{20} are the associated excited state linewidths, and N_{ef} is the effective number of π bond electrons which are believed to be the primary participants in nonlinear excitation. $N_{ef} = \left[\sum_i N_i\right]^{1/2}$ where N_i is the number of electrons involved in double and triple bonds and the sum is over 'submolecules.' Submolecules are mutually exclusive electronic domains within a molecule internally connected through conjugated bonds[22].

In the case of hemoglobin the four heme centers are the optically active sites. Each heme has a conjugated cycle consisting of 11 double bonds (22 electrons) and two side appendages each with one double bond (see Appendix III.B), thus the effective number of π bond electrons at heme sites is $N_{ef} = (4x(22^2 + 2x2^2))^{.5} = 44.4$. The relevant one-photon and two-photon excited state energies E_{10} and E_{20} are approximately 2.2eV and 3eV corresponding to absorption peaks at 578 nm and 418 nm. We estimate the line widths (the full width half maximum) of the primary absorption peaks to be Γ_{10} = .08 and Γ_{20} =.3 eV respectively. Over the range of excitation wavelengths of interest the index of refraction of hemoglobin is ~1.356 (Appendix IIA.) These parameters and Eq. 4 provide a theoretical estimate of the maximum TPA cross-section, σ_{TPA_MAX}, that varies linearly from ~1260 to 1600 GM over the wavelength range of 880 to 780nm.

Results and Conclusions

Rhodamine Dyes. Our measurements of the TPA cross-section in rhodamine 6G and B at 800 nm, *i.e.*, σ_{TPA} = 13.4 GM and σ_{TPA} = 21 GM respectively, are in excellent correspondence with previous work[23-25] at similar concentrations (see Fig. 3.3). We measured TPA in R6G solutions at concentrations ranging from 4- 30 mM and found little evidence that the TPA cross-section was a function of concentration under these circumstances. Lower concentrations could not be resolved.

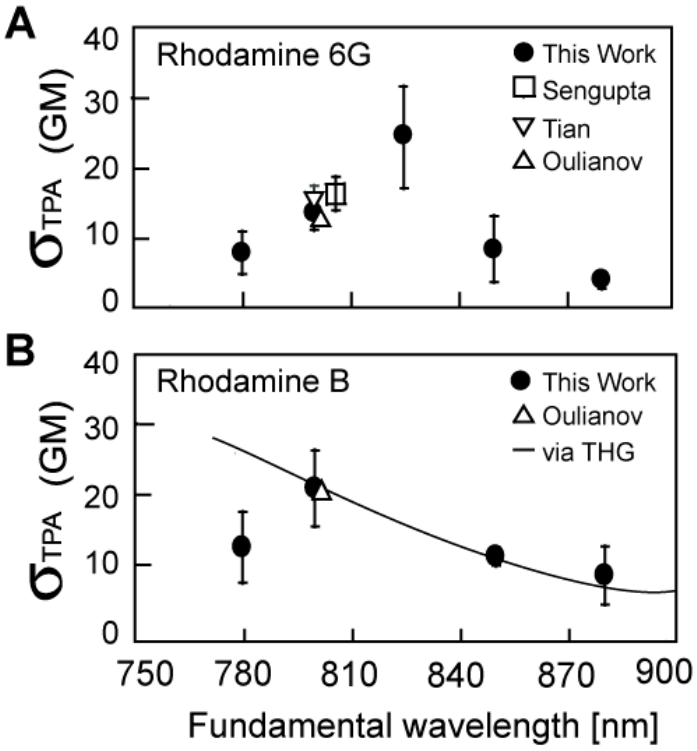

Figure 3.3. The TPA cross-sections (Eq. 3) of 8.3-mM solutions of rhodamine 6G (panel A) and rhodamine B (panel B) in methanol are shown along with previously measured values by Segupta *et al.* (10-mM)[23], Tian and Warren (30-mM)[24], and Oulianov *et al.* (20 and 23-mM, respectively)[25]. Error bars in our data only capture random uncertainties. In panel B, the curve represents two-photon enhanced THG from a 1-mM aqueous solution of rhodamine B[26]. The THG curve has been amplitude scaled.

We also measured TPA in these dyes at other wavelengths between 780 nm and 880 nm (Fig. 3.3, 3.5.) Third harmonic generation (THG) micro-spectroscopy studies[26] on an aqueous solution of rhodamine B demonstrates a TPA resonance with a similar, though not exactly conforming, spectral profile to what we find here (black line in figure 3.3B). Naive comparisons with existing TPEF measurements made with solutions of rhodamine, typically at concentrations of 100 μM or less, are inappropriate in light of the complex concentration dependence of the optical properties of these dyes[27-29] (See Appendix III.A. for a detailed discussion of this issue.)

Hemoglobin. For hemoglobin, the TPA spectra roughly tracks the linear absorption at half the wavelength (Fig. 3.3), as might be expected for two-photon absorption. Hemoglobin has a spectral peak in TPA absorption at 825 nm, with σ_{TPA} = 150 GM. The two-photon peak corresponds to a one-photon absorption peak at ~420 nm (Figs. 3.3A and 3.3B), which is assigned to the Soret band. The approximately 15 nm blue shift in the measured TPA peak compared to the location expected from the position of the linear absorption peak at half the wavelength is also detected in TPA resonance enhanced THG spectra of the same solutions (gray curves in figures 3A and 3B)[26]. Similar shifts in TPA peaks have been observed in TPEF measurements of auto-fluorescent proteins[30].

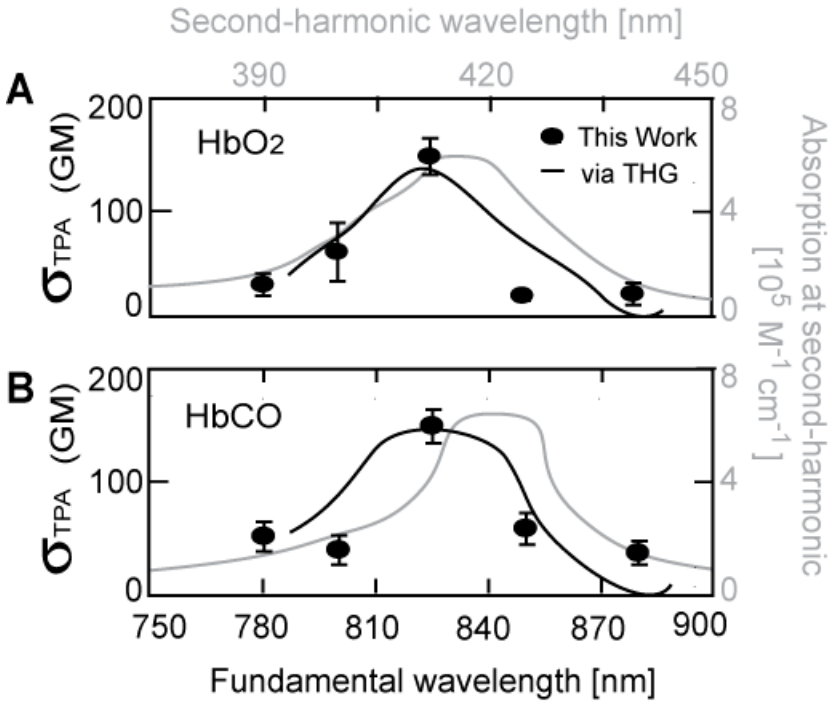

Figure 3.4. The TPA cross-sections (Eq. 3) of HbO_2 (panel A) and HbCO (panel B) are plotted (left-hand scale) along with the linear absorption coefficient (gray lines, right hand scale) at twice the incident photon energy (upper wavelength scale). A statistically significant difference in the TPA cross-section of HbO_2 and HbCO is found at $\lambda = 850$ nm. Systematic uncertainties are not included in the error bars. The dark lines represent amplitude scaled, TPA resonance enhanced THG spectra of these same solutions[26]. The THG curves have been amplitude scaled.

The cross-section of hemoglobin is substantial, even off of resonance, *e.g.*, $\sigma_{TPA} \sim 20$ to 60 GM. As mentioned above it has been suggested that a fruitful means of evaluating TPA efficiency in a molecule is by normalizing the measured value of σ_{TPA} by the theoretical maximum value, σ_{TPA_MAX} (Eq. 4.) This procedure has been applied to several studies of over dozens of conjugated organic chains where the value of σ_{TPA} has thus far always found to be less than 2% (.15% on average) of the quantum mechanically allowed limit [22, 31]. The off resonance ratio

$\sigma_{TPA}/\sigma_{TPA\_MAX}$ of hemoglobin as measured and calculated here (with an ~50% systematic uncertainty), varies between 2- 4% On resonance, at 825 nm, the measured value of σ_{TPA} is ~10% of the theoretical maximum. These results suggest TPA conversion efficiency in heme, perhaps due to its cyclic structure, is substantially greater than in conjugated organic chains.

Our data confirms theoretical expectations of large TPA cross-sections in porphyrins as a result of Soret band states[17]. The TPA resonance appears less prominent than its one-photon counterpart, a feature which is also noticed in the third harmonic studies[26]. The two ligand states HbO_2 and HbCO have significantly different TPA cross-sections near the edge of the resonance band that is centered at 850 nm. This difference confirms the results of previous THG work that shows that the nonlinear optical properties of hemoglobin may be used to distinguish among oxidation states[26].

The large TPA cross-section and relatively high concentration of hemoglobin in red blood cells, ~ 4-mM, supports the contention that these cells may be good candidates for nonlinear imaging and spectroscopy studies *in vivo*. On resonance, λ = 825 nm, and at the highest imaging powers, I ~ $5x10^{11}$ W/cm^2, the energy deposition in a red blood cell at the focus that results from TPA in hemoglobin approaches that due to one photon absorption, *i.e.*, $\beta I / \alpha \sim 1$ (Eq. 1). This suggests that under focussed high intensity illumination, TPA in hemoglobin may provide a basis for imaging contrast that rivals that of linear processes.

Appendix A

TPA Spectroscopy: Nonlinear Transmission vs TPEF

Introduction

The reported values of the TPA cross-section, $\sigma_{TPA,}$ of rhodamine B and 6G, derived through ultrafast TPEF spectroscopy are substantially larger than those values found through nonlinear transmission approaches[23, 32]. The σ_{TPA} values found here are in excellent agreement with single wavelength literature values produced by nonlinear transmission (Fig. 3.3) thus they are not typically in good agreement with TPEF derived values as reported (Fig. 3.5.) It has been variously suggested that the difference in the values measured between techniques is either due to the corruption of nonlinear transmission measurements by confounding effects from other nonlinear processes[25] or to incorrect assumptions regarding the fluorescent quantum yield in TPEF based derivations[14]. In fact, substantial differences in the reported σ_{TPA} of rhodamine 6G and B are apparent even when only comparing TPEF based measurements. The two most extensive ultrafast TPEF studies of rhodamine B (RB) in this spectral range[33, 34] report values for σ_{TPA} that differ on average by ~400 GM. (Fig. 3.5A.) Similarly, ultrafast TPEF spectroscopy studies[34, 35] on rhodamine 6G (R6G) have, on average, a large difference, $\delta\sigma_{TPA}$ ~165 GM (Fig. 3.5B). TPEF studies of fluorescein, another xanthene, are more consistent, with only the largest $\delta\sigma_{TPA}$ values across four studies[33-36] exceeding 100 GM (Fig. 3.5C.) Resolving these apparently large

discrepancies in measured values of σ_{TPA} is important to quantitative TPEF microscopy and nonlinear spectroscopy.

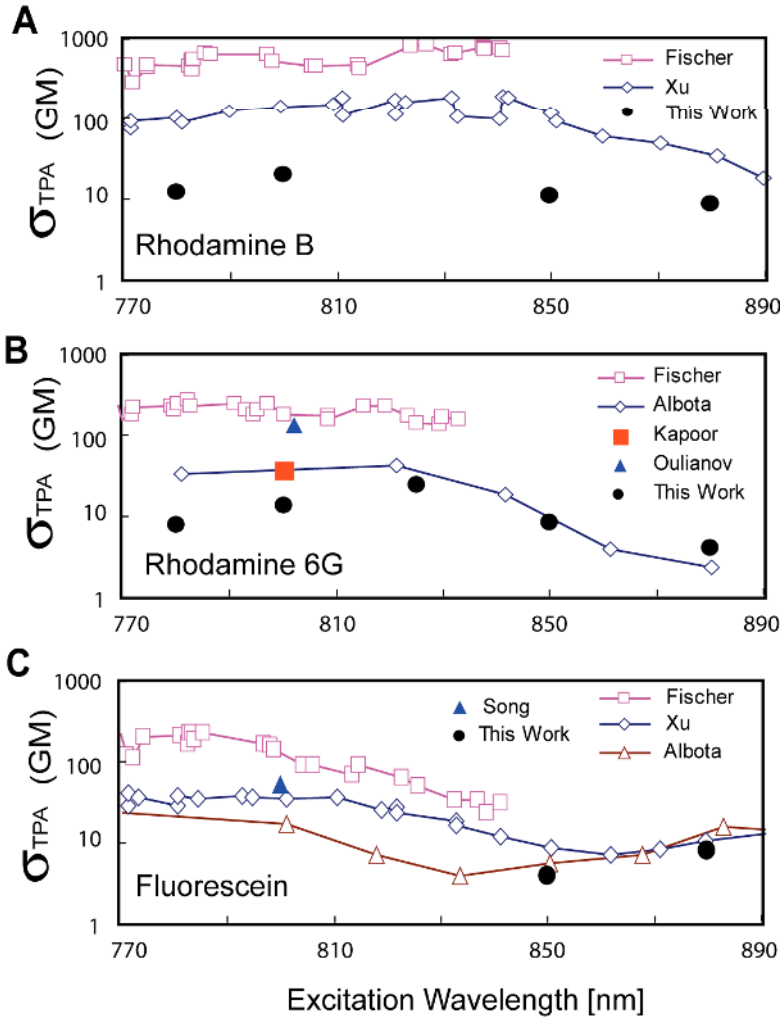

Figure. 3.5. Ultrafast TPEF based TPA measurements and this work show similar spectral profiles but significant differences in absolute values. **A.** TPEF studies on rhodamine B in methanol by Fischer et al[34] at .01-mM, Xu et al[33] at .1-mM, and this work at 8.3-mM. **B.** TPEF studies on rhodamine 6G by Fischer et al[34] at .01-mM, Albota et al[35] at .11-mM, Kapoor et al[32] at .031-mM, Oulianov et al at .04-mM and this work at 8.3-mM. The solvent was methanol in all cases except Kapoor et al[32] which used ethanol. **C.** TPEF studies on Fluorescein by Fischer et al[34] at .01-mM, Xu et al[33] at .1-mM, Albota et al[35] at .11-mM, Song et al[36] at .001-mM and this work at 10-mM. The solvent was buffered water (pH 11) in all cases except this work used ethanol. Song et al[36] used a dextran-fluorescein.

A consistent confound in comparing TPEF and TPA measurements on RB and R6G across the literature is dye concentration (Fig 3.5.) Nonlinear transmission studies depend on directly detecting the ~ $1/10^6$ photons lost due to TPA, thus these experiments tend to involve dye concentrations ranging from ~10-30 mM (Fig. 3.3.) TPEF studies make use of the spectral separation between the excitation beam and fluorescence emission and are thus typically applied to dye concentrations ranging between ~.001-.1 mM (Fig 3.5.)

Concentration and temperature dependent changes in the linear absorption spectrum of xanthenes was reported as early as the 1920's[37]. Renewed interest in these effects accompanied the use of rhodamine dyes as a laser medium[38, 39]. Proposed mechanisms for the influence of concentration on linear absorption and one-photon induced fluorescence include dimerization[38] and higher order aggregation[40] (trimerization[41] etc), conformational states of the monomer[42-45] and dimer[46, 47], interactions between these molecular states[48, 49], and solvation effects [39, 42-46]. Non-monotonic concentration dependence of TPA has been observed in R6G using ~10ns long laser pulses to induced photoacoustic[29] and thermal lensing[50] effects. Concentration dependence in the TPEF spectral features of RB has been noticed in ultrafast TPEF spectroscopy[28], and one set of investigators has reported σ_{TPA} as a function of concentration at 435 and 600 nm[27].

In this report we measure the concentration dependence of TPEF in these molecules at several wavelengths. We show that concentration related quenching can account for the bulk of the discrepancies in the reported values for σ_{TPA}.

TPEF Measurement

8.3 mM solutions of R6G and RB in methanol and a 10 mM solution of Fluorescein in ethanol were diluted by factors of 10, 100, and 1000. TPEF was collected from these solutions at 800, 850, and 880 nm. TPEF was collected on the transmission side of the beam path (see the fluorescence block in Fig. 3.1.) A long pass dichroic reflected the TPEF through a colored glass infrared blocking filter and onto a PMT. With the probe beam blocked the pump frequency modulation in the PMT voltage served to report TPEF power.

The TPEF power, denoted P_{TPEF} was measured as a function of incident pump power, denoted P. Two parameter power law fits to the TPEF power dependent data (Fig 3.6) confirmed its quadratic dependence on power, i.e. $P_{TPEF} = \varepsilon P^2$, typically to within 5% across wavelengths and samples. The quadratic fit parameters, denoted ε, are related to the two-photon cross section, σ_{TPA} in the following way.

(5) $$\varepsilon = kC\,\phi\,\sigma_{TPA}$$

where k is a constant of proportionality that includes geometric factors, C is the concentration of the fluorophore, and ϕ is the fluorescence quantum efficiency. Both the quantum yield ϕ and the TPA cross-section σ_{TPA} may demonstrate

concentration dependence, for this reason and in order to avoid making assumptions about ϕ we introduce the TPEF cross-section:

(6) $$\sigma_{TPEF} = \phi\, \sigma_{TPA} = \varepsilon/(kC)$$

The ratio of the TPEF cross-sections measured at two different concentrations, ie. $\sigma_{TPEF}(C_1)/\sigma_{TPEF}(C_2) = (\varepsilon(C_1)C_2)/(\varepsilon(C_2)C_1)$ is useful as a probe of the concentration dependence of the quantum yield and TPA.

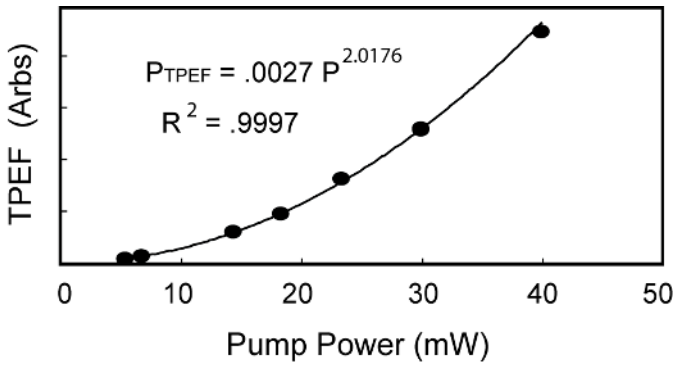

Figure. 3.6. TPEF from a 8.3mM solution of rhodamine B at 850 nm. The close fit to a quadratic demonstrates the anticipated power dependence. Pump Power is measured at the back aperature of the focussing objective. All studies were performed at 21 C.

Results

TPEF in xanthene dyes was found to vary with concentration over the range of .008-10mM, confirming previous results. A plot of $\sigma_{TPEF}(C)/\sigma_{TPEF}(C_{Max})$, where C_{Max} is 8.3 mM for the rhodamines and 10 mM for fluorescein shows that over this range of concentrations, σ_{TPEF} varies by over an order of magnitude (Fig. 3.7). These concentration effects tend to differ across wavelength and show some indication that they may be non-monotonic with concentration which confirms and extends previous findings[27, 28 29, 50].

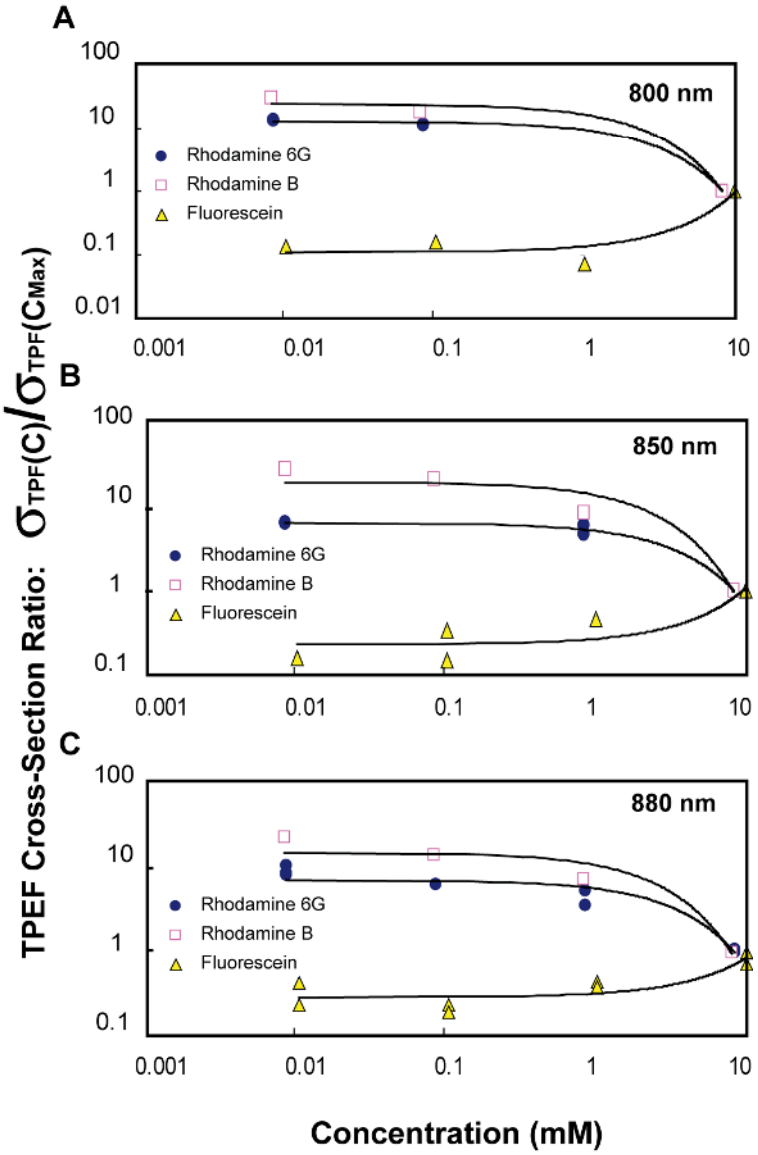

Figure. 3.7. TPEF Quenching: The TPEF cross-section ratio σ_{TPEF}, measured in the xanthene dyes, rhodamine 6G, rhodamine B, and fluorescein as a function of concentration. The yields are normalized by the yield of the maximum concentration measured, i.e. 8.3mM in methanol for the rhodamine dyes and 10mM in ethanol for fluorescein. Curves are two parameter exponential fits and are intended only to guide the eye. At 800 and 850 nm the 8.3mM measurement on rhodamine 6G is obscured by rhodamine B symbol.

Concentration Scaling

The TPEF cross-section ratio data shown in Fig 3.7 can be used to provide a rough scaling between TPEF based literature measurements of σ_{TPA} taken at different concentrations, i.e $\sigma_{TPA}(C_1) = [\sigma_{TPEF}(C_1)/\sigma_{TPEF}(C_2)] \times \sigma_{TPA}(C_2)$. We scale previous ultrafast TPEF spectroscopy studies of σ_{TPA} in RB and R6G to a concentration of 8.3-mM, the same concentration as our TPA samples. For example, the value of the two photon cross section, σ_{TPA} ~440 GM, reported for a .01-mM solution of RB at 800 nm by Fischer et al is multiplied by the TPEF ratio; σ_{TPEF}(8.3-mM) /σ_{TPEF}(.001-mM) ~30 (Fig. 3.5A), this results in an estimate of the TPA cross-section, σ_{TPA} ~22 GM, at a concentration of 8.3-mM. In this case the estimated value lies quite close to our measured value, σ_{TPA} ~20 GM. We extend this concentration scaling to wavelengths other than 800, 850, and 880 nm and to measurements made at concentrations intermediate to our measurements through piece-wise linear approximation.

Rhodamine B. In RB, the average absolute difference in the cross-section data of Fischer et al.[34] data measured at ~.01-mM and that of Xu et al.[33] measured at ~.1-mM is ~500 GM (Fig 3.6A.) After both data sets are scaled to 8.3-mM their average difference in absolute cross-section, denoted $\delta\sigma_{TPA}$, is ~15 GM (Fig 3.6B.) The average reduction in the relative magnitudes of the two measurements, σ_{TPA}(.01mM)/σ_{TPA}(.1mM), due to scaling is a more modest 10%. The most dramatic reductions in absolute and relative magnitudes due to scaling in RB is the difference between literature values and the measurements made here. The average absolute difference between the σ_{TPA} values measured here and that of

Fischer et al.[34] is reduced from ~500 GM to ~3 GM in the scaled data, while the average ratio of the cross-sectional values measured by the two studies was reduced from σ_{TPA} (.01mM)/σ_{TPA} (8.3mM) ~40 to ~1. Scaling the cross section values of Xu et al.[33] from .1mM to 8.3mM also reduced the average differences with the σ_{TPA} values measured here; in this case scaling reduced $\delta\sigma_{TPA}$ from ~83 GM to ~8 GM, and the average cross-section ratio σ_{TPA}(.1mM)/σ_{TPA} (8.3mM) from ~7 to ~1/3.

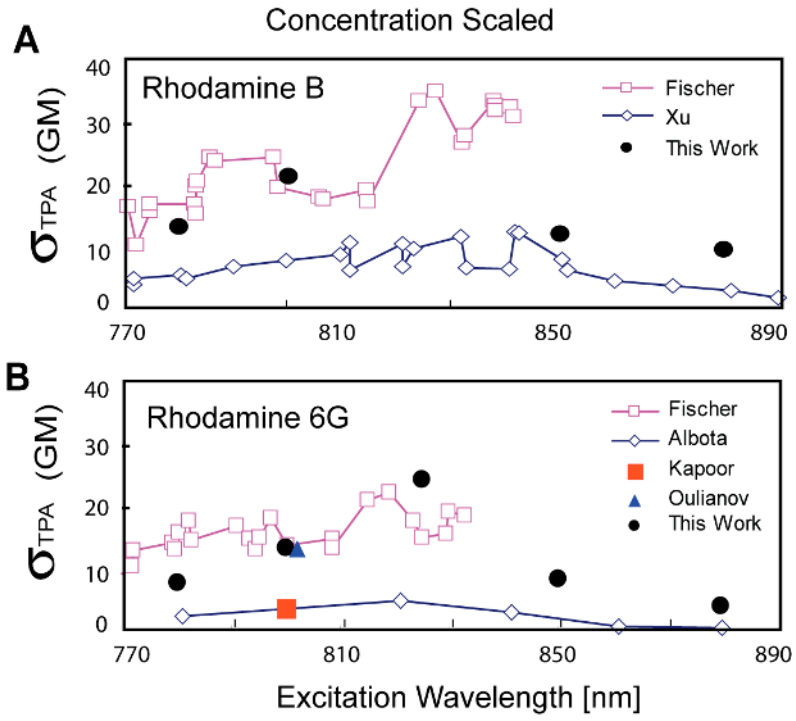

Figure. 3.8. Comparison of ultrafast TPEF based TPA measurements scaled to 8.3-mM shows improved correspondance between most studies. **A.** The concentration scaled TPEF studies on rhodamine B in methanol by Fischer et al[34] at .01-mM, Xu et al at .1-mM, are plotted along with this work at 8.3-mM. **B.** The concentration scaled TPEF studies on rhodamine 6G by Fischer et al[34] at .01-mM, Albota et al[35] at .11-mM, Kapoor et al[32] at .031-mM, Oulianov et al at .04-mM shown with this work at 8.3-mM. The solvent was methanol in all cases except Kapoor et al[32] which used ethanol.

Rhodamine 6G. In R6G, the average absolute difference in the cross-section data of Fischer et al.[34] data measured at ~.01-mM and that of Albota et al.[33] measured at .11-mM is ~200 GM (Fig 3.6A.) After both data sets are scaled to 8.3-mM their average difference in absolute cross-section, denoted $\delta\sigma_{TPA}$, is ~10 GM (Fig 3.6B.) The average relative magnitudes of the two measurements, σ_{TPA}(.01mM)/σ_{TPA}(.1mM), drops from ~6 to ~3.6. As with RB, the most dramatic reductions in absolute and relative magnitudes due to scaling in R6G is the difference between literature values and the measurements made here. The average absolute difference between the σ_{TPA} values measured here and that of Fischer et al.[34] is reduced from ~210 GM to ~6 GM in the scaled data, while the average ratio of the cross-sectional values measured by the two studies was reduced from σ_{TPA} (.01mM)/σ_{TPA} (8.3mM) ~23 to ~1.7. Scaling the cross section values of Albota et al.[33] from .1mM to 8.3mM slightly reduced the average absolute difference $\delta\sigma_{TPA}$ from 14 GM to 9.5 GM, but the average cross-section ratio σ_{TPA}(.1mM)/σ_{TPA} (8.3mM) actually increased from ~3 to ~6.6.

Fluorescein. Fluorescein in ethanol shows little or no quenching of TPEF with concentrations from .01- 1mM, above 1mM the TPEF yield actually increases. The TPEF measurements on fluorescein are also much closer in value across studies and concentrations than are the rhodamines. They also stand in good agreement with the measurements made here at 850 and 880nm. (Fig 3.5.) The use of different renders it impossible to apply the concentration dependent TPEF measurements here to the bulk of the literature.

Conclusion

Significant differences exist in the reported values of the two photon cross-section of the xanthene dyes rhodamine B, 6G, and Fluorescein. A clear resolution of these differences is important to the development of quantitative TPEF microscopy and spectroscopy.

We construct a crude empirically generated concentration scaling function to facilitate comparisons between measurements on the two-photon cross-section, σ_{TPA} performed at different dye concentrations. We find that the disparity between the values of the absolute TPA cross-section of rhodamine dyes found in previous studies is largely an effect of concentration. In particular the σ_{TPA} values generated through direct nonlinear transmission measurements and those generated by TPEF are shown to be relatively consistent (typically within estimated errors) after scaling the data to a common concentration. These results do not assist in the identification of fluorescence quenching mechanisms but do demonstrate that much of the previous inconsistency between cross-section measurements is a material property and not due to experimental or methodological errors.

Appendix B

Chemical Structures of Xanthene Dyes and Heme

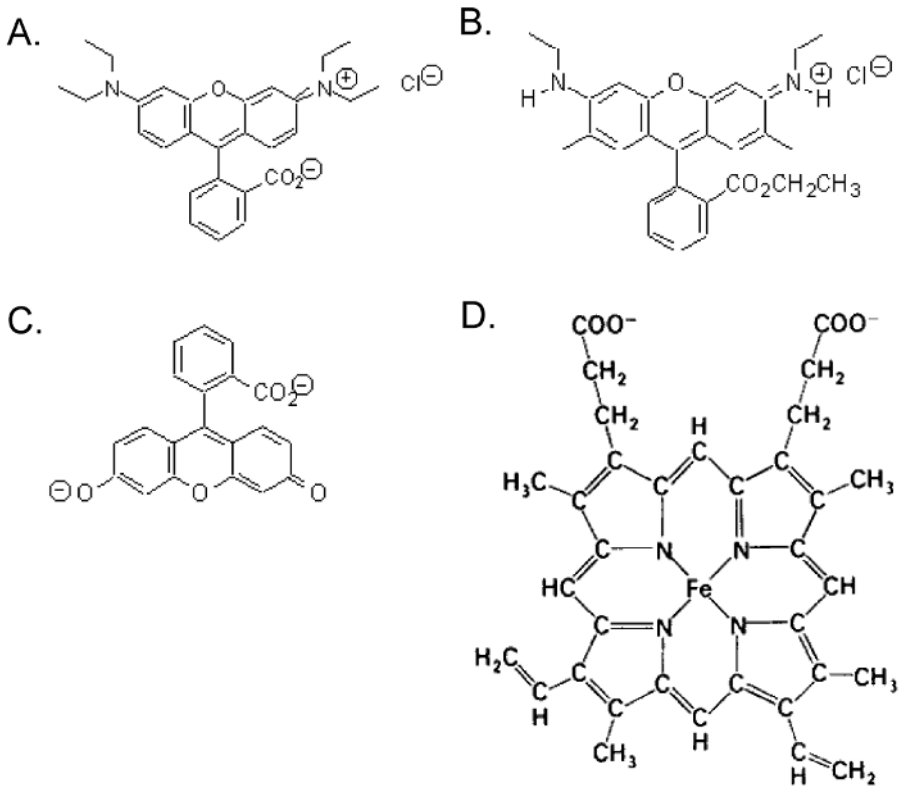

Figure. 3.9. Chemical structures of xanthene dyes and heme[51]. **A.** Rhodamine B. **B.** Rhodamine 6G **C.** Fluorescein **D.** Heme.

Acknowledgements

I would like to acknowledge useful discussions with Peifang Tian and technical support from Earl Dolnick and Phil Tsai.

The Following work was used in part or in full in Chapter III:

> Large two-photon absorption cross-section of hemoglobin in the infrared range of 780 - 880 nm. G. O. Clay, C. B. Schaffer and D. Kleinfeld. submitted.

References

1. D. M. Friedrich and W. M. McClain, "Two-Photon Molecular Electronic Spectroscopy," Annual Review Physical Chemistry **31**, 559-577 (1980).

2. W. Denk, J. H. Strickler, and W. W. Webb, "Two-photon laser scanning fluorescence microscopy," Science **248**, 73-76 (1990).

3. J. E. Ehrlich, X. L. Wu, I.-Y. S. Lee, Z.-Y. Hu, H. Rockel, S. R. Marder, and J. W. Perry, "Two-photon absorption and broadband optical limiting with bis-doner stilbenes," Optics Letters **22**, 1843-1846 (1997).

4. S. Jeon, V. Malyarchuk, J. A. Rogers, and G. P. Wiederrecht, "Fabricating three dimensional nanostructures using two-photon lithography in a single exposure step," Optics Express **14**, 2300 (2006).

5. A. Karotki, M. Khurana, J. R. Lepock, and B. C. Wilson, "Simultaneous Two-photon Excitation of Photofrin in Relation to Photodynamic Therapy," Photochemistry and Photobiology **82**, 443-452 (2006).

6. D. Day, M. Gu, and A. Smallridge, "Use of two-photon excitation for erasable-rewritable three-dimensional bit optical data storage in a photorefractive polymer," Optics Letters **24**, 948-951 (1999).

7. K. Konig, T. W. Becker, P. Fischer, I. Riemann, and K.-J. Halbhuber, "Pulse-length dependence of cellular response to intense near-infrared laser pulses in multiphoton microscopes," Optics Letters **24**, 113-115 (1999).

8. K. Konig, P. T. C. So, W. W. Mantulin, and E. Gratton, "Cellular response to near-infrared femtosecond laser pulses in two-photon microscopes," Optics Letters **22**, 135-138 (1997).

9. T. Shimada, W. Watanabe, S. Matsunaga, T. Higashi, H. Ishii, K. Fukui, K. Isobe, and K. Itoh, "Intracellular disruption of mitochondria in a living HeLa cell with a 76-MHz femtosecond laser oscillator," Optics Express **13**, 9869 (2005).

10. K. Konig, I. Riemann, and P. Fischer, "Photodynamic therapy by nonresonant two-photon excitation," presented at the Conference on Optical Methods for Tumor Treatment and Detection: Mechanisms and Techniques in PHotodynamic Therapy VIII, San Jose, CA, 1999.

11. A. Karotki, M. Kruk, M. Drobizhev, A. Rebane, E. Nickel, and C. W. Spangler, "Efficient Singlet Oxygen Generation Upon Two-Photon Excitation of New Porphyrn With Enhanced Nonlinear Absorption," IEEE Journal On Selected Topics in Quantum Electronics **7**, 971-975 (2001).

12. M. C. Fischer, T. Ye, G. Yurtsever, A. Miller, M. Ciocca, W. Wagner, and W. S. Warren, "Two-photon absorption and self-phase modulation measurements with shaped femtosecond laser pulses," Optics Letters **30**(12), 1551-1553 (2005).

13. C.-K. Sun, C.-C. Chen, S.-W. Chu, T.-H. Tsai, Y.-C. Chen, and B.-L. Lin, "Multiharmonic-generation biopsy of skin," Optics Letters **28**, 2488-2490 (2003).

14. P. Tian and W. Warren, "Ultrafast measurement of two-photon absorption by loss modulation," Optics Letters **27**, 1634-1636 (2002).

15. D. Kleinfeld, P. P. Mitra, F. Helmchen, and W. Denk, "Fluctuations and stimulus-induced changes in blood flow observed in individual capillaries in layers 2 through 4 of rat neocortex," Proceedings of the National Academy of Sciences USA **95**, 15741-15746 (1998).

16. E. Chaigneau, M. Oheim, E. Audinat, and S. Charpak, "Two-photon imaging of capillary blood flow in olfactory bulb glomeruli," Proceedings of the National Academy of Sciences USA **100**, 13081-13086 (2003).

17. M. B. Masthay, L. A. Findsen, B. M. Pierce, D. F. Bocian, J. S. Lindsey, and R. R. Birge, "A theoretical investigation of the one and two photon properties of porphyrins," Journal of Chemical Physics **7**(1), 3901-3915 (1986).

18. S. Frolov and Z. Vardeny, "Double-modulation electro-optic samping for pump-probe ultrafast corretlation measurements," Review of Scientific Instruments **69**, 1257 (1998).

19. R. Sutherland, L., *Handbook of Nonlinear Optics* (Marcel Dekker, Inc, New York, 2003), p. 971.

20. M. Albota, D. Beljonne, J.-L. Bredas, J. E. Ehrlich, J.-Y. Fu, A. A. Heikal, S. E. Hess, T. Kigej, M. D. Levin, S. R. Marder, D. McCord-Maughon, J. W. Perry, H. Rockel, M. Rumi, G. Subramaniam, W. W. Webb, X. L. Wu, and C. Xu, "Design of Organic Molecules with Large Two-Photon Absorption Cross Sections," Science **281**, 1653-1656 (1998).

21. M. G. Kuzyk, "Physical Limits on Electronic Nonlinear Molecular Susceptibilities," Physical Review Letters **85**, 1218-1221 (2000).

22. M. G. Kuzyk, "Fundamental limits on two-photon absorption cross-sections," Journal of Chemical Physics **119**, 8327-8334 (2003).

23. P. Sengupta, J. Balaji, S. Banerjee, R. Philip, R. Kumar, and S. Maiti, "Sensitive measurement of absolute two-photon absorption cross sections," Journal of Chemical Physics **112**, 9201-9205 (2000).

24. P. Tian and W. Warren, "Ultrafast measurement of two-photon absorption by loss modulation," Optics Letters **27**, 1634 (2002).

25. D. A. Oulianov, A. S. Tomov, A. S. Dvornikov, and P. M. Rentzepis, "Observations on the measurement of two-photon absorption cross-section," Optics Communications **191**, 235-243 (2001).

26. G. O. Clay, A. C. Millard, C. B. Schaffer, J. Aus-der-Au, P. S. Tsai, J. A. Squier, and D. Kleinfeld, "Spectroscopy of third harmonic generation: Evidence for resonances in model compounds and ligated hemoglobin," Journal of the Optical Society of America B **23**, 932-950 (2006).

27. N. K. M. N. Srinivas, S. V. Rao, and D. N. Rao, "Saturable and reverse saturable absorption of Rhodamine B in methanol and water," Journal of the Optical Society of America B **20**(12), 2470-2479 (2003).

28. C. H. Wang, O. Y. H. Tai, Y. Wang, T. H. Tsai, and N. C. Chang, "Non-quadratic-intensity dependence of two-photon absorption induced flurescence of organic chromophores in solution," The Journal of Chemical Physics **122**, 084509-084501, 084509-084507 (2005).

29. R. Philip, P. Sathy, V. P. N. Nampoori, J. Philip, and C. P. G. Vallabhan, "Characteristics of two-photon absorption in methanol solutions of Rhodamine 6G using laser induced pulsed photoacoustics," Journal of Physics B **25**, 155-161 (1992).

30. G. A. Blab, P. H. M. Lommerse, L. Cognet, G. S. Harms, and T. Schmidt, "Two-photon excitation action cross-sections of the autofluorescent proteins," Chemical Physical Letters **350**, 71-77 (2001).

31. M. G. Kuzyk and J. P. Moreno, "Fundamental Limits of the Dispersion of the Two-Photon Absorption Cross-Section," Journal of Chemical Physics **123**, 194101 (2006).

32. R. Kapoor, C. S. Friend, and A. Patra, "Two-photon-excited absolute emission cross-sectional measurements calibrated with a luminance meter," Journal of the Optical Society of America B **20**, 1550-1554 (2003).

33. C. Xu and W. W. Webb, "Measurement of two-photon excitation cross sections of molecular fluorophores with data from 690 to 1050 nm," Journal Optical Society of America **13**, 481-491 (1996).

34. A. Fischer, C. Cremer, and E. Stelzer, "Fluorescence of coumarins and xanthenes after two-photon absorption with a pulsed titanium-sapphire laser," Applied Optics **34**, 1989 (1995).

35. M. Albota, C. Xu, and W. W. Webb, "Two-photon fluorescence excitation cross-sections of biomolecular probes from 690-960 nm," Applied Optics **37**, 7352 (1998).

36. J. M. Song, T. Inoue, H. Kawazumi, and T. Ogawa, "Determination of Two Photon Absorption Cross Section of Fluorescein," Analytical Sciences **15**, 601-603 (1999).

37. W. Speas, "A quantitiative study of the changes produced in the absorption bands of certain organic fluorescent dye solutions by alternations of concentration and temperature," Physical Review **31**, 569-578 (1928).

38. J. E. Selwyn and J. I. Steinfeld, "Aggregation Equilibria of Xanthene Dyes," The Journal of Physical Chemistry **76**, 762-774 (1971).

39. J. Fergusen and A. W. H. Mau, "Absorption studies of acid-base equilibria of dye solutions," Chemical Physical Letters **17**, 543-546 (1972).

40. D. Toptygin, B. Z. Packard, and L. Brand, "Resolution of absorption spectra of rhodamine 6G aggregates in aqueous solution using the law of mass action," Chemical Physical Letters **277**, 430-435 (1997).

41. F. Lopez-Arbeloa, P. Ruiz-Ojeda, and I. Lopez-Arbeloa, "On the Aggregation of rhodamine B in ethanol," Chemical Physical Letters **148**, 253-258 (1988).

42. M. J. Snare, F. E. Treloar, K. P. Ghiggiinio, and P. J. Thistlethwaite, "The Photophysics of Rhodamine B," Journal of Photochemistry **18**(1982), 335-346 (1982).

43. K. G. Casey and E. L. Quitevis, "Effect of Sovent Polarity on Nonradiative Processes in Xanthene Dyes: Rhodamine B in Normal Alcohols," Journal of Physical Chemistry **92**, 6590-6594 (1988).

44. P. J. Sadkowski and G. R. Fleming, "Photophysics of acid and base forms of rhodmane B," Chemical Physical Letters **57**, 526-529 (1978).

45. D. A. Hinckley, P. G. Seybold, and D. P. Borris, "Solvatochromism and thermochromism of rhodamine solutions," Spectochimica Acta **42A**, 747-754 (1986).

46. M. Faraggi, P. Peretz, I. Rosenthal, and D. Weinraub, "Solution properties of dye lasers. Rhodamine B in alcohols," Chemical Physical Letters **103**, 310-314 (1984).

47. V. I. Gavrilenko and M. A. Noginov, "Ab initio study of optical properties of rhodamine 6G molecular dimers," The Journal of Chemical Physics **124**, 044301 (2006).

48. F. Lopez-Arbeloa, P. Ruiz-Ojeda, and I. Lopez-Arbeloa, "Fluorescence self-quenching of the molecular forms of rhodamine B in aqueous and ethanolic solutions," Journal of Luminescence **44**, 105-112 (1989).

49. F. Lopez-Arbeloa, P. Ruiz-Ojeda, and I. Lopez-Arbeloa, "The fluorescence quenching mechanisms of rhodamine 6G in concentrated ethanolic solution," Journal of Photochemistry and Photobiology, A **45**, 313-323 (1988).

50. C. V. Bindhu, S. S. Harilal, V. P. N. Nampoori, and C. P. G. Vallabhan, "Studies of nonlinear absorption and aggregation in aqueous solutions of rhodamine 6G using a transient thermal lens technique," Journal of Physics D **32**, 407-411 (1998).

51. H. Du, R. A. Fuh, J. Li, A. Corkan, and J. S. Lindsey, "PhotochemCAD: A computer-aided design and research tool in photochemistry," Photochemistry and Photobiology **68**, 141-142 (1998).